

**Impact of Mouse Strain on Arrested Alveolarization
in Response to Hyperoxia Exposure as Neonates**

Inauguraldissertation

zur Erlangung des Grades eines Doktors der Humanmedizin

des Fachbereichs Medizin

der Justus-Liebig-Universität Gießen

vorgelegt von **Tiono, Jennifer**

aus Bremen, Deutschland

Gießen 2023

Aus dem Fachbereich Medizin der Justus-Liebig-Universität Gießen

Herz- und Lungenforschung, Bad Nauheim
Abteilung: Entwicklung und Umbau der Lunge

Gutachter: Prof. Dr. Werner Seeger

Gutachterin: Prof. Dr. Veronika Grau

Tag der Disputation: 05.03.2024

*„Der Beginn aller Wissenschaften ist das Erstaunen,
dass die Dinge sind, wie sie sind.“*

— Aristoteles —

I. Table of Contents

I.	Table of Contents	I
II.	List of figures	III
III.	List of tables	V
IV.	List of abbreviation	VII
1.	Introduction	1
1.1	Human lung development	1
1.1.1	Early lung development	1
1.1.2	Late lung development	2
1.2	Pathogenesis of BPD	3
1.3	Old and new BPD	4
1.4	Animal models of bronchopulmonary dysplasia	5
1.5	Mouse strains	6
1.6	Antioxidants	7
2.	Hypothesis and aims of the study	9
3.	Material and Methods	10
3.1	Material	10
3.1.1	Equipment	10
3.1.2	Reagents	12
3.2	Methods	15
3.2.1	Water Purification	15
3.2.2	Animal experiments	15
3.2.3	Organ isolation	16
3.2.4	Lung fixation and embedding	17
3.2.5	Design-based stereology	19
3.2.6	Gene expression level assessment	21

3.2.7	Protein expression analysis	28
3.2.8	Statistical analysis	33
4.	Results	34
4.1	Hyperoxia was tolerated by five out of six mouse strains.....	34
4.2	The genetic background impacts the outcome of lung development under the effect of hyperoxia	36
4.3	The genetic background impacts the gene expression of the lung antioxidant response under the effect of hyperoxia	46
5.	Discussion	62
5.1	Method Discussion	62
5.1.1	Polymerase Chain Reaction	62
5.1.2	Immunoblot	64
5.1.3	Statistical analysis	65
5.2	Selection of mouse strains and experimental design.....	66
5.3	Lung development in mouse strains under hyperoxia.....	67
5.4	Lung antioxidant gene expression in mouse strains under hyperoxia.....	69
6.	Conclusion.....	75
7.	Summary.....	76
8.	Zusammenfassung.....	78
9.	References	80
10.	Declaration	89
11.	Publication directory.....	90
12.	Acknowledgements.....	91

II. List of figures

Figure 1 The experimental BPD model.....	16
Figure 2 Phylogenetic Tree.	35
Figure 3 Survival rate of six mouse strains.	36
Figure 4 Representative plastic-embedded lung tissue sections from five mouse strains exposed to 21% O ₂ or 85% O ₂	37
Figure 5 Quantitative analysis of alveoli number by design-based stereology.....	40
Figure 6 Quantitative analysis of alveolar density by design-based stereology.	41
Figure 7 Quantitative analysis of lung volume by design-based stereology.....	42
Figure 8 Quantitative analysis of septal thickness by design-based stereology.....	43
Figure 9 Quantitative analysis of mean linear intercept (MLI) by design-based stereology.	44
Figure 10 Expression of superoxide dismutase 1, 2 and 3 in five different inbred mouse strains exposed to hyperoxia.	48
Figure 11 Expression of superoxide dismutase 3 in five different inbred mouse strains exposed to normoxia or hyperoxia.	49
Figure 12 Expression of glutathione in five different inbred mouse strains exposed to hyperoxia.	50
Figure 13 Expression of glutathione synthetase in five different inbred mouse strains exposed to normoxia or hyperoxia.	51
Figure 14 Expression of glutathione peroxidase 1 and glutathione disulfide reductase in five different inbred mouse strains exposed to normoxia or hyperoxia.	53

Figure 15 Expression of thioredoxin and catalase in five different inbred mouse strains exposed to normoxia or hyperoxia.	54
Figure 16 Expression of thioredoxin reductase 1 and 2 in five different inbred mouse strains exposed to normoxia or hyperoxia.....	55
Figure 17 Expression of nuclear factor (erythroid-derived 2) -like 2 in five different inbred mouse strains exposed to normoxia or hyperoxia.	56
Figure 18 Expression of peroxiredoxin 1, 5 and 6 in five different inbred mouse strains exposed to normoxia or hyperoxia.	58
Figure 19 Expression of peroxiredoxin 2, 3 and 4 in five different inbred mouse strains exposed to normoxia or hyperoxia.	59
Figure 20 Expression of paroxonase 1,2 and 3 in five different inbred mouse strains exposed to normoxia or hyperoxia.	60
Figure 21 Expression of hemoxygenase-1 in five different inbred mouse strains exposed to normoxia or hyperoxia.	61

III. List of tables

Table 1 The five stages of human lung development.....	1
Table 2 Composition for Paraformaldehyde 1.5%.....	17
Table 3 Buffers required for treatment of lungs and embedding in Technovit 7100.....	18
Table 4 Richardson's stain - stock solution	19
Table 5 Steps used for the reverse transcription reaction.....	21
Table 6 Mastermix composition for cDNA synthesis	22
Table 7 Primers for RT-PCR.....	23
Table 8 Composition of the reaction mix for real-time PCR analysis	25
Table 9 Real-time PCR reaction program	25
Table 10 Composition for TENS buffer.....	26
Table 11 Composition for TE buffer.....	26
Table 12 Composition for PCR genotyping reaction mix for sex determination.....	27
Table 13 PCR genotyping reaction program for sex determination.....	27
Table 14 Primers employed for sex determination	28
Table 15 Composition of protein lysis buffer	29
Table 16 Composition of 10% stacking / resolving gel used for immunoblot analysis..	30
Table 17 Composition of 10× SDS running buffer for immunoblot analysis.....	30
Table 18 Composition of 5% milk-blocking buffer for immunoblot analysis.....	31
Table 19 Composition of 1× PBS washing buffer for immunoblot analysis	32
Table 20 Primary and secondary antibodies used for western blot analysis.....	32

Table 21 Composition of stripping buffer for immunoblot analysis.....	33
Table 22 Structural parameters of lungs from mice exposed to 21% O ₂ normoxia for 14 days postnatal life. Assessed by design-based stereology.....	38
Table 23 Structural parameters of lungs from mice exposed to 85% O ₂ hyperoxia for 14 days postnatal life. Assessed by design-based stereology.....	39
Table 24 Percentage analysis of parameters by design-based stereology	45

IV. List of abbreviation

APS	Ammonium persulfate
bp.....	Base pairs
BPD.....	Bronchopulmonary dysplasia
CAT.....	Catalase
cDNA	Complementary DNA
CE	Coefficient of error
COPD.....	Chronic obstructive pulmonary disease
C _t	Cycle threshold
CV	Coefficient of variation
DNA.....	Desoxyribonucleic acid
dNTPs	Deoxyribonucleotide triphosphate
dsDNA	Double-stranded template DNA
E	Embryonic day
ECM.....	Extracellular matrix
EDTA.....	Ethylendinitrilo-N, N, N, N'-tetra-acetic-acid
EGTA.....	Ethylene glycol-bis (β-aminoethyl ether)- N,N,N',N'-tetraacetic acid
g.....	acceleration due to gravity
GA.....	Glutaraldehyde
GPX.....	Glutathione peroxidase
GSR.....	Glutathione-Disulfide Reductase
GSS	Glutathione Synthetase
HEPES	4-(2-hydroxyethyl)-1-piperazineethanesulfonic acid
HMOX	Heme Oxygenase
HRP	Horseradish peroxidase
i.e.....	<i>id est</i>
MLI	Mean linear intercept
MuLV.....	Murine leukemia virus
Nfe212	Nuclear factor erythroid 2-related factor 2
NP-40.....	Nonyl phenoxy polyethoxyethanol, Tergitol-type NP-40
OsO ₄	Osmium tetroxide
P	Postnatal day
PBS	Phosphate buffered saline

PFA	Paraformaldehyde
POLR2A	RNA Polymerase II Subunit A
PON.....	Paraoxonase
PRDX1	Peroxiredoxin
RDS.....	Respiratory distress syndrome
RNA	Ribonucleic acid
ROS.....	Reactive oxygen species
RT-PCR.....	Reverse transcriptase polymerase chain reaction
SDS	Sodium dodecyl sulfate
SOD.....	Superoxide dismutase
TAE.....	Tris-acetate-EDTA
TE.....	Tris-EDTA
TEMED.....	Tetramethylethylenediamine
tRNA	Transfer RNA
TXN1	Thioredoxin-1
TXNRD1.....	Thioredoxin reductase
UrAc.....	Uranyl acetate
UV	Ultraviolet
vol	Volume
wt.....	Weight

1. Introduction

1.1 Human lung development

The lung is one of the most crucial organs for air-breathing mammals. Its primary function is to transport oxygen into the bloodstream, providing fresh oxygen for the body while releasing carbon dioxide. Gas exchange occurs in certain units within a complex network called the alveoli. The alveoli-capillary barrier consists of several layers, including epithelial cells supported by the extracellular matrix and surrounded by capillaries [1]. The lung can be described as a tree that divides into numerous branches and eventually terminates in the alveoli. This structure provides a large surface area while also keeping the thickness as thin as possible, facilitating maximal efficiency of gas exchange and function within a minimum amount of space [2].

Lung development is a process divided into five stages, which are further subdivided into early (mostly prenatal) and late (mostly postnatal) lung development [3]–[5].

Table 1 *The five stages of human lung development*

Early lung development	
Embryonic	0–7 weeks <i>in utero</i>
Pseudoglandular,	7–17 weeks <i>in utero</i>
Canalicular	17–27 weeks <i>in utero</i>
Saccular	28–36 weeks <i>in utero</i>
Late lung development	
Alveolar	36 weeks <i>in utero</i> –2 years post-natal

Table constructed from [3]

1.1.1 Early lung development

Embryonic stage

The embryonic period occurs during the 4- 7th week post-conception in humans (Mouse: E9.5-E12). Lung buds form from the ventral wall of the primitive foregut and branch into the left and right primary bronchial buds, which eventually develop into the left and right bronchial trees. The lung buds then elongate, grow into the surrounding mesenchyme, and begin branching. By the conclusion of the 7th week, the lung

transitions into the pseudoglandular stage, exhibiting characteristics reminiscent of a small tubule-acinar gland [3], [6], [7].

Pseudoglandular stage: The pseudoglandular stage occurs between the 7th and 17th weeks post-conception in humans (Mouse: E12-E16.5). This stage is characterized by ongoing tubular branching of the conducting airways, establishment of blood vessels, and the development of terminal bronchioles enveloped by mesenchyme. By the culmination of this stage, the respiratory system resembles a tree-like structure, indicative of its advancing maturation. [3], [6], [8].

Canalicular stage: During the canalicular stage (occurring between the 16th and 27th weeks post-conception in humans – Mouse: E16.5-E17.5), the formation of acinar structures begins, which include respiratory bronchioles, alveolar ducts, and primitive alveoli. The pulmonary epithelium differentiates into the alveolar-capillary barrier, and type I/II pneumocytes undergo differentiation. Surfactant protein becomes detectable in the 24th week, facilitating gas exchange [7]. Consequently, the canalicular stage (specifically the 24th week) represents the earliest viable timeframe for the successful delivery of a preterm infant.[6], [8].

Saccular stage: During the saccular stage (24th–38th week post-conception in humans and E18-postnatal day (P4) in mice), peripheral airways expand, alveolar sacs form, and surfactant production begins. The air-blood barrier also undergoes further thinning to increase the gas-exchanging surface area [3], [8], [9].

1.1.2 Late lung development

The following stages occur mainly during the postnatal period and represent the last stages of lung development in both humans and mice. While the establishment of the number of airway generations and branching patterns occurs after birth, the development of the pulmonary parenchyma persists for several years [5]. Notably, over 90% of all alveoli develop postnatally [5].

Alveolar stage: The alveolar stage occurs during the 36th week post-conception in humans until age 2-3 [3]. It takes place between postnatal days PN5-PN30 in mice [10].

During this stage, secondary septation, formation of definitive alveoli, and microvascular maturation occur [3].

Postnatal lung development: At the time of birth, the lung typically contains approximately 20-50 million alveoli [11]. However, during the postnatal period, alveolar multiplication occurs, leading to a substantial increase in the total number of alveoli in the fully developed lung. As a result, the final count ranges from 300 to 600 million alveoli [5].

1.2 Pathogenesis of BPD

Bronchopulmonary dysplasia (BPD) was first described more than 50 years ago by William Northway in 1967 [12]. It primarily affects preterm infants who experience surfactant deficiency and develop respiratory distress syndrome (RDS), requiring mechanical ventilation for survival [12]. While mechanical ventilation increased the survival rate of premature infants with RDS, it also gave rise to a new lung injury known as BPD. Northway discovered changes in the lungs of prematurely born infants suffering from RDS and treated with positive-pressure ventilation and high oxygen concentrations to maintain the necessary blood oxygen saturation [12].

BPD is most prevalent in very preterm infants (28-31 weeks of gestation) and extremely preterm infants (<28 weeks of gestation) [13] with birth weights <1,250 g [14], occurring in the late canalicular or saccular stage of lung development [13].

It is a multifactorial long-term lung complication, and the exact cause of its development is unknown. Various pre-, peri-, and post-natal factors contribute to the changes in the lung. Ante- and perinatal factors include lung immaturity with surfactant homeostasis, intrauterine and perinatal infections, decreased host antioxidants defence, patent ductus arteriosus, and genetics. Postnatal causes include oxygen toxicity and oxidative stress, where newborns receive oxygen supplementation to manage acute respiratory failure as well as baro- and volutrauma caused by mechanical ventilation [15], [16]. Long-term hyperoxia exposure through oxygen supplementation remains the most critical cause of BPD pathogenesis [17].

Disturbances in the lung development process during the late canalicular or saccular stage, which is a critical period of lung development, can cause BPD in preterm infants [16].

Despite major treatment advances, BPD remains a common chronic lung disease with an incidence above 30% in preterm infants below 30 weeks of gestation in most European countries [18]. In a recent study, the reported global incidence range of BPD in infants born <28 weeks was found to be 10% to 89% (10% to 73% in Europe, 18% to 89% in North America, 18% to 82% in Asia, and 30% to 62% in Oceania) [19]. In Germany alone, approximately 11,000 preterm infants (<32 weeks of gestation) are born and treated in neonatal intensive care units each year, with BPD occurring in 15% of these cases [20].

The consequences of BPD include lifelong restrictions of pulmonary function, increased risk of respiratory problems, and a higher risk for abnormal somatic and psychomotor development [13]. Most pulmonary restrictions persist into adolescence, leading to obstructive respiratory disorders [21]. Current studies suggest that former preterm infants are predisposed to developing chronic pulmonary diseases such as COPD or Asthma bronchiale in adolescence [22], [23].

In recent decades, significant progress has been made in understanding the mechanism and pathogenesis of BPD, as well as medical advances in treatment. However, as stated above, the incidence of BPD remains high, and therapeutic options are limited [24]. Therefore, further research is necessary to provide a deeper understanding of the pathophysiology of BPD.

1.3 Old and new BPD

Over the course of several years, the epidemiology and pathology of BPD have changed due to medical advances. These advances include the introduction of prenatal and postnatal steroid therapy [25],[26], postnatal caffeine, vitamin A [27], postnatal administration of exogenous intratracheal surfactant [28], a better understanding of pH, pCO₂, and pO₂ physiological effects, and improvement of the mechanical ventilation [29].

The demographic shift resulting from these advances led to increased survival rates of infants, including extremely preterm infants from the 23rd-28th week of intrauterine life and <1000 g birth weight, with lungs being developed in the late canalicular/early saccular stage [30], [31].

The morphology of BPD also changed along with the shift, leading to differentiation between "old" BPD, representing the original severe form, and "new" BPD, the currently most common less severe form, termed in 1999 by Jobe [32].

The "old" BPD was characterized by severe morphologic changes such as emphysema, atelectasis, fibrosis, airway smooth muscle hypertrophy, and pulmonary vascular hypertensive changes, leading to airway obstruction, pulmonary hypertension, and *cor pulmonale* [12], [33]. Whereas "new" BPD is mainly characterized by developmental disorders [33]. The current main histopathology feature of "new BPD" is the stunting of lung alveolarization and aberrant lung vascular development [34], leading to larger, simplified alveoli, decreased septation of airspace and decreased branching of the pulmonary vasculature [33]. Alveolar septal fibrosis, airway injury and inflammation, which were common in "old" BPD, are now observed in fewer cases.[35].

1.4 Animal models of bronchopulmonary dysplasia

BPD is a multifactorial long-term lung complication with contributing factors including lung immaturity, volu- and barotrauma through mechanical ventilation, as well as infection and inflammation [15], [16], leading to an impairment of alveolar and vascular development [34].

The majority of knowledge regarding the pathogenesis of BPD has been obtained from animal models, particularly rodents and non-human primates [36]. These models aim to replicate the pulmonary phenotype observed in human BPD by subjecting animals to various stimuli, including hyperoxic gas and/or mechanical ventilation [37].

A crucial aspect of reliable animal models is their ability to reproduce similar features observed in preterm infants with BPD [38].

In the past, both large animal models (baboons, sheep, lambs, and pigs) and small animal models (rabbits, rats, and mice) have been used for clinical studies on BPD. [38]. Large animal models, such as preterm lambs and preterm baboons, probably represent the best models of human disease, but they come with high maintenance costs and ethical debate [39]. Overall, rodents have been proven to be the most suitable and commonly used mammalian research model [40], [41].

Lung development is typically categorized into five stages: embryonic, pseudoglandular, canalicular, saccular and alveolar stage [3]. While the lung development of term-born infants coincides with the alveolar stage, the lungs of preterm infants often find themselves in the late canalicular or saccular stage [13].

Rodents are born at a developmental stage equivalent to that of extremely preterm infants (i.e., saccular stage), which provides another significant advantage for studying BPD in experimental settings [38], [41]. Although term-born rodents are structurally

immature in the saccular stage, their lungs are functionally mature and capable of efficient gas exchange. As a result, these rodents do not require life-saving interventions such as intubation, ventilation, or surfactant therapy, which are commonly needed in larger animal models. This feature highlights the advantage of using term-born rodents for studying lung development and diseases like BPD. [38], [41].

Rodents also have relatively short estrous cycles, gestation periods, and large litter and pup sizes [38]. These factors provide many opportunities for easy planning of pregnancies, multiple litters in a short time, a higher number of subjects per pregnancy, and the relatively larger birth size eases surgical manipulation and provides a larger amount of tissue when harvested [38].

Since the lung development of rodents is nearly complete within 2 and 3 weeks after birth, monitoring postnatal lung maturation is convenient [41]. According to Burri et al., alveolar formation occurs in approximately 10 days, specifically from postnatal day 4 to day 13 [4].

Rodents offer several additional benefits for research purposes. Their small size makes them convenient to handle and house in laboratory settings. Additionally, rodents have short life cycles, allowing researchers to conduct studies within a relatively short timeframe. Furthermore, there is a wide availability of antibodies specifically designed for rodents, facilitating experimental investigations. Moreover, rodents serve as a cost-effective model, not only in terms of their initial purchase but also in terms of ongoing maintenance, making them a highly appealing choice for many researchers [42].

1.5 Mouse strains

An inbred strain is defined as a population of animals that results from at least 20 sequential generations of brother-sister mating [43]. This process of inbreeding leads to a state of high homozygosity, with each mating increasing homozygosity at gene loci by approximately 19.1% per generation. [44], [45]. After 20 generations, homozygosity reaches approximately 98%, resulting in an inbred strain that is nearly genetically identical. [44].

To date, around 400 inbred mouse and 200 inbred rat strains have been developed [44]. The following listing from Overbeek et al. contains the most frequently used strains along with their pigmentations: “A (albino), BALB/c (albino), C3H (agouti), C57BL/6 (black), C57BL/10 (black), C57BR (brown), C58 (black), DBA (dilute brown), FVB

(albino), NZB (black), NZW (white), SJL (albino), SWR (albino) and 129/Sv (usually albino or chinchilla)” [46].

A wide range of mouse strains are utilized in BPD research, with C57BL/6 being a well-established neonatal model for hyperoxia-induced injury. Other frequently employed mouse strains in BPD research include BALB/c, A/J, C3H/He, FVB/N, and DBA/2 [39].

Past studies have shown the significance of the role of mouse and rat strains in experiments. These studies have shown that the genetic background of mice can result in different outcomes in the same experiments involving environmental exposure, genetic manipulation, or specific treatments [47].

Nichols et al. demonstrated that the genetic background of mice contributes to the level of lung inflammation observed when newborn mouse pups from 36 different inbred strains are exposed to hyperoxia for 72 hours after birth [48]. Also, Whitehead et al. observed that the impact of oxygen injury is partly influenced by the genetic background in an experiment involving nine genetically diverse inbred strains exposed to hyperoxia [49]. Additionally, studies have identified strain-independent and strain-dependent gene expression patterns in the lungs of C57BL/6J, A/J, and C3H/HeJ mice [50]. Therefore, it is crucial to consider the mouse strains used in preclinical studies on bronchopulmonary dysplasia (BPD) to ensure accurate and consistent results.

These findings highlight the importance of considering the employed mouse strains in preclinical studies on bronchopulmonary dysplasia (BPD) and should be considered when designing, interpreting and comparing experiments.

1.6 Antioxidants

Reactive oxygen species (ROS), including superoxide radical ($O_2^{\cdot-}$), hydrogen peroxide (H_2O_2) and the hydroxyl radical ($\cdot OH$) are normal metabolic byproducts of cellular metabolism in aerobic organisms [51]. ROS are highly reactive, and at low to moderate concentrations, contribute to essential cellular processes. However, excessive levels of ROS can lead to oxidative damage to important molecules, such as lipid peroxidation, protein denaturation, and DNA modification [52]. This oxidative damage can trigger a local inflammatory response [53]. Antioxidants, on the other hand, act as defense mechanisms that inhibit oxidation [54]. Oxidation is a chemical reaction that can generate free radicals, leading to cellular damage [55]. An antioxidant is defined as “any

substance that can eliminate reactive oxygen species directly or indirectly, acting as a regulator of the antioxidant defence, or inhibiting the production of those species” [56]. Enzymatic and non-enzymatic antioxidant systems in the body include superoxide dismutase (SOD), catalase (CAT), glutathione peroxidase (GPX), lipid-soluble vitamin E, carotenes, and water-soluble vitamin C [55].

An imbalance between oxidants, such as ROS, and antioxidants in favor of the oxidants is termed "oxidative stress," which can lead to oxidative damage to macromolecules when the antioxidant system becomes overwhelmed [54]. Pathophysiological conditions, including exposure to hyperoxia, cigarette smoke, ozone, ionizing radiation, and others, result in heightened production of oxidants [57]. In such circumstances, the lungs undergo increased production of oxygen radicals, surpassing the cellular antioxidant defense capacity and causing pulmonary injury [58].

2. Hypothesis and aims of the study

Bronchopulmonary dysplasia (BPD) remains one of the most common complications of preterm birth, leading to significant morbidity and mortality in neonatal intensive care units [18]. Consequently, there is an urgent need for further research to understand the pathomechanism of BPD. Preclinical mouse models are frequently used to mimic the physiological and histological characteristics of BPD. However, conflicting findings can arise due to the utilization of different mouse strains. Currently, no comprehensive study has been conducted to compare lung alveolarization and the gene expression of key components involved in the lung antioxidant response across commonly used mouse strains.

The objectives of this study are as follows:

1. To determine whether the genetic background of five different inbred mouse strains — C57BL/6J, BALB/cJ, FVB/NJ, C3H/HeJ, and DBA/2J — affects lung development in the presence of hyperoxia.
2. To investigate whether the genetic background influences the gene expression of central components involved in the lung antioxidant response.

The hypothesis of this study posits that the genetic background of mice plays a significant role in shaping the outcomes of lung development under hyperoxic conditions.

3. Material and Methods

3.1 Material

3.1.1 Equipment

Name	Company
Agar cutting mould	custom made
Agar embedding moulds	custom made
Barnstead™ GenPure™ Pro Water Purification System	Thermo Scientific
Blotting membrane, Trans-Blot® Turbo™ Transfer Pack	Bio-Rad, Germany
Camera, D5300	NIKON, USA
Cell culture dish, 100 mm	Greiner Bio-One, Germany
CELLSTAR® 96 Well Plates	Greiner Bio-One, Germany
Centrifuge 5430/ 5430 R	Eppendorf, Germany
Centrifuge MiniSpin®	Eppendorf, Germany
Cover slides	Roth, Germany
Digital slide scanner, NanoZoomer-XR C12000	Hamamatsu, Germany
Electrophoresis chambers, Mini Protean® Tetra system	Bio-Rad, Germany
Electrophoresis chambers, Wide Mini-Sub® Cell GT	Bio-Rad, Germany
Filter tips, 10 µl, 100 µl, 200 µl, 300 µl, 1000 µl	Sarstedt, Germany
Fully Automated Rotary Microtome	Leica Biosystems, Germany
Heating plate	Medax, Germany
Heraeus Multifuge 3SR Plus	Thermo Scientific
Histobloc	Heareus, Germany
Histoform Q mould	Heareus, Germany
HLC Heating-ThermoMixer MHR 11	DITABIS, Germany
Homogenizing kit for soft tissue, Precellys®	PEQLAB, Germany
Homogenyzer, Precellys® 24-Dual homogenizer	PEQLAB, Germany
Imager ImageQuant® LAS 4000	GE health care, USA
InoLab® pH meter	WTW, Germany
Knife holder NZ RM2200 silver	Leica Biosystems, Germany

MicroAmp™ Optical 96-Well Reaction Plate	Applied Biosystems, USA
MicroAmp™ Optical Adhesive Film	Applied Biosystems, USA
Microcentrifuge tubes, 0.5, 1.5, 2 ml	Eppendorf, Germany
Microplate reader, VersaMax ELISA	Molecular devices, USA
Microscope slides, SUPERFROST ULTRA PLUS®	Thermo Fisher Scientific, USA
Microtome knife, 16cm long, profile d, steel assy	Leica Biosystems, Germany
NanoDrop® ND-1000 spectrophotometer	Thermo Scientific, USA
NanoDrop™ One/OneC Mikrovolumen-UV-Vis-Spektrophotometer mit WLAN	Thermo Scientific, USA
Objective, AF-S DX Micro NIKKOR, 85mm	NIKON, USA
Pasteur pipette, 3.5 ml	Sarstedt, Germany
PCR-thermocycler, peqSTAR 2X	VWR, USA
Pipetboy®	Integra, Switzerland
Pipettes Eppendorf Research® plus, manual, 10 µl, 20 µl, 100 µl, 200 µl, 1000 µl	Eppendorf, Germany
Pipettes Eppendorf Xplorer®, automatic, 10 µl, 100 µl, 300 µl	Eppendorf, Germany
Pipettes, multichannel, 300 µl	Eppendorf, Germany
Pipettes, serological, 2 ml, 5 ml, 10 ml, 25 ml, 50 ml	Falcon, USA
PowerPac™ Basic Power Supply	Bio-Rad, Germany
Precision Plus Protein® Dual color standard	Bio-Rad, Germany
Refrigerated microcentrifuge CT15RE	VWR, USA
Silica Gel Orange	Roth, Germany
Single use needles, FINE-JECT®	HENKE SASS WOLF, Germany
Snap-cap vials, Rotilabo®	Roth, Germany
Snap-on lids	Roth, Germany
Spectrafuge™ Mini Laboratory Centrifuges	Labnet, USA
StepOnePlus™ Real-Time PCR System	Applied Biosystems, USA
Surgical instruments – scissors, tweezers	F.S.T., Germany
Technovit® 3040/Histobloc®	Heareus, Germany
Test tubes, 15 ml, 50ml	Greiner Bio-One, Germany
Trans-Blot® Turbo™ Transfer System	Bio-Rad, Germany

Ultraviolet (UV) Transilluminator, Gel Imager	Intas, Germany
Unimax 2010	Heidolph, Germany
ViiA 7 Real-Time PCR System	Applied Biosystems, USA
VisiopharmNewCast software	Visiopharm, Denmark
Vortex mixer	VWR, USA
Water bath, for histological slides	Vogel, Germany
White light transilluminator, TW-26	UVP, UK

3.1.2 Reagents

Name	Company
2-Mercaptoethanol	Bio-Rad, Germany
4× Laemmli Sample Buffer	Bio-Rad, Germany
Acetone, > 99.7% (vol/vol)	Roth, Germany
Acrylamide/Bisacrylamide stock solution (Rotiphorese Gel 30)	Roth, Germany
Agar for microbiology (Agar-agar)	Sigma-Aldrich, Germany
Agarose	Promega, USA
Ammonium persulfate (APS)	Promega, Germany
Azure II	Sigma-Aldrich, Germany
Bovine serum albumin (BSA)	Thermo Fisher Scientific, USA
Complete® protease inhibitor	Roche, Germany
Deoxynucleotide Triphosphates (dNTPs)	Promega, USA
Deoxynucleotide Triphosphates (dNTPs)	Promega, USA
Di-Sodium tetraborate Decahydrate	Roth, Germany
Double-distilled water (ddH ₂ O)	Thermo Fisher Scientific, USA
Ethanol, 70% (vol/vol)	Roth, Germany
Ethanol, absolute	Roth, Germany
Ethidium bromide	Promega, USA
Ethylendinitrilo-N, N, N, N'-tetra-acetic-acid (EDTA)	Sigma-Aldrich, Germany
Ethylene glycol-bis (2-amino-ethylether)-N, N, N', N'-tetraacetic-acid (EGTA)	Sigma-Aldrich, Germany

Glutaraldehyde stock solution 50%	Sigma-Aldrich, Germany
Glycine	Roth, Germany
GoTaq® DNA-Polymerase	Promega, USA
GoTaq® Flexi Reaction Buffers	Promega, USA
HEPES	Sigma-Aldrich, Germany
Isopropanol	Merck, Germany
Liquid nitrogen	Air Liquide, Germany
Magnesium chloride stock solution (25 nM)	Applied Biosystems, USA
Magnesium chloride stock solution (50 nM)	Applied Biosystems, USA
Methylene blue	Roth, Germany
MuLV Reverse Transcriptase	Applied Biosystems, USA
NARCOREN , Pentobarbital Sodium	Merial GmbH
Non-fat dry milk powder	Roth, Germany
NP-40	Fluka Biochemika, UK
Nuclease-Free Water	Invitrogen, UK
Osmium tetroxide	Roth, Germany
Paraformaldehyde (PFA)	Sigma-Aldrich, Germany
PCR Nucleotide Mix (10 mM)	Promega, USA
PCR-Buffer II 10×	Applied Biosystems, USA
Phosphate buffered saline (PBS) 1×, 10×	Sigma-Aldrich, Germany
Platinum™ SYBR™ Green qPCR SuperMix-UDG	Invitrogen, UK
Ponceau S	Sigma-Aldrich, Germany
Precision Plus Protein Dual Color Standards	Bio-Rad, Germany
Proteinase K	Promega, USA
QuickStart® Bradford 1×Dye Reagent	Bio-Rad, Germany
Random Hexamers (50 µM)	Invitrogen, UK
RIPA® buffer	Sigma-Aldrich, Germany
RNase free water	Qiagen, Germany
RNase Inhibitor	Applied Biosystems, USA
RNaseZAP™	Sigma-Aldrich, Germany
SDS / Natriumlaurylsulfat ≥ 99% powder	Roth, Germany
Sodium cacodylate	Serva, Germany

Sodium dodecyl sulfate (SDS), 10% solution	Promega, USA
Sodium orthovanadate	Sigma-Aldrich, Germany
SuperSignal® West Femto chemiluminescent substrate	ThermoFisher Scientific, USA
Technovit 3040	HeareusKulzer, Germany
Technovit 7100	HeareusKulzer, Germany
Technovit, universal liquid	HeareusKulzer, Germany
Tetramethylethylenediamine (TEMED)	Bio-Rad, Germany
Tris Buffer (Tris-HCl) (pH 6.8, 0.5M)	Thermo Scientific, USA
Tris Buffer (Tris-HCl) (pH 7.5, 1M)	Thermo Scientific, USA
Tris Buffer (Tris-HCl) (pH 8.8, 1.5M)	Thermo Scientific, USA
Tris Buffer ≥ 99% Powder	Roth, Germany
Tris-acetate-EDTA (TAE) buffer, 50×	Roth, Germany
Tween® 20	Sigma-Aldrich, Germany
Uranyl acetate	Serva, Germany
Xylol, > 98.5% (vol/vol)	Roth, Germany

3.2 Methods

3.2.1 Water Purification

To ensure the quality and purity of water used in all experiments, a water purification system Barnstead GenPure Pro Water Purification System was employed. This system employs a combination of purification techniques to achieve a high level of water purity. The resulting double-distilled water was used as the primary water source for the experimental procedures described in this thesis.

3.2.2 Animal experiments

3.2.2.1 Normobaric hyperoxia-based mouse model of BPD

The C57BL/6J, BALB/cJ, FVB/NJ, C3H/HeJ and DBA/2J mouse strains were purchased from The Jackson Laboratory (Bar Harbor, MA, USA), and the 129S2/SvPasOrlRj mouse strain was purchased from Janvier (Le Genest-Saint-Isle, Mayenne, France). To obtain an appropriate animal model for this study, newborn mouse pups were randomized within 2 hours of birth to litter sizes of either four or five. From the day of birth (designated P1) until the 14th day of postnatal life (P14), the mouse pups were exposed to normoxic (21% O₂) or hyperoxic (85% O₂) conditions (see Figure 1). Nursing dams were rotated every 24 h between normoxia- and hyperoxia-exposed litters to minimize oxygen toxicity. All animals had access to food and water and were maintained at room temperature (22 °C) and lighting in a 12/12 h light/dark cycle. The health status of experimental animals was monitored daily using a ScoreSheet approved by the “Regierungspräsidium”, as per regulations. Strict guidelines and regulations for animal care and welfare were followed, as well as maintaining high standards of hygiene and sanitation to ensure the health and well-being of the animals involved in research. Mouse pups were euthanized on day P14 by pentobarbital overdose (500 mg/kg, intraperitoneal).

All animal procedures were approved by the local authorities, the Regierungspräsidium Darmstadt (approval B2/1108).

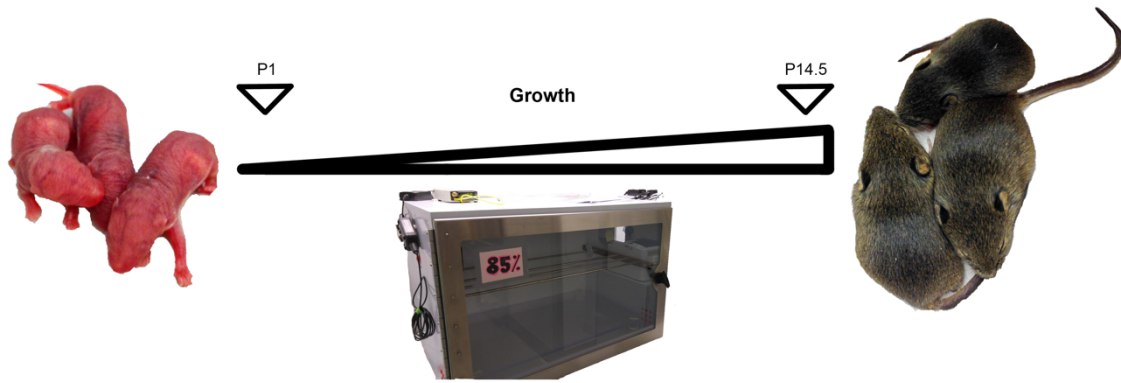


Figure 1 The experimental BPD model.

Mouse strains were exposed to hyperoxia from the day of birth (post-natal day 1, P1) for 14 days of postnatal life (P14.5).

3.2.3 Organ isolation

After soaking the body in 70% ethanol, the abdomen was opened using surgical scissors and tweezers. The diaphragm was then punctured to allow the lungs to retract.

After the lungs were successfully isolated, the following steps were taken for further treatment.

3.2.3.1 Lungs isolated for RNA and protein analysis

To exsanguinate the mouse, the lungs were perfused with 1x PBS by cannulating the right ventricle. This procedure removes the blood from the pulmonary vascular system.

To improve the perfusion, the inferior vena cava and trachea were cut.

After perfusion, both lung lobes were extracted and immediately frozen in liquid nitrogen. All samples were kept at -80°C for further processing.

3.2.3.2 Lungs isolated for embedding in plastic resin and stereological analysis

Lungs were instillation-fixed via a tracheal cannula under a 20 cm H_2O hydrostatic pressure with a fixation solution containing 1.5% (wt/vol) paraformaldehyde, 1.5% (wt/vol) glutaraldehyde in 150 mM HEPES, pH 7.4. Measurements are listed in Table 2.

Lungs were dissected and all samples were kept 24 h at 4°C in fixation solution before further processing.

Table 2 Composition for Paraformaldehyde 1.5%

Reagent	Volume
GA (50%)	6 ml
HEPES 1M	30 ml
PFA	3 g
PBS 1%	164 ml
Total Volume	200ml

GA, glutaraldehyde; HEPES, hydroxyethyl-piperazineethane-sulfonic acid; PFA, paraformaldehyde; PBS, phosphate buffered saline

3.2.4 Lung fixation and embedding

3.2.4.1 Embedding in agar and lung volume estimation

After the lungs were stored 24 h in fixation solution, the heart, trachea and thymus were removed. Afterwards, the lungs were embedded *in toto* in 2% (wt/vol) agar-agar overnight in specific custom-made agar embedding moulds.

The hardened agar blocks were then cut via a custom-made agar cutting mould into 3 mm slices. Photographs were taken of the same side of each slice. Lung pieces within the agar were preserved for further embedding procedures.

The photographs were used to calculate the lung volume by the Cavalieri Principle using Visiopharm NewCast computer-assisted stereology system and Stepanizer. The lung volume estimation with the Cavalieri estimator is performed using a point grid within 100% of each lung section. The Cavalieri's principle has been previously described [59].

3.2.4.2 Embedding in plastic resin

Recovered lung pieces were transferred into Snap-cap vials for a five-day process of embedding in Technovit 7100 inside a fume hood. Buffers required for the treatment of lungs and embedding are defined in Table 3.

Day 1: Lungs were washed 4×5 min in 0.1 M sodium cacodylate buffer then treated for 2 h with 1% osmium tetroxide (OsO_4) in 0.1 M sodium cacodylate buffer. Next, the lungs were rewashed for 4×5 min in 0.1 M sodium cacodylate buffer, then 2×5 min in double-distilled water and afterwards for 1 h in double-distilled water, changing every

15 min. Eventually, the samples were blocked overnight at room temperature in half-saturated uranyl acetate (UrAc) buffer protected from light.

Day 2: Samples were washed 4×5 min in double-distilled water, followed by the dehydration process. In this process, lungs were dehydrated 2×1 h in 70% acetone, then 2×1 h in 90% acetone and finally 1×1 h in acetone absolute. Lungs were then embedded overnight in a 1:1 solution of Technovit + Härter 1 and acetone absolute.

Day 3: Samples were infiltrated overnight in Technovit + Härter 1.

Day 4 & 5: Samples were embedded in Technovit + Härter 1 + Härter 2 for 5 min constantly stirring in the vials. The Lungs were then transferred into a Histoform Q mould and left for at least 48 h to solidify, which includes day five.

After 48 h, the plastic blocks were removed from the moulds with Technovit universal liquid and Technovit 3040 using the Histobloc adaptors.

Table 3 Buffers required for treatment of lungs and embedding in Technovit 7100.

Buffer	Dilution
Sodium cacodylate	0.1 M in ddH ₂ O
Osmium tetroxide	2% (wt/vol) stock solution, in water for injections 1% (wt/vol) working solution, in 0.1 M sodium cacodylate
Uranyl acetate	saturated stock solution in ddH ₂ O half-saturated working solution in ddH ₂ O
Acetone	70% (vol/vol), 90% (vol/vol), 100% (vol/vol), in ddH ₂ O
Technovit 7100	undiluted solution
Technovit 7100 + Härter 1	1% (wt/vol) Härter 1 in Technovit 7100
Technovit 7100 + Härter 1 + Härter 2	200 µl Härter 2 in 3 ml Technovit 7100- Härter 1
Technovit 3040 + Technovit universal liquid	2:1 ratio

ddH₂O, Double distilled water

3.2.4.3 Plastic sectioning

The lungs embedded in Technovit blocks were sliced into 2 µm sections using a fully automated rotary microtome. A 16 cm long, profile D, steel assy microtome knife was used for this purpose. Every tenth section from a consecutive series was placed on Superfrost Ultra Plus adhesion slides for subsequent staining. To determine the total

number of alveoli and alveolar density, the first and third sections from a consecutive series were collected, while the second section was discarded. All slides were dried on a heating plate at 65 °C.

3.2.4.4 Richardson's staining

The plastic sections were stained with Richardson's stain at 65 °C for 30 seconds, followed by a brief rinse in ice-cold tap water, hot tap water, and a final wash in normal temperature ddH₂O. Finally, the slides were immersed in Xylol for a few seconds.

To prepare Richardson's stain, two stock solutions are required. For stock solution I, di-sodium tetraborate decahydrate is dissolved in ddH₂O, afterwards methylene blue is added. For stock solution II, Azur II powder is dissolved in ddH₂O. Subsequently, both stock solutions are combined. The measurements for the stock solutions are detailed in Table 4. Prior to use, the final stock solution should be filtered through filter paper and diluted 1:1 with tap water.

Table 4 Richardson's stain - stock solution

Reagent	Volume
Stock solution I	
Methylene blue	0,5 g
di-sodium tetraborate decahydrate	0,5 g
ddH ₂ O	50 ml
Stock solution II	
Azur II powder	0,5 g
ddH ₂ O	50 ml

ddH₂O, Double distilled water

3.2.5 Design-based stereology

Lung structure analyses were performed following the American Thoracic Society/European Respiratory Society recommendations [60]. Tissue section images were captured using a NanoZoomer-XR C12000 Digital slide scanner. Digital tissue sections were analyzed using the Visiopharm newCAST computer-assisted stereology system (VIS 4.5.3). The analyses included the determination of gas-exchange surface area, mean linear intercept (MLI; representing an approximate diameter of an alveolus), arithmetic mean septal thickness, alveolar density, and total alveoli number. Assessment of alveolar and septal volume was conducted by point counting on a corresponding point grid, while surface density was measured by point and intersection counting on a

“line grid” within the lung parenchyma. Counting newly appearing alveolar bridges using a physical dissector allowed estimation of alveolar density. Additionally, lung volume was estimated using Cavalieri’s principle, as stated previously [59].

To ensure measurement accuracy, the coefficient of error (CE), the coefficient of variation (CV), and the squared ratio between both (CE^2/CV^2) were calculated, with a requirement of $CE^2/CV^2 < 0.5$.

3.2.6 Gene expression level assessment

3.2.6.1 Total RNA isolation

Approximately 50 mg of mouse lung tissue was homogenized in RNA lysis buffer (part of the Precellys® Tissue RNA-Kit) using a Precellys® 24 homogenizer. Total RNA was then isolated using the Precellys® Tissue RNA-Kit according to the manufacturer's instructions ¹. After homogenization, the resulting suspension was applied to a DNA removing column, where DNA selectively binds to the silica membrane. The flow-through liquid was subsequently applied to the PerfectBind RNA column, where the RNA binds to the silica. The total RNA was then eluted in ddH₂O.

3.2.6.2 Reverse transcription reaction for cDNA synthesis

Reverse transcriptase is an RNA-dependent DNA polymerase that catalyzes DNA synthesis using RNA as a template, resulting in the formation of complementary DNA (cDNA). The steps involved in the reverse transcription reaction are outlined in Table 5. For the preparation of the reverse transcription reaction, RNase-free water was added to 1000 ng of the total RNA sample, containing the desired mRNA to a total RNA volume of 20 µl. The reaction mixture was then denatured for 10 minutes at 70 °C in a PCR machine. After denaturation, 20 µl of mastermix (Table 6) was added, and reverse transcriptase was performed in the PCR machine. The resulting cDNA was diluted with 60 µl of ddH₂O and stored at -20 °C, ensuring its stability and preservation for future use. A no reverse transcriptase (no RT) control was conducted, wherein reverse transcriptase was replaced by RNase-free water during the reverse transcription reaction.

Table 5 Steps used for the reverse transcription reaction

Cycle	Temperature [°C]	Duration [min]	Effect
1	21 °C	10 min	Attachment of random hexamers
2	43 °C	75 min	Reverse transcription
3	99 °C	5 min	Reverse transcriptase inactivation
4	4 °C	not specific	Cool down

¹ https://at.vwr.com/assetsvc/asset/de_AT/id/17039043/contents

Table 6 Mastermix composition for cDNA synthesis

Reagent	Volume [μ l]
10 \times PCR-buffer	4
MgCl ₂ stock solution (25 mM)	8
PCR nucleotide mix	2
Random hexamers	2
RNase inhibitor	1
MuLV reverse transcriptase	2
RNase free water	1
Total Volume	20

PCR, Polymerase chain reaction; RNase, Ribonuclease; MuLV, Murine leukemia virus

3.2.6.3 Real-time polymerase chain reaction (RT-PCR)

The real-time polymerase chain reaction (RT-PCR) is a technique used to exponentially amplify a specific cDNA sequence and quantify gene expression levels. The Platinum SYBR® Green qPCR Mix-UDG – Kit from Invitrogen was used with primer pairs obtained online from a Primer Bank database² or designed using Primer-BLAST software³. The employed primers are listed in Table 7. The primers were synthesized and delivered by Eurofins Genomics.

The RT-PCR consists of three major steps and each reaction generally runs for 40 cycles. The composition of the reaction mix and the reaction program for RT-PCR are described in Table 8 and Table 9. The three major steps are as follows:

- 1. Denaturation:** The double-stranded template DNA (dsDNA) is melted into two single strands.
- 2. Annealing:** The temperature is lowered to enable the binding of the primer to the corresponding sequence of single DNA strands.
- 3. Extension:** Double-stranded DNA is exponentially amplified from single-stranded DNA by DNA polymerase.

² <https://pga.mgh.harvard.edu/primerbank/>

³ <https://www.ncbi.nlm.nih.gov/tools/primer-blast/index.cgi>

Applying fluorescent dye (SYBR® Green I) to the reaction mix allows the amount of DNA to be measured after each cycle via the fluorescent signal.

The dye binds directly to double-stranded DNA and the fluorescence signal increases in direct proportion to the number of PCR product molecules amplified. The StepOnePlus™ Real-time PCR System, which includes thermal cycling and fluorescent dye scanning capability, was used to detect the fluorescence signal change over the reaction. To view the accumulation of PCR product over the reaction, the system generates an amplification plot by plotting fluorescence against the cycle number. A melting curve analysis was performed for each primer to differentiate the amplified PCR product from unspecific primer dimers. A melting curve with a single peak melting curve indicated a specific PCR product.

Samples were always tested in duplicate, and *Polr2a* was used as the reference gene (housekeeping) to analyze the relative expression of specific genes.

When a new primer pair was tested for the first time, the PCR product was separated and resolved on a 1.5% (wt/vol) agarose gel containing 0.002% ethidium bromide in 1×TAE buffer using the Wide Mini-Sub® Cell GT electrophoresis chambers. Following electrophoresis, the gel was imaged under UV transillumination to visualize the DNA bands. The purpose of this method was to confirm the presence of a single amplicon, indicating the successful amplification of the target sequence by the primer pair.

The efficiency of all used RT-PCR primers was tested before in a separate primer dilution test in which the primers proved to function at a dilution up to 1:5000 (m/v).

Table 7 Primers for RT-PCR

Gene	Primer	Primer sequence, 5' - 3'	Primer size, bp	Amplicon size, bp	T _m , °C	Location, bp	Accession number
<i>Txn1</i>	Forward	GGGAGTTCTCCGGTGCTAAC	20	128	61.4	459-478	NM_011660
	Reverse	AGCAGTGGCTTAGGGGACTA	20		59.4	586-565	
<i>Sod1</i>	Forward	GTCGGCTTCTCGTCTTGC	18	155	61.4	701-720	NM_011434
	Reverse	CCCATGCTGGCCTTCAGTTA	20		59.4	855-836	
<i>Sod2</i>	Forward	GCCTGCTCTAATCAGGACCC	20	138	61.4	1386-1405	NM_013671
	Reverse	AGACTACAGCACCCAGTCA	20		59.4	1523-1504	
<i>Sod3</i>	Forward	CCTTCTGTTCTACGGCTTGC	21	117	59.8	93-113	NM_011435
	Reverse	TCGCCTATCTTCTCAACCAGG	22		59.4	209-118	
<i>Cat</i>	Forward	ACCGTGCTCTGTGCATCTTAT	21	125	57.9	91-113	NM_009804
	Reverse	GGAAGCCCTACAGGGAAAAACT	22		60.3	215-193	
<i>Nfe2l2</i>	Forward	CAGAGTGATGGTTGCCACT	20	154	59.4	102-121	NM_010902
	Reverse	GACACTGGTCACACTGGGTT	20		59.4	255-234	

<i>Gpx1</i>	Forward	AGTCCACCGTGTATGCCTTCT	21	124	59.8	830-849	NM_008160
	Reverse	GAGACGCGACATTCTCAATGA	21		57.9	953-934	
<i>Gsr</i>	Forward	GACACCTCTTCCTTCGACTACC	22	117	62.1	1302-1322	NM_010344
	Reverse	CCCAGCTTGTGACTCTCCAC	20		61.4	1418-1397	
<i>Gss</i>	Forward	CAAAGCAGGCCATAGACAGGG	21	138	61.8	1386-1405	NM_008180
	Reverse	AAAAGCGTGAATGGGGCATAAC	21		57.9	1523-1504	
<i>Txnrd1</i>	Forward	CATTGAAGGAGAAGCCCTGGT	21	117	52.4	93-113	NM_001042513
	Reverse	GAGGGCAGATACAGGGGTCA	20		61.4	209-118	
<i>Txnrd2</i>	Forward	GATCCGGTGGCCTAGCTTG	19	125	61	91-113	NM_013711
	Reverse	TCGGGGAGAAGGTTCCACAT	20		59.4	215-193	
<i>Prdx1</i>	Forward	GTCTGAGCTGTGTTTTGGGC	20	154	59.4	102-121	NM_011034
	Reverse	ATGGTACACATGCTGGGAAA	21		57.9	255-234	
<i>Prdx2</i>	Reverse	CACCTGGCGTGGATCAATACC	21	124	61.8	830-849	NM_011563
	Forward	GACCCCTGTAAGCAATGCC	20		61.4	953-934	
<i>Prdx3</i>	Reverse	GGTTGCTCGTCATGCAAGTG	20	155	59.4	701-720	NM_007452
	Forward	CCACAGTATGTCTGTCAAACAGG	23		60.6	855-836	
<i>Prdx4</i>	Reverse	TCCTGTTGCGGACCGAATC	19	138	58.8	1386-1405	NM_001313711
	Forward	CCACCAGCGTAGAAGTGGC	19		61.6	1523-1504	
<i>Prdx5</i>	Reverse	GGCTGTTCTAAGACCCACCTG	21	117	58.8	93-113	NM_012021
	Forward	GGAGCCGAACCTTGCCCTC	19		61.0	209-118	
<i>Prdx6</i>	Reverse	CGCCAGAGTTTGCCAAGAG	19	125	61.8	91-113	NM_007453
	Forward	TCCGTGGGTGTTTACCATTG	21		61.0	215-193	
<i>Pon1</i>	Reverse	CGGAAGGGGAGAACAGTGCAA	20	154	58.8	102-121	NM_011134
	Forward	CAGGTCGGCTACAATATCGTC	21		59.8	255-234	
<i>Pon2</i>	Reverse	AGGAATCGAACTGGAGCTGA	21	124	59.4	830-849	NM_183308
	Forward	AGTGCTAATGCCATGTGGGT	20		59.8	953-934	
<i>Pon3</i>	Reverse	GCACCGTGGCTTCTGTGTAT	20	117	57.9	1302-1322	NM_173006
	Forward	GGGTGTTGGGCACATACAGT	20		57.3	1418-1397	
<i>Hmx1</i>	Reverse	AAATGCAATACTGGCCCCCA	21	117	59.4	1302-1322	NM_010442
	Forward	ACAGCTGCTTTTACAGGCCA	20		59.4	1418-1397	
<i>Polr2a</i>	Reverse	CTAAGGGGCAGCCAAAGAAAC	21	209	59.5	808-828	NM_001291068
	Forward	CCATTCAGCATACAACCTAGGC	23		59.2	1016-994	

bp, base pairs; *T_m*, melting temperature

Table 8 Composition of the reaction mix for real-time PCR analysis

Reagent	Volume [μ l]
Platinum® SYBR® Green qPCR SuperMix-UDG	13
MgCl ₂ stock solution (50 mM)	1
10 μ M forward primer	0.5
10 μ M reverse primer	0.5
ddH ₂ O	8
cDNA	2
Total	25

ddH₂O, Double distilled water; cDNA, Complementary DNA

Table 9 Real-time PCR reaction program

Step	Temperature [°C]	Duration	Cycles
Initialization/polymerase activation	95	10 min	1
Denaturation	95	10 s	40
Annealing of primers	59	10 s	40
Elongation	72	10 s	40
Denaturation	95	1 min	40
Melting curve	55 - 95	Variable	1
Cooling down	25	Not specific	1

3.2.6.4 Determining mRNA expression by StepOne Software

StepOne Software was used to determine mRNA expression. The C_t (cycle threshold) is the intersection between an amplification curve and a threshold line. It indicates the number of cycles needed for the SYBR Green fluorescent signal to surpass the threshold, which is a significantly higher fluorescent signal compared to the background fluorescence. C_t levels are inversely proportional to the quantity of target nucleic acid present in the sample [61].

To analyze the data, the ΔC_t -values of each sample was calculated, by subtracting the C_t -Mean of the reference gene with the C_t -Mean of the gene of interest [C_t (reference gene) - C_t (gene of interest) = ΔC_t]. To ensure robustness and reliability, technical

replicates were performed for each ΔC_t -values. Specifically, duplicate C_t measurements were obtained for both the reference gene and the gene of interest within each sample, resulting in two technical replicates for each gene in every sample. This approach allows for the assessment of technical variability and enhances the accuracy of the experimental results.

3.2.6.5 Deoxyribonucleic acid isolation

To extract genomic DNA, mouse tail biopsies were digested by shaking them in 500 μ l TENS buffer (Table 10) + 5 μ l Proteinase K overnight at 56 °C. The samples were then centrifuged, and the supernatant was transferred to a new tube containing 400 μ l isopropanol. After a brief vortex, the samples were centrifuged for 15 minutes at $16,200 \times g$ in a refrigerated microcentrifuge at 4 °C. The resulting pellet was then diluted with 500 μ l of 70% ethanol and spun down again. The ethanol was removed, and the samples in the tubes were allowed to dry at room temperature. Once dried, the samples were reconstituted in 100 μ l TE buffer (Table 11) and incubated at 56 °C for 30 minutes. The purity and quantification of the DNA solution were determined using a NanoDrop® ND-1000 spectrophotometer.

Table 10 Composition for TENS buffer

Reagent	Concentration
1 M Tris-HCL pH 8	10 mM
0.5 M EDTA pH 8	1 mM
NaCl	100 mM
SDS	0.5% (w/v)

EDTA, Ethylenediaminetetraacetic acid; SDS, Sodium Dodecyl Sulfate

Table 11 Composition for TE buffer

Reagent	Volume [ml]
1 M Tris-HCL pH 8	10
0.5 M EDTA pH 8	2
ddH ₂ O	988

EDTA, Ethylenediaminetetraacetic acid; ddH₂O, Double distilled water

3.2.6.6 Sex determination in mouse pups

To determine the sex of mouse pups, PCR amplification was utilized to detect a male-specific sequence, known as *Sry*, located on the Y chromosome. The detection of the sex independent *I|3* gene (chromosome 11) confirms the correct amplification of the template DNA isolated before and serves as an internal control of PCR amplification. The employed primers are listed below (Table 14).

The protocol for the PCR genotyping reaction mix is provided in Table 12 along with the reaction program for sex determination listed in Table 13.

Table 12 Composition for PCR genotyping reaction mix for sex determination

Reagent	Volume [μ l]
ddH ₂ O	31.15
5× Green GoTaq flexi PCR buffer	10
dNTPs 1 mM	1
Primer <i>I 3</i> (10 μ M)	0,6
Primer <i>Sry</i> (10 μ M)	1
MgCl ₂ stock solution (25 mM)	4
GoTaq polymerase (5 U/ μ l)	0,25
DNA	2
Total	50

ddH₂O, Double distilled water; *dNTP*, Deoxyribonucleotide triphosphate;

DNA, Desoxyribonucleic acid

Table 13 PCR genotyping reaction program for sex determination

	Step	Temperature [$^{\circ}$ C]	Duration
	Heat lid	95	4.5 min
	Start loop		
33 cycles	Denaturation	95	35 s
	Primer annealing	50	1 min
	Product elongation	72	1 min
	Close loop		
	Incubation	72	5 min
	Store	8	∞

Table 14 Primers employed for sex determination

Gene	Primer	Primer sequence, 5' - 3'	Primer size, bp	Amplicon size, bp
<i>Il3</i>	Forward	GGGACTCCAAGCTTCAATCA	20	544
	Reverse	TGGAGGAGGAAGAAAAGCAA	20	
<i>Sry</i>	Forward	TGGACTGGTGACAATTGTC	20	402
	Reverse	GAGTACAGGTGTGCAGCTCT	20	

bp, base pairs

After the PCR reaction, aliquots of the amplified products were transferred on a 1.5% (wt/vol) agarose gel containing 0.002% (wt/vol) ethidium bromide. Subsequently, electrophoresis was performed in 1× TAE buffer for 30 minutes using Wide Mini-Sub® Cell GT electrophoresis chambers. The results were imaged under UV transillumination, allowing for the detection of DNA bands indicative of the *Sry* and *Il3* genes.

To ensure the reliability and accuracy of the PCR assay, positive controls were included in the analysis. These positive controls consisted of DNA samples extracted from both male and female mice with known sex. These controls served as a reference for confirming the expected amplification patterns and validating the experimental results.

3.2.7 Protein expression analysis

3.2.7.1 Protein Isolation

To isolate protein from lung tissue, approximately 50 µg of tissue were homogenized by using the Precellys® 24-Dual homogenizer in Precellys lysis tubes filled with 1.5 mm ceramic beads and 250 µl lysis buffer (Table 15) supplemented by 40 µl of sodium ortho vanadate and 160 µl of Complete™ protease inhibitor. After homogenization, the samples were centrifuged in a MiniSpin personal microcentrifuge at 10,000 × g for 2 min to obtain a clean supernatant. Next, the supernatant was transferred into a new 1,5ml tube and incubated on ice for 30-60 min (vortexed every 5 min). The samples were then centrifuged for 15 minutes at 4°C at 16,200 × g in a refrigerated microcentrifuge. Finally, the supernatant was collected and stored at -80°C.

Table 15 Composition of protein lysis buffer

Reagent	Concentration
Tris, pH 7.5	20 mM
NaCl	150 mM
1 mM EDTA	1 mM
1 mM EGTA	1 mM
1% (vol/vol) NP-40	0.5%

EDTA, Ethylenediaminetetraacetic acid; EGTA, Ethylene glycol-bis (2-amino-ethylether)-N, N, N', N'-tetraacetic-acid; NP-40, Nonyl phenoxypolyethoxylethanol, Tergitol-type NP-40

3.2.7.2 Determining protein concentrations

Protein concentrations were determined using the Bradford assay, a colorimetric assay based on the Bradford dye-binding method [62]. This method is based on the binding of the dye Coomassie Blue G250 to proteins in a proportional manner. When protein molecules bind to Coomassie dye under acidic conditions, a color change from brown to blue occurs, resulting in a shift in the absorption maximum from 465 nm to 595 nm. The number of developed complexes in the solution is an indicator of the protein concentration and is estimated by measuring absorbance.

To perform the Bradford assay, protein samples were diluted with ddH₂O in a 1:50 ratio. Next, 10 µL of each sample was applied to a 96-well plate along with 200 µL of Quick Start™ Bradford dye reagent. To create a standard curve, defined concentrations of bovine serum albumin ranging from 0.05-0.5 µL were also added to the 96-well plate. The blank control consisted of ddH₂O. After incubating for 5 minutes, the absorbance was measured using a VersaMax ELISA Microplate reader and SoftMax® Pro Software. The assay was performed according to the instruction manual⁴ provided by Bio-Rad Laboratories, the manufacturer of the Quick Start™ Bradford dye reagent.

3.2.7.3 SDS polyacrylamide gel electrophoresis

Before blotting, protein samples must be separated according to their sizes using SDS polyacrylamide gel electrophoresis.

⁴ <https://www.bio-rad.com/webroot/web/pdf/lsr/literature/4110065A.pdf>

Preparation of the gels: To prepare the gels, resolving gel (Table 16) was poured into two glass plates separated by a spacer with isopropanol on top. After 30 minutes of polymerization, the isopropanol was removed, and stacking gels (Table 16) were poured on top of the polymerized resolving gel using a comb to form wells in the gel.

Table 16 Composition of 10% stacking / resolving gel used for immunoblot analysis

Stacking gel	Volume	Resolving gel	Volume
dH ₂ O	2,975 ml	dH ₂ O	3.8 ml
0.5 M Tris-HCl pH 6.8	1.25 ml	1.5 M Tris-HCl pH 8.8	2.6 ml
10% SDS stock solution	50 µl	10% SDS stock solution	100 µl
(30%/0.8%) Acrylamide/Bisacrylamide	0.67 ml	(30%/0.8%) Acrylamide/Bisacrylamide	3.4 ml
10% APS	50 µl	10% APS	100 µl
TEMED	5 µl	TEMED	10 µl

dH₂O, distilled water; *M*, molar mass; *SDS*, Sodium dodecyl sulfate; *APS*, Ammonium persulfate; *TEMED*, Tetramethylethylenediamine

Gel electrophoreses: Proteins were mixed with 4× sample buffer supplemented with 10% (v/v) 2-mercaptoethanol in a 1:1 ratio. The samples were then denatured for 10 minutes at 95°C. The denatured protein samples were pipetted into the corresponding wells of the polyacrylamide gel. To verify that the observed bands corresponded to the expected molecular weights of the target antigens, ten micrograms of Precision Plus Protein Dual Color Standards were pipetted into the first well, serving as a protein marker. These markers consist of a mixture of purified proteins with known molecular weights. The amount of protein samples pipetted into the wells was calculated to achieve a total amount of 30 µg protein per well. The gel electrophoresis was then performed at 110 volts for 90 minutes in 1× running buffer.

Table 17 Composition of 10× SDS running buffer for immunoblot analysis

Reagent	Amount
Tris	30 g
Glycine	144 g
SDS Powder	10 g
ddH ₂ O	Up to 1000 ml
Total	1000 ml

SDS, Sodium dodecyl sulfate; *ddH₂O*, Double distilled water

3.2.7.4 Immunoblot analysis

Immunoblot analysis is used to detect and visualize protein levels through a combination of gel electrophoresis and antigen-antibody interaction. The process involves four stages: 1) separation by SDS polyacrylamide gel electrophoresis, 2) transfer onto a second matrix, 3) blocking, and 4) visualization via antigen-antibody interaction. To ensure the specificity of the Western blots, the primary antibody listed in Table 20 employed in this study was carefully chosen based on its established specificity for the target antigen. The antibody's specificity has been previously validated and confirmed by the manufacturer.

3.2.7.4.1 Immunoblotting

After the proteins were separated by SDS polyacrylamide gel electrophoresis, they were transferred from the SDS-polyacrylamide gel onto a 0.2 μm nitrocellulose membrane using the Trans-Blot® Turbo™ western blot transfer system. The transfer was conducted at 110 volts for 60 minutes. The nitrocellulose membrane was incubated for 5 min with Ponceau S to observe the correct loading and transfer. The transferred membranes were then blocked in 5% milk-blocking buffer (Table 18) for 60 minutes at room temperature. This blocking step prevents nonspecific binding of antibodies. Following the blocking step, the membrane was incubated overnight at 4°C with the primary antibody (Table 20) diluted in the blocking buffer.

Table 18 Composition of 5% milk-blocking buffer for immunoblot analysis

Reagent	Amount
Non-fat dry milk	5 g
1× PBS washing buffer	100 ml

PBS, phosphate buffered saline

3.2.7.4.2 Protein visualization

After the overnight incubation of the membrane with the primary antibody, the membranes were washed the next day for 60 minutes using a 1× PBS washing buffer. During the washing process, the PBS washing buffer was changed every 10 minutes to ensure comprehensive and effective removal of any unbound or nonspecifically bound antibodies.

Table 19 Composition of 1× PBS washing buffer for immunoblot analysis

Reagent	Volume [ml]
10× PBS	99
Tween 20	1
ddH ₂ O	900

PBS, phosphate buffered saline; ddH₂O, Double distilled water

After the washing process, the membrane was incubated with the secondary antibody (Table 20) for 1 h at 4 °C. Following this incubation, the membranes underwent a series of three washes with 1× PBS washing buffer, each lasting 10 minutes. During the washing process, the buffer was changed every 10 minutes to ensure effective removal of any unbound secondary antibody. The secondary antibody was selected based on the species in which the primary antibody was raised.

To visualize the protein bands, the membranes were treated with SuperSignal® West Femto chemiluminescent substrate. Visualization was accomplished using a LAS-4000 luminescent image analyzer, which is a digital imaging system for sensitive and quantitative imaging of blots by chemiluminescence. After visualizing the protein bands, the membranes were rewashed with another series of three washes with 1× PBS washing buffer, each lasting 10 minutes. During the washing process, the buffer was changed every 10 minutes.

To serve as a loading control and confirm equal protein loading (30 µg protein) across the polyacrylamide gel wells, the membranes were subsequently incubated overnight at 4 °C with the primary antibody against anti-β-Actin (Table 20). The following day, the steps from the previous day were repeated. The visualized protein bands served as a control to validate equal loading of protein samples within the polyacrylamide gel wells.

Table 20 Primary and secondary antibodies used for western blot analysis.

Antibody	Company	Catalog number	Dilution	Host
Primary Antibody				
Anti-superoxide dismutase 3 antibody	Abcam	ab80946	1/1000	Mouse
Anti-glutathione synthetase antibody	Abcam	ab133592	1/1000	Rabbit
Anti-β-Actin	Cell Signaling Technology	4967	1/1000	Rabbit

Secondary Antibody				
Goat anti-mouse IgG (H+L) Secondary antibody, HRP	Thermo Scientific	31430	1/5000	Goat
Goat anti-rabbit IgG (H+L) Secondary antibody, HRP	Thermo Scientific	31460	1/2000	Goat

3.2.7.4.3 Membrane stripping

To strip and reprobe a western blot, the primary and secondary antibodies were removed from the membrane. For this purpose, the membrane was washed in washing buffer (Table 19) for a duration of 1×5 minutes. The membrane was then stripped in 50 ml stripping buffer (Table 21) and 347 µl of β-mercaptoethanol at 52 °C for 5 minutes effectively stripping off the previously bound antibodies.

After the stripping procedure, the membrane was rewashed in washing buffer (2×5 minutes) for removal of any residual stripping reagents and then blocked in blocking buffer for 1 h. Following that, protein visualization could be repeated as described above in section 3.2.7.4.2.

Table 21 Composition of stripping buffer for immunoblot analysis

Reagent	Volume [ml]
1.0 M Tris, pH 6.8	31
10% SDS	10
1× PBS washing buffer	459

SDS, Sodium dodecyl sulfate; PBS, phosphate buffered saline

3.2.8 Statistical analysis

Data are indicated in scatter plots as mean ± SD. The unpaired Student t test was used for statistical comparisons of two different groups. All statistical analyses were performed with GraphPad Prism 6.0. Values of $P < 0.05$ were considered as significant. The dataset underwent screening for statistical outliers using the Grubbs test, and any identified outliers were subsequently removed from the analysis to ensure data integrity.

4. Results

4.1 Hyperoxia was tolerated by five out of six mouse strains

In this study, we selected six different mouse strains to mimic the bronchopulmonary dysplasia (BPD) phenotype by exposing them to hyperoxia. The mouse strains were C57BL/6J, BALB/cJ, FVB/NJ, C3H/HeJ, DBA/2J, and 129S2/SvPasOrlRj, chosen to provide a wide genetic strain diversity. Figure 2 presents a mouse family tree that illustrates the origins and relationships of inbred mouse strains, based on 1,638 informative single-nucleotide polymorphisms compared in 102 inbred mouse strains generated by Petkov et al. [63].

We observed variations in survival rates among the six mouse strains. Out of the investigated strains, five strains demonstrated survival under both normoxia (21% O₂) and hyperoxia (85% O₂) exposure during the initial 14 days of postnatal life. These strains were C57BL/6J, BALB/cJ, FVB/NJ, C3H/HeJ, and DBA/2J, with respective survival rates of 100% (C57BL/6J and BALB/cJ), 89% (FVB/NJ), 78% (C3H/HeJ), and 67% (DBA/2J) (Figure 3). However, the 129S2/ SvPasOrlRj strain demonstrated low resistance to hyperoxia, with a mortality rate of 100% within the fourth day within multiple experimental runs. Non-surviving mice were either found dead in the cages or cannibalized by the nursing dam. Therefore, we did not consider the 129S2/SvPasOrlRj strain for further experiments.

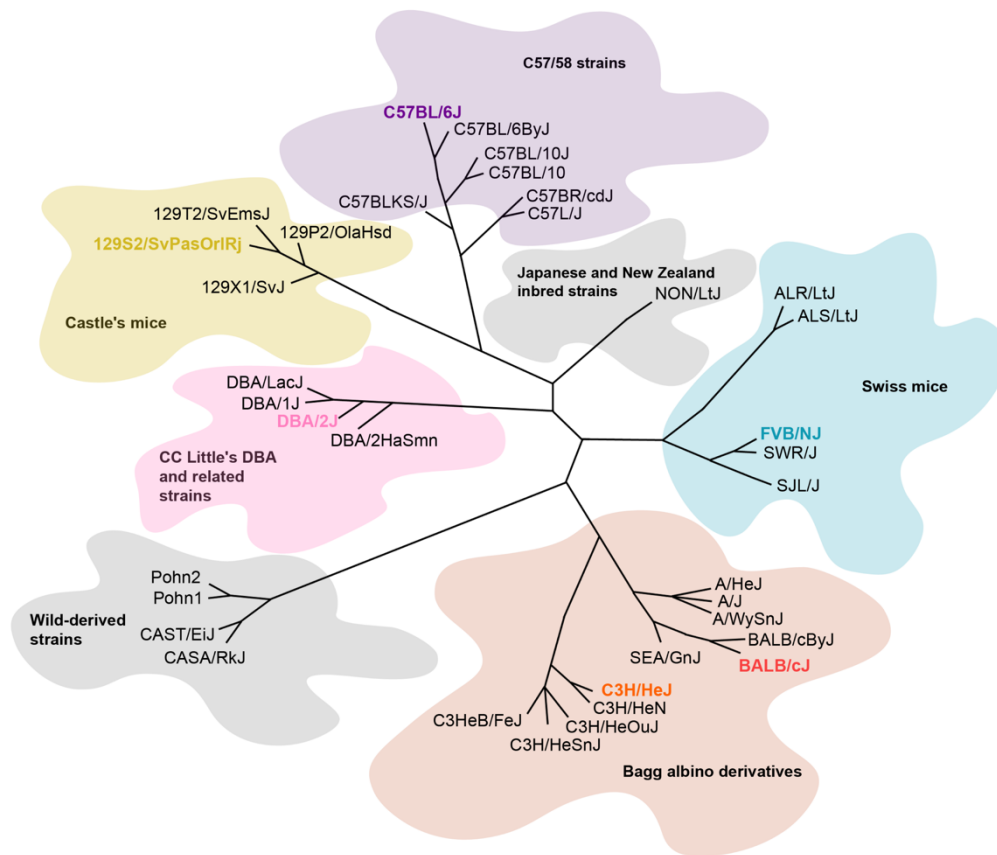


Figure 2 Phylogenetic Tree.

Classification of 102 mouse strains into seven groups based on their genetic backgrounds: Group 1, Bagg albino derivatives; Group 2, Swiss mice; Group 3, Japanese and New Zealand inbred strains; Group 4, C57/58 strains; Group 5, Castle's mice; Group 6, C.C. Little's DBA and related strains; Group 7, wild-derived strains. The highlighted strains in the tree, namely C57BL/6J, BALB/cJ, FVB/NJ, C3H/HeJ, DBA/2J, and 129S2/SvPasOrlRj, are highlighted in the tree using colored fonts. These strains were specifically chosen to represent a diverse range of genotypes and are commonly used in preclinical studies on bronchopulmonary dysplasia (BPD).

Adapted from "Mouse genetic background impacts susceptibility to hyperoxia-driven perturbations to lung maturation" by J. Tiono, R.E. Morty, W. Seeger, 2018, *Pediatric Pulmonology*, 54, p. 7. Copyright 2020 by John Wiley and Sons. Reprinted with permission.

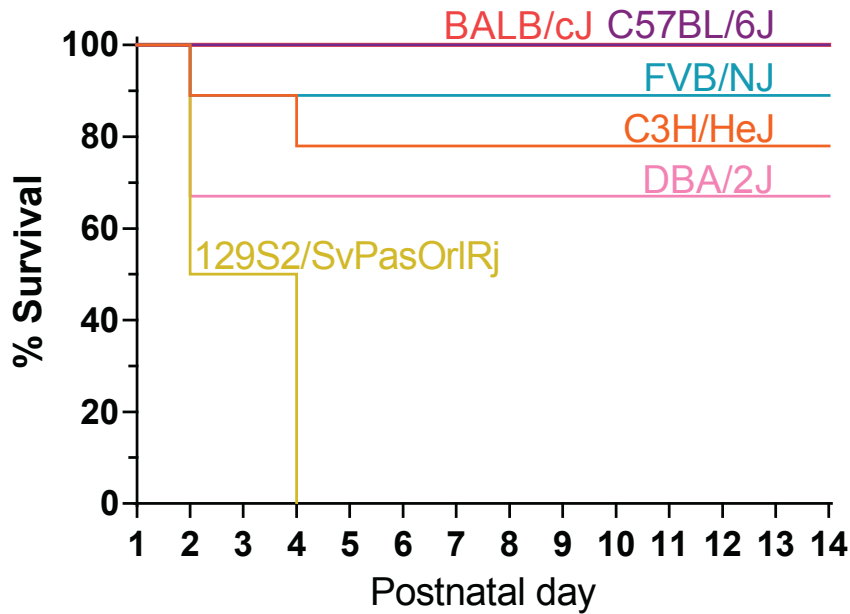


Figure 3 Survival rate of six mouse strains.

Six strains of newborn mice were exposed to hyperoxia 85% O₂ for 14 days of postnatal life. The survival percentage of each group is depicted in the graph, with eight mice in each group. The strains are represented in the graph using colored fonts, corresponding to the font color employed in the phylogenetic tree (Figure 2).

Adapted from [64]. Copyright 2020 by John Wiley and Sons. Reprinted with permission.

4.2 The genetic background impacts the outcome of lung development under the effect of hyperoxia

To investigate the impact of genetic background on lung development under hyperoxic conditions, we exposed five different inbred mouse strains (C57BL/6J, BALB/cJ, FVB/NJ, C3H/HeJ, and DBA/2J) to normoxia (21% O₂) or hyperoxia (85% O₂) for 14 days after birth. This experimental setup aimed to mimic the physiological and histological features of BPD [38]. As BPD is characterized by an arrest in alveolarization, increased lung volume, MLI, and septal thickness, and decreased alveolar number and density [33], [34], design-based stereology was used to quantify these parameters.

Upon visual examination of Richardson-stained lung tissue sections embedded in plastic, we observed that the mean alveolar diameter in the normoxia-exposed C3H/HeJ mouse lungs exceeded that of the other strains. Overall, exposure to hyperoxia resulted in visible enlargement of alveolar size across all strains to varying degrees. The disparity in alveolar size between mice treated with normoxia and those exposed to

hyperoxia was more pronounced in the C57BL/6J, BALB/cJ, and FVB/NJ strains, while it was less prominent in the C3H/HeJ and DBA/2J strains. (Figure 4).

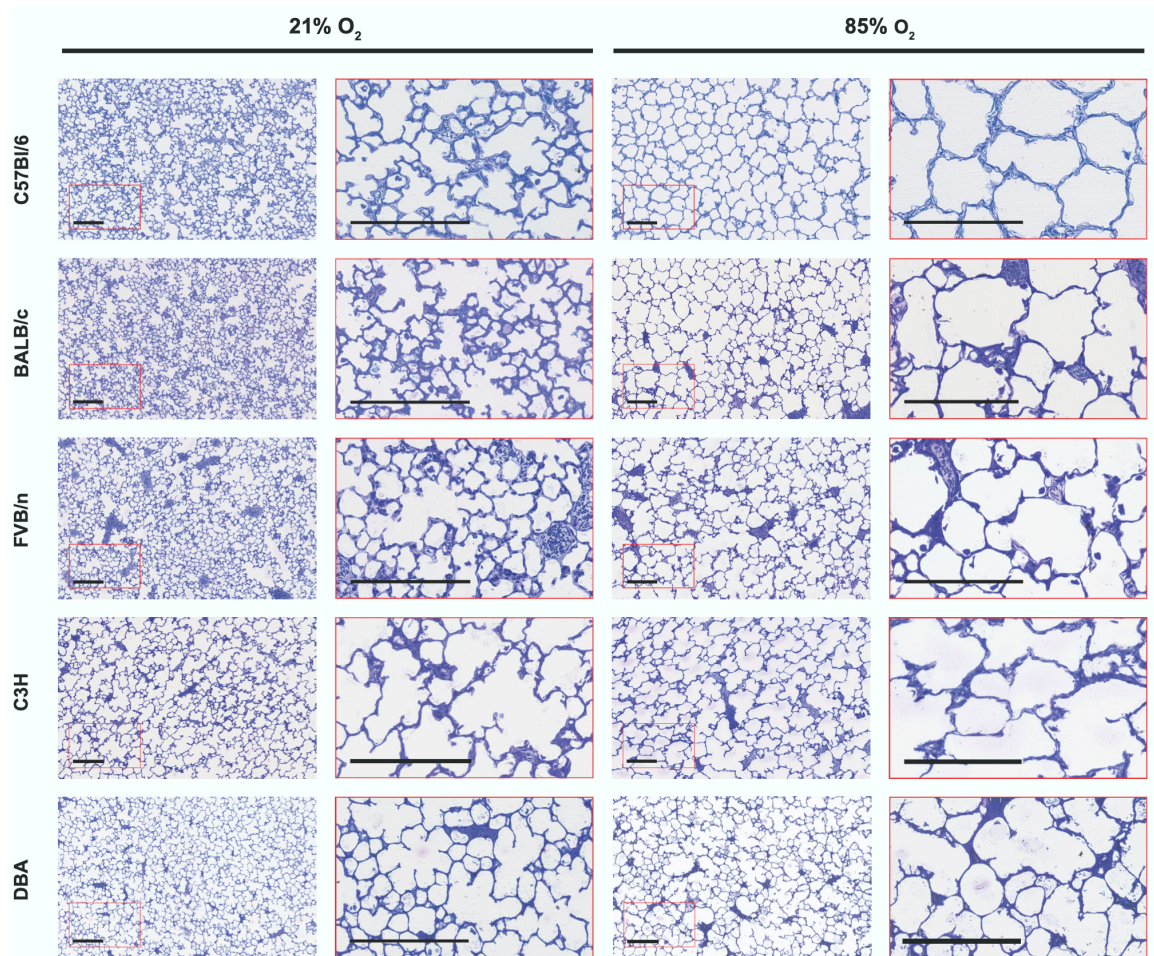


Figure 4 Representative plastic-embedded lung tissue sections from five mouse strains exposed to 21% O₂ or 85% O₂.

Richardson-stained plastic-embedded lung tissue sections from five different mouse strains (C57BL/6J, BALB/cJ, FVB/NJ, C3H/HeJ, and DBA/2J) exposed to either normoxic (21% O₂) or hyperoxic (85% O₂) conditions for 14 days postnatal life. Upon visual inspection, an observable enlargement of alveolar size was noted in all strains following exposure to hyperoxia. The magnified section on the right side is indicated by the red box. Scale bar = 200 μ m.

Adapted from [64]. Copyright 2020 by John Wiley and Sons. Adapted with permission.

Table 22 Structural parameters of lungs from mice exposed to 21% O₂ normoxia for 14 days postnatal life. Assessed by design-based stereology.

Parameter	C57BL/6J		BALB/cJ		FVB/NJ		C3H/HeJ		DBA/2J								
	mean ± (SD)		mean ± (SD)		mean ± (SD)		mean ± (SD)		mean ± (SD)								
V (lung) [cm ³]	0.3631 (0.05834)		0.2641 (0.07081)		0.2432 (0.03140)		0.3142 (0.07904)		0.2414 (0.07284)								
CE	CV	CE ² /CV ²	0.072	0.160	0.200	0.120	0.268	0.200	0.058	0.129	0.200	0.113	0.251	0.200	0.135	0.3017	0.200
V_V (par/lung) [%]			0.9328 (0.0051)		0.9377 (0.0220)		0.9441 (0.0306)		0.8986 (0.0124)						0.9326 (0.0415)		
CE	CV	CE ² /CV ²	0.003	0.005	0.250	0.010	0.023	0.200	0.014	0.032	0.200	0.006	0.014	0.200	0.020	0.045	0.250
N (alv, lung) 10 ⁶			5.01 (0.719)		4.31 (1.00)				3.65 (0.444)					3.51 (0.907)			
CE	CV	CE ² /CV ²	0.064	0.143	0.201	0.104	0.232	0.202	0.055	0.121	0.201	0.116	0.258	0.200	0.101	0.226	0.199
N_V (alv/par, lung) 10 ⁷ [cm ⁻³]			1.508 (0.2383)		1.764 (0.2053)				1.594 (0.1091)					1.249 (0.1785)			
CE	CV	CE ² /CV ²	0.071	0.158	0.200	0.052	0.116	0.200	0.031	0.068	0.200	0.064	0.143	0.200	0.133	0.296	0.200
S_V (lung) [cm ⁻¹]			804 (46.73)		888.8 (51.47)				8691 (70.47)					634.2 (42.38)			
CE	CV	CE ² /CV ²	0.026	0.058	0.200	0.026	0.058	0.200	0.036	0.081	0.200	0.030	0.067	0.200	0.039	0.086	0.200
S (alv epi, lung) [cm ²]			269.0 (34.94)		219.2 (55.07)				199.2 (27.98)					178.2 (42.15)			
CE	CV	CE ² /CV ²	0.058	0.130	0.200	0.112	0.251	0.200	0.063	0.140	0.200	0.106	0.237	0.200	0.110	0.245	0.200
τ (sep, lung) [μ m]			8.090 (1.487)		7.208 (1.117)				6.909 (1.191)					10.16 (0.7125)			
CE	CV	CE ² /CV ²	0.082	0.184	0.200	0.069	0.155	0.200	0.077	0.172	0.200	0.031	0.070	0.200	0.086	0.193	0.200
MLI (lung) [μ m]			33.71 (2.165)		30.7 (2.51)				32.44 (5.317)					42.99 (4.328)			
CE	CV	CE ² /CV ²	0.029	0.064	0.200	0.037	0.082	0.200	0.073	0.164	0.200	0.045	0.101	0.200	0.027	0.060	0.250

Abreviation: alv, alveoli; alv epi, alveolar epithelium; CE, coefficient of error; CV, coefficient of variation; MLI, mean linear intercept; N, alveoli number; N_V , numerical density; par, parenchyma; S, surface area; S_V , surface density; τ (sep), arithmetic mean septal wall thickness; V, volume; V_V , volume density. Values are presented as mean ± SD, n=5 lungs per group for all strains except for the DBA group (n=4).

Table 23 Structural parameters of lungs from mice exposed to 85% O₂ hyperoxia for 14 days postnatal life. Assessed by design-based stereology.

Parameter	C57BL/6J		BALB/cJ		FVB/NJ		C3H/HeJ		DBA/2J	
	mean ± (SD)	mean ± (SD)	mean ± (SD)	mean ± (SD)	mean ± (SD)	mean ± (SD)				
<i>V</i> (lung) [cm ³]	0.2631 (0.04713)	0.3392 (0.02554)	0.2388 (0.03994)	0.3044 (0.06942)	0.2240 (0.04921)					
<i>CE</i> <i>CV</i> <i>CE</i> ² / <i>CV</i> ²	0.080 0.179 0.200	0.034 0.075 0.200	0.075 0.167 0.200	0.102 0.228 0.200	0.110 0.220 0.200					
<i>V_v</i> (par/lung) [%]	0.9382 (0.0130)	0.9085 (0.0317)	0.9253 (0.0416)	0.8891 (0.0200)	0.9177 (0.0296)					
<i>CE</i> <i>CV</i> <i>CE</i> ² / <i>CV</i> ²	0.006 0.014 0.200	0.016 0.035 0.200	0.020 0.045 0.200	0.010 0.022 0.200	0.016 0.032 0.250					
<i>N</i> (alv, lung) 10 ⁶	1.28 (0.205)	2.85 (0.251)	1.77 (0.101)	2.17 (0.512)	2.09 (0.541)					
<i>CE</i> <i>CV</i> <i>CE</i> ² / <i>CV</i> ²	0.072 0.160 0.200	0.039 0.088 0.199	0.026 0.057 0.202	0.106 0.236 0.200	0.130 0.259 0.251					
<i>N_v</i> (alv/par, lung) 10 ⁷ [cm ⁻³]	0.5304 (0.1047)	0.9279 (0.06918)	0.8157 (0.116)	0.8003 (0.09154)	0.6665 (0.09813)					
<i>CE</i> <i>CV</i> <i>CE</i> ² / <i>CV</i> ²	0.088 0.197 0.200	0.033 0.075 0.200	0.064 0.142 0.200	0.051 0.114 0.200	0.074 0.147 0.250					
<i>S_v</i> (lung) [cm ⁻¹]	462.7 (23.74)	549 (34.08)	505.4 (42.94)	477.7 (38.95)	473.1 (85.6)					
<i>CE</i> <i>CV</i> <i>CE</i> ² / <i>CV</i> ²	0.023 0.051 0.200	0.028 0.062 0.200	0.038 0.085 0.200	0.036 0.082 0.200	0.090 0.181 0.250					
<i>S</i> (alv epi, lung) [cm ⁻¹]	114.3 (21.86)	169.3 (19.52)	110.9 (14.29)	130.5 (36.21)	147.0 (32.01)					
<i>CE</i> <i>CV</i> <i>CE</i> ² / <i>CV</i> ²	0.035 0.079 0.200	0.062 0.138 0.200	0.096 0.214 0.200	0.052 0.117 0.200	0.140 0.279 0.200					
<i>τ</i> (sep, lung) [μm]	10.54 (0.8286)	9.677 (1.332)	11.43 (2.448)	13.82 (1.622)	11.69 (3.262)					
<i>CE</i> <i>CV</i> <i>CE</i> ² / <i>CV</i> ²	0.035 0.079 0.200	0.062 0.138 0.200	0.096 0.214 0.200	0.052 0.117 0.200	0.140 0.279 0.250					
MLI (lung) [μm]	65.55 (4.628)	53.73 (4.777)	56.72 (6.646)	56.59 (10.68)	63.62 (12.44)					
<i>CE</i> <i>CV</i> <i>CE</i> ² / <i>CV</i> ²	0.032 0.071 0.200	0.040 0.089 0.200	0.052 0.117 0.200	0.084 0.189 0.200	0.098 0.196 0.250					

Abbreviation: *alv*, alveoli; *alv epi*, alveolar epithelium; *CE*, coefficient of error; *CV*, coefficient of variation; *MLI*, mean linear intercept; *N*, alveoli number; *N_v*, numerical density; *par*, parenchyma; *S*, surface area; *S_v*, surface density; *τ* (sep), arithmetic mean septal wall thickness; *V*, volume; *V_v*, volume density. Values are presented as mean ± SD; n=5 lungs per group for all strains except for the DBA group (n=4).

Exposure of the five mouse strains to hyperoxia from birth until P14 led to changes in postnatal lung architecture maturation in all strains to a different degree. The changes were quantified using design-based stereology. Hyperoxia caused a reduction in the number of alveoli in all mouse strains, except for the DBA strain, which exhibited no significant change compared to the normoxia group. A striking reduction in alveoli number occurred in C57BL/6J mouse pups (74.5%), while the other strains were affected to a lesser degree (27.7%–51.5%) (Figure 5).

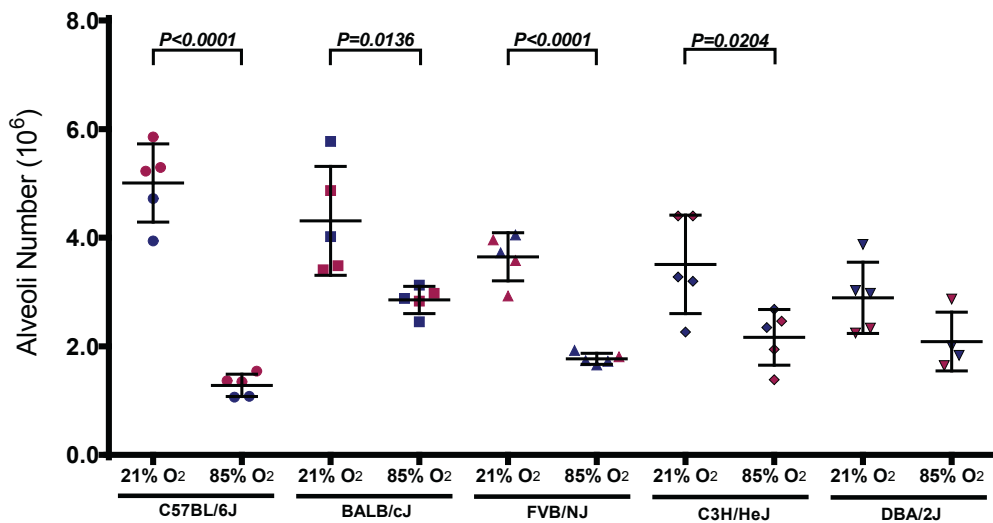


Figure 5 Quantitative analysis of alveoli number by design-based stereology.

Quantitative analysis of alveoli number using design-based stereology was performed in five different inbred mouse strains exposed to normoxic conditions (21% O₂) or hyperoxic conditions (85% O₂) during the first 14 days of postnatal life. Values represent mean \pm SD values ($n = 5$ per group, except for DBA with $n = 4$), with individual animals represented by colored dots (red for females, blue for males). Statistical comparisons between the normoxia and hyperoxia groups within each strain were conducted using the unpaired Student *t*-test, with *p*-values < 0.05 indicated. Additional lung structure data and percentage analysis can be found in Table 22, Table 23 and Table 24.

Adapted from [64]. Copyright 2020 by John Wiley and Sons. Adapted with permission.

Upon exposure to hyperoxia, alveolar density significantly decreased in all strains. Among the strains, C57BL/6J mouse pups exhibited the greatest reduction, with a decrease of 64.8% in alveolar density. BALB/cJ and FVB/NJ strains were less affected, with a decrease of 46.6% to 47.4% in alveolar density. The strains that were least affected were C3H/HeJ and DBA/2J, which showed a reduction of 35.9% and 45.9% in alveolar density (Figure 6).

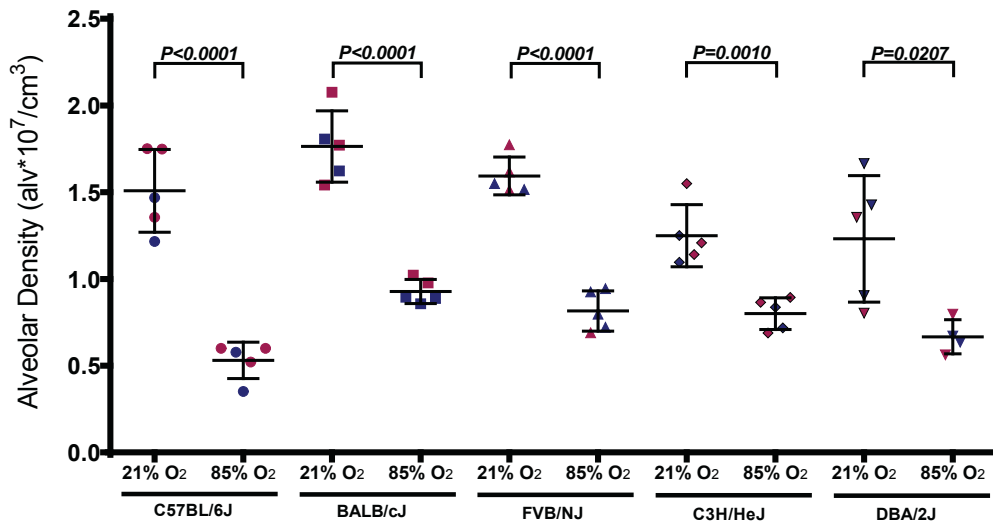


Figure 6 Quantitative analysis of alveolar density by design-based stereology.

Quantitative analysis of alveolar density using design-based stereology was performed in five different inbred mouse strains exposed to normoxic conditions (21% O₂) or hyperoxic conditions (85% O₂) during the first 14 days of postnatal life. Values represent mean \pm SD values ($n = 5$ per group, except for DBA with $n = 4$), with individual animals represented by colored dots (red for females, blue for males). Statistical comparisons between the normoxia and hyperoxia groups within each strain were conducted using the unpaired Student *t*-test, with *p*-values < 0.05 indicated. Additional lung structure data and percentage analysis can be found in Table 22, Table 23 and Table 24. Adapted from [64]. Copyright 2020 by John Wiley and Sons. Adapted with permission.

All strains, except for the C57BL/6J strain, were not affected by hyperoxia in terms of lung volume. The C57BL/6J strain exhibited a decrease of 27.5%. (Figure 7).

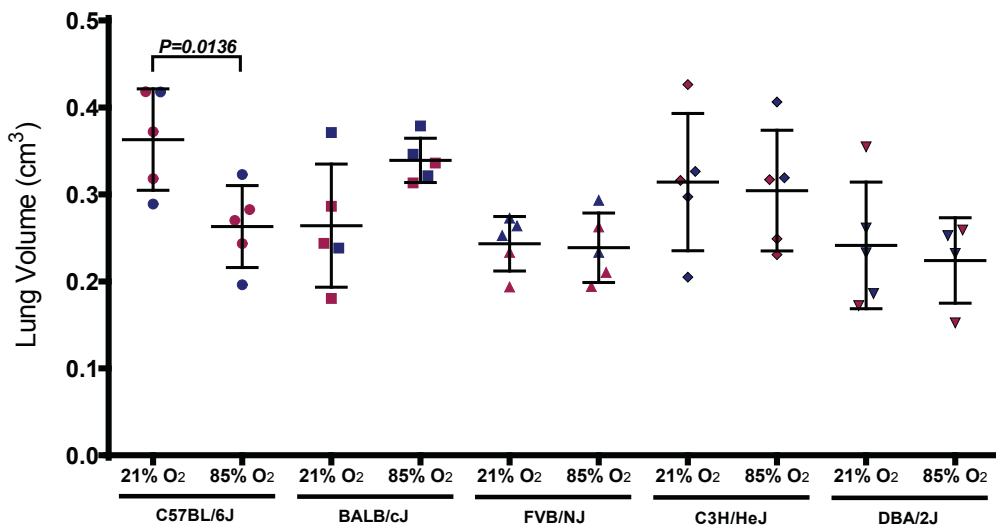


Figure 7 Quantitative analysis of lung volume by design-based stereology.

Quantitative analysis of lung volume using design-based stereology was performed in five different inbred mouse strains exposed to normoxic conditions (21% O₂) or hyperoxic conditions (85% O₂) during the first 14 days of postnatal life. Values represent mean \pm SD values ($n = 5$ per group, except for DBA with $n = 4$), with individual animals represented by colored dots (red for females, blue for males). Statistical comparisons between the normoxia and hyperoxia groups within each strain were conducted using the unpaired Student *t*-test, with *p*-values < 0.05 indicated. Additional lung structure data and percentage analysis can be found in Table 22, Table 23 and Table 24. Adapted from [64]. Copyright 2020 by John Wiley and Sons. Adapted with permission.

In response to hyperoxia, four out of five strains demonstrated an increase in septal thickness. The FVB/Nj strain had the greatest increase at 65.4%, followed by the C3H/HeJ strain with a 36% increase. The C57BL/6J and BALB/cJ strains demonstrated relatively smaller increases in septal thickness, ranging from 30.3% to 34.3%. In contrast, the DBA/2J strain did not show any significant change in septal thickness (Figure 8).

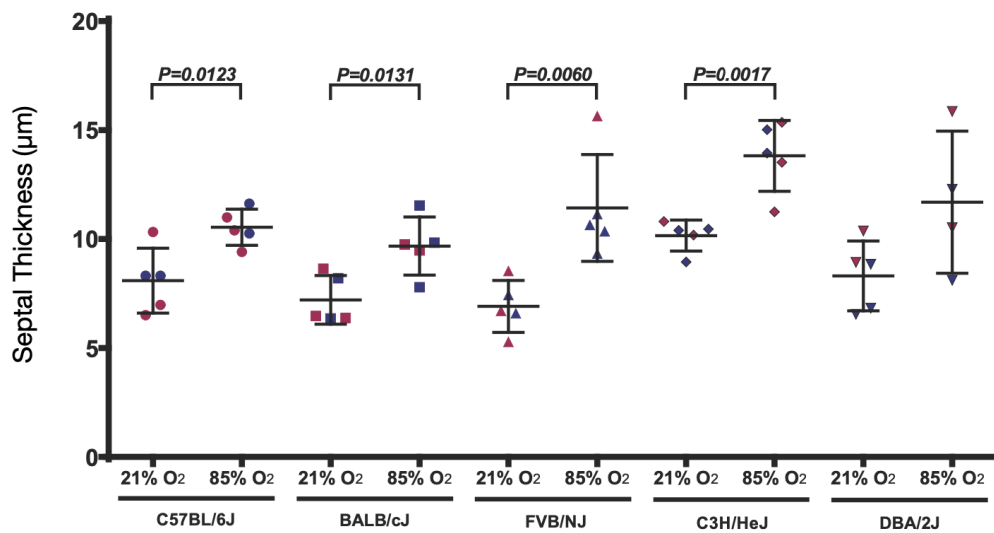


Figure 8 Quantitative analysis of septal thickness by design-based stereology.

Quantitative analysis of septal thickness using design-based stereology was performed in five different inbred mouse strains exposed to normoxic conditions (21% O₂) or hyperoxic conditions (85% O₂) during the first 14 days of postnatal life. Values represent mean \pm SD values ($n = 5$ per group, except for DBA with $n = 4$), with individual animals represented by colored dots (red for females, blue for males). Statistical comparisons between the normoxia and hyperoxia groups within each strain were conducted using the unpaired Student *t*-test, with *p*-values < 0.05 indicated. Additional lung structure data and percentage analysis can be found in Table 22, Table 23 and Table 24. Adapted from [64]. Copyright 2020 by John Wiley and Sons. Adapted with permission.

All five mouse strains demonstrated an increase in MLI following exposure to hyperoxia. The C57BL/6J strain exhibited the greatest increase at 94.5%, followed by the DBA/2J (79.92%), BALB/cJ (75.02%), and FVB/NJ strains (74.85%). The C3H/HeJ strain was the least affected by hyperoxia, with an increase of 31.65% (Figure 9).

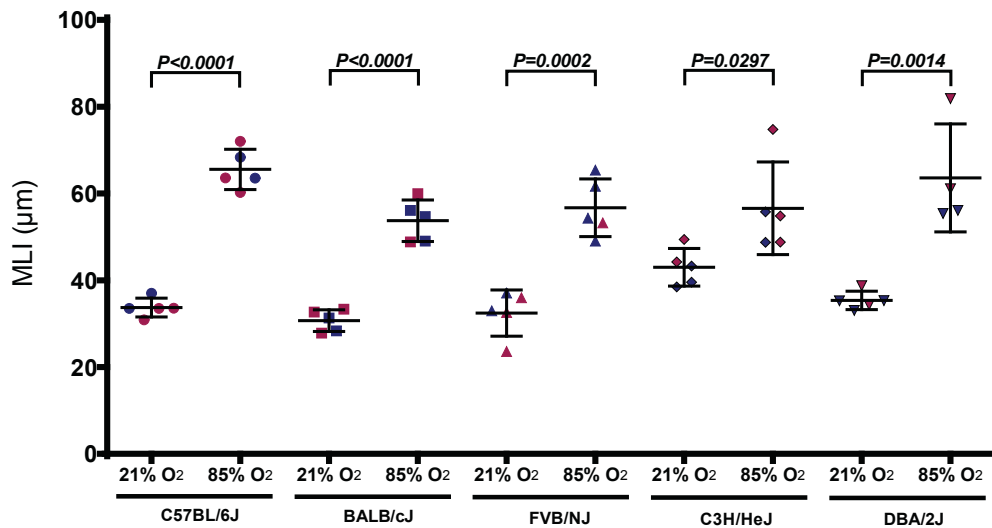


Figure 9 Quantitative analysis of mean linear intercept (MLI) by design-based stereology.

Quantitative analysis of mean linear intercept (MLI) using design-based stereology was performed in five different inbred mouse strains exposed to normoxic conditions (21% O₂) or hyperoxic conditions (85% O₂) during the first 14 days of postnatal life. Values represent mean \pm SD values ($n = 5$ per group, except for DBA with $n = 4$), with individual animals represented by colored dots (red for females, blue for males). Statistical comparisons between the normoxia and hyperoxia groups within each strain were conducted using the unpaired Student *t*-test, with *p*-values < 0.05 indicated. Additional lung structure data and percentage analysis can be found in Table 22, Table 23 and Table 24. Adapted from [64]. Copyright 2020 by John Wiley and Sons. Adapted with permission.

Exposure to hyperoxia during the first 14 days of postnatal life affected lung development in all five mouse strains, leading to a distinct lung architecture compared to the normoxia-treated group. The impact of hyperoxia varied among the different strains, with the C57BL/6J strain showing the most pronounced changes in alveoli number, density, and mean linear intercept (MLI). The FVB/NJ strain exhibited the most notable changes in septal thickness after of hyperoxia exposure (Table 23).

Table 24 Percentage analysis of parameters by design-based stereology

	C57BL/6J	BALB/cJ	FVB/NJ	C3H/HeJ	DBA/2J
Alveoli Number $\times 10^6$	74.5%	73.9%	51.5%	38.2%	27.7%
Alveolar Density $\times 10^7/ \text{cm}^3$	64.8%	46.4%	47.4%	35.9%	45.9%
Lung Volume cm^3	27.5%	unaffected	unaffected	unaffected	unaffected
Septal Thickness (μm)	30.3%	34.3%	65.4%,	36 %	unaffected
MLI (μm)	94.5%	75.0%	74.9%	31.7%.	79.9%

Percentage of change in evaluated parameters according to the investigated strain after exposure to hyperoxia. Values of alveoli number, alveolar density, and lung volume are considered decreasing, while values of septal thickness and MLI are considered increasing. The most significant degree of change in the number is visually emphasized with a darker background.

4.3 The genetic background impacts the gene expression of the lung antioxidant response under the effect of hyperoxia

BPD is a multifactorial lung complication, with premature exposure to hyperoxia as the primary risk factor. Hyperoxia leads to the generation of reactive oxygen species (ROS) and an imbalance between ROS and antioxidants, resulting in oxidative stress [17], [56]. Antioxidant enzyme gene expression is stimulated by oxidative stress [65], as antioxidants act as defense mechanisms against oxidation [56]. Therefore, this study investigated the expression of a spectrum of genes encoding antioxidant enzymes and selected protein expression using RT-PCR and immunoblot techniques. A list of the profiled genes is provided in Table 7.

The genes *Sod1*, *Sod2*, and *Sod3* encode the enzyme superoxide dismutase 1/2/3. After exposure to hyperoxia, the C57BL/6J strain exhibited a significant increase in mRNA levels of *Sod1*, *Sod2*, and *Sod3*. In the other strains, the mRNA levels of *Sod1* genes remained unchanged, while the mRNA levels of *Sod2* and *Sod3* genes either increased or remained unchanged (Figure 10).

The SOD3 protein expression level was assessed by immunoblot, which validated the measured *Sod3* gene mRNA levels under hyperoxia exposure. An exception to this was observed in hyperoxia-exposed BALB/cJ mouse pups, where an increase in SOD3 protein expression was observed without a corresponding change in the measured *Sod3* gene mRNA levels (Figure 11).

The observed molecular masses of the bands closely matched the manufacturer's predicted band sizes. SOD3 exhibited a band size of 25 kDa, slightly lower than the manufacturer's prediction of 26 kDa⁵, while β -Actin displaying a band size of 45 kDa, aligning with the expected molecular weight⁶. This indicates that the observed protein bands are in line with the expected molecular weights, despite a slight variation in the case of SOD3.

⁵ <https://www.abcam.com/products/primary-antibodies/superoxide-dismutase-3ec-sod-antibody-4g11g6-ab80946.html>

⁶ <https://www.cellsignal.com/products/primary-antibodies/b-actin-antibody/4967>

In all blots conducted with SOD3, a consistent additional band at 52 kDa was observed. This additional band coincided with the manufacturer's reported presence of extra bands at 54 kDa. The manufacturer has stated uncertainty regarding the identity of this extra band. However, its presence was consistently observed in our experimental results. These additional bands were not presented in Figure 11 due to cropping, which aimed to highlight the main findings.

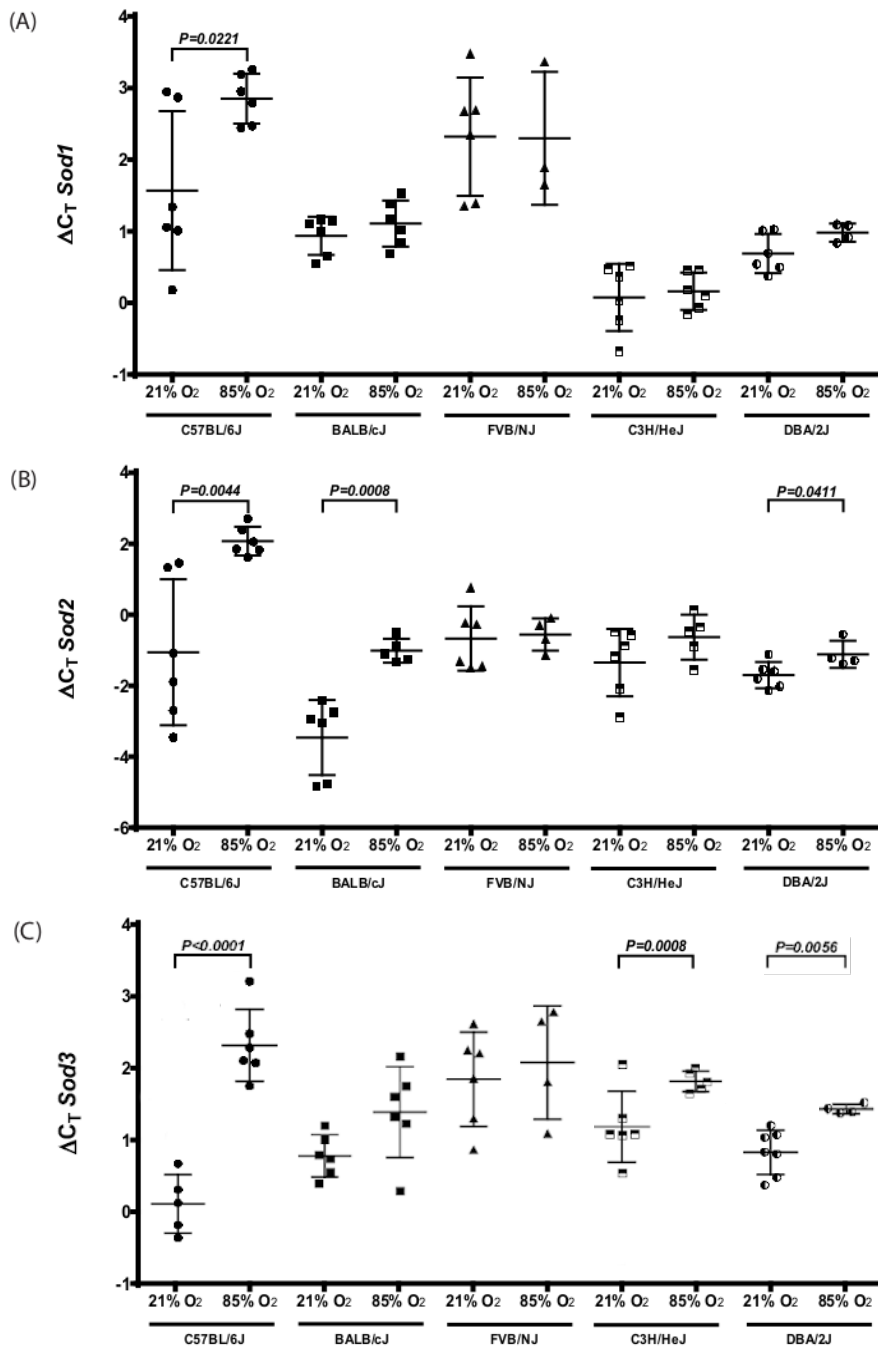


Figure 10 Expression of superoxide dismutase 1, 2 and 3 in five different inbred mouse strains exposed to hyperoxia.

mRNA levels of (A) Sod1, (B) Sod2 and (C) Sod3 in lungs of mouse pups from inbred mouse strains on the 14th day of postnatal life. Parameters were assessed by real-time RT-PCR from five different inbred mouse strains exposed to normoxic (21% O₂) or hyperoxic (85% O₂) conditions for the first 14 days of postnatal life. Utilized primers are listed in Table 7.

Values represent mean $\Delta C_t \pm SD$ ($n = 3-7$, outliers were removed using the Grubbs test), per group. Each dot represents an individual animal. Comparisons between the data from 21% O₂ and 85% O₂ exposed animals of the same strain were made by the unpaired Student *t* test. *P* values below 0.05 are indicated. mRNA, messenger RNA; real-time RT-PCR, real-time polymerase chain reaction; Sod, superoxide dismutase

Adapted from [64]. Copyright 2020 by John Wiley and Sons. Adapted with permission.

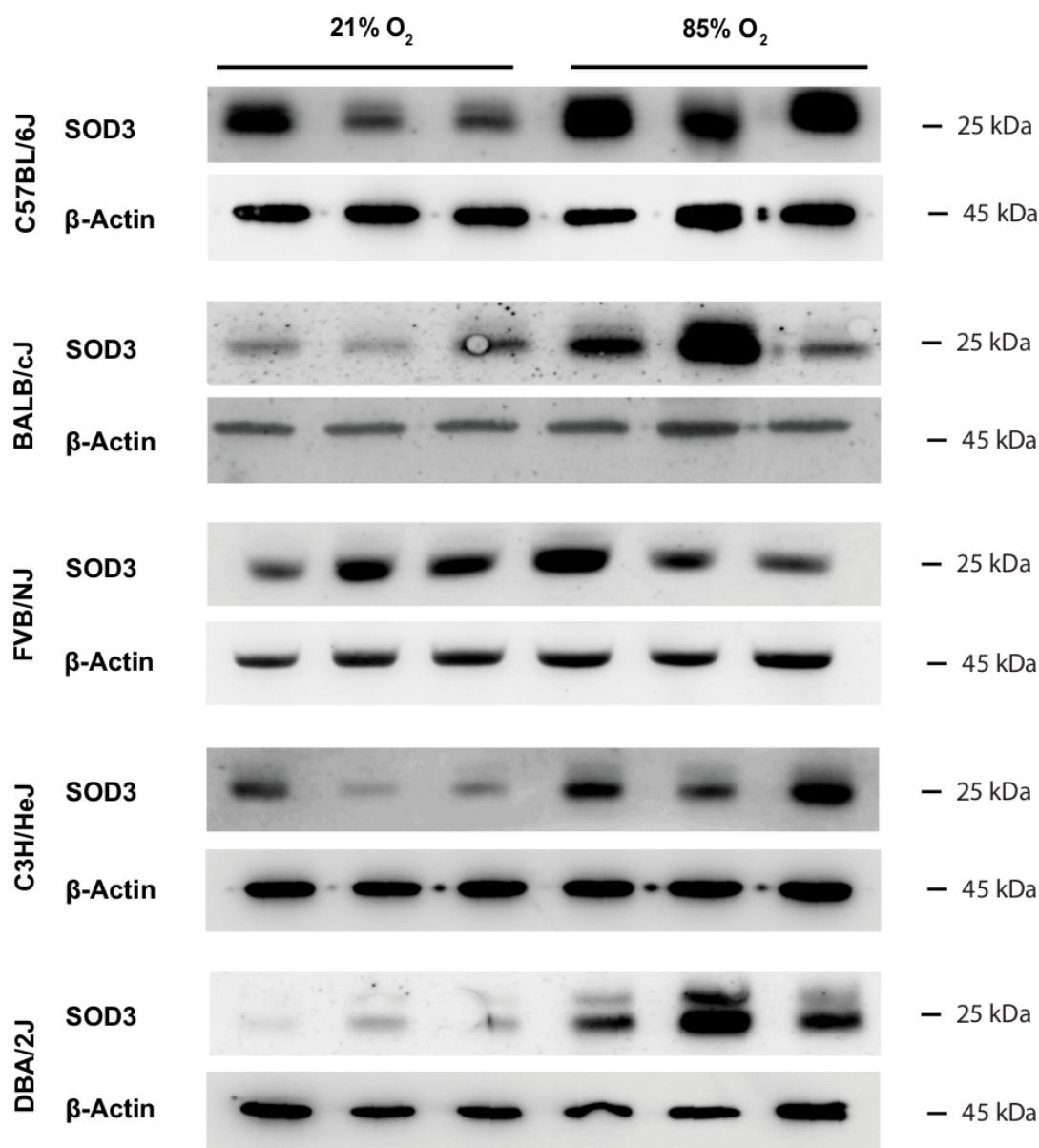


Figure 11 Expression of superoxide dismutase 3 in five different inbred mouse strains exposed to normoxia or hyperoxia.

SOD3 protein levels in lungs of mouse pups from inbred mouse strains on the 14th day of postnatal life. Parameters were assessed by immunoblot from five different inbred mouse strains exposed to normoxic (21% O_2) or hyperoxic (85% O_2) conditions for the first 14 days of postnatal life. The three immunoreactive bands on the left side each represent individual 21% O_2 -exposed animal, whilst the three immunoreactive bands on the right side each represent one individual 85% O_2 -exposed animal. β -actin levels serve as the loading equivalence.

mRNA, messenger RNA; real-time RT-PCR, real-time polymerase chain reaction; SOD3, superoxide dismutase 3. Adapted from [64]. Copyright 2020 by John Wiley and Sons. Adapted with permission.

Exposure to hyperoxia induced the upregulation of glutathione metabolizing lung enzymes. The *Gss* genes encode the enzymes responsible for glutathione synthesis. After hyperoxia exposure, increased lung mRNA levels of *Gss* were observed consistently across the C57BL/6J, BALB/cJ, and DBA/2J strains. Additionally, increased protein levels of GSS were detected in all five mouse strains, as depicted in Figure 12 and Figure 13. The molecular masses of the observed bands were consistent with the predicted sizes for GSS (52 kDa ⁷) and β -Actin (45 kDa ⁸), as indicated by the manufacturer's specifications. The detected protein bands correspond to the expected molecular weights. No additional bands were detected.

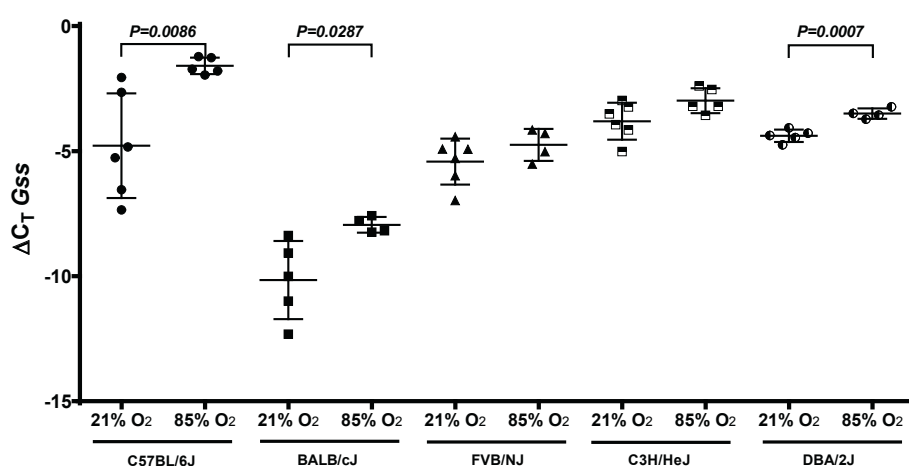


Figure 12 Expression of glutathione in five different inbred mouse strains exposed to hyperoxia.

mRNA levels of *Gss* in lungs of mouse pups from inbred mouse strains on the 14th day of postnatal life. Parameters were assessed by real-time RT-PCR from five different inbred mouse strains exposed to normoxic (21% O₂) or hyperoxic (85% O₂) conditions for the first 14 days of postnatal life. Utilized primers are listed in Table 7.

Values represent mean $\Delta C_t \pm SD$ ($n = 4-6$, outliers were removed using the Grubbs test). Each dot represents an individual animal. Comparisons between the data from 21% O₂ and 85% O₂ exposed animals of the same strain were made by the unpaired Student *t* test. *P* values below 0.05 are indicated. mRNA, messenger RNA; real-time RT-PCR, real-time polymerase chain reaction; *Gss*, glutathione. Adapted from [64]. Copyright 2020 by John Wiley and Sons. Adapted with permission.

⁷ <https://www.abcam.com/products/primary-antibodies/glutathione-synthetase-antibody-epr6563-ab133592.html>

⁸ <https://www.cellsignal.com/products/primary-antibodies/b-actin-antibody/4967>

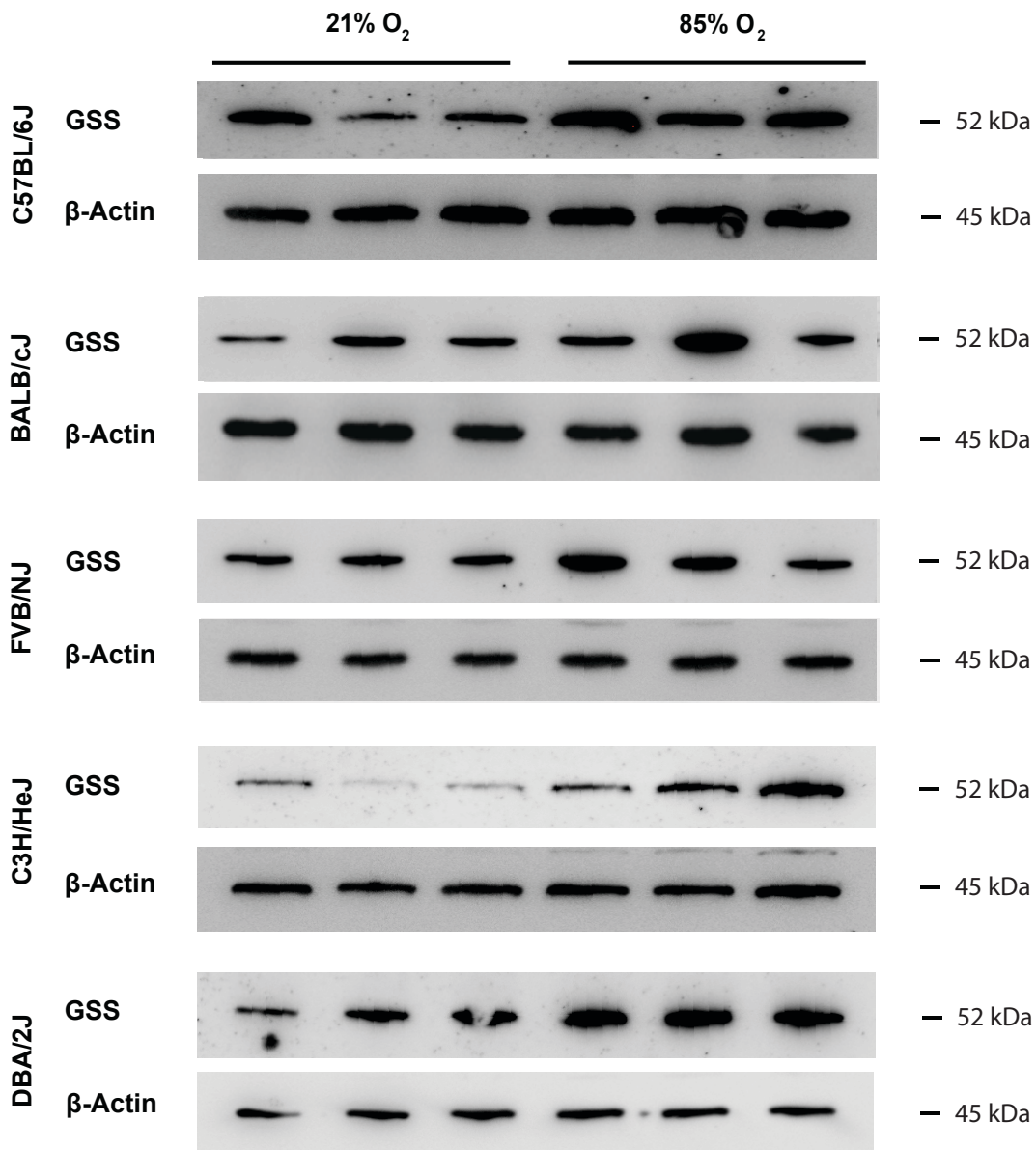


Figure 13 Expression of glutathione synthetase in five different inbred mouse strains exposed to normoxia or hyperoxia.

GSS protein levels in lungs of mouse pups from inbred mouse strains on the 14th day of postnatal life. Parameters were assessed by immunoblot from five different inbred mouse strains exposed to normoxic (21% O₂) or hyperoxic (85% O₂) conditions for the first 14 days of postnatal life. The three immunoreactive bands on the left side each represent individual 21% O₂-exposed animal, whilst the three immunoreactive bands on the right side each represent one individual 85% O₂-exposed animal. β-actin levels serve as the loading equivalence.

mRNA, messenger RNA; real-time RT-PCR, real-time polymerase chain reaction; GSS, glutathione. Adapted from [64]. Copyright 2020 by John Wiley and Sons. Adapted with permission.

Glutathione peroxidase 1 enzyme is encoded by the *Gpx1* gene. The mRNA levels of *Gpx1* were increased in the C57BL/6J, BALB/cJ, and FVB/NJ strains in response to hyperoxia exposure, while other strains were unaffected (Figure 14).

The mRNA levels of the *Gsr* gene, encoding glutathione disulfide reductase, remained unchanged across all strains except for the FVB/NJ strain, where an increase was observed (Figure 14).

The mRNA levels of *Txn1*, which encodes the protein thioredoxin, were decreased in the BALB/cJ and C3H/HeJ strains following hyperoxia exposure, while remaining unchanged in the other strains. Notably, the mRNA level of *Txn1* in the C57BL/6J strain was exceptionally lower compared to the other strains (Figure 15).

A decrease in the mRNA levels of *Cat*, encoding catalase, was observed in the C57BL/6J, BALB/cJ, and C3H/HeJ strains after exposure to hyperoxia. Among all the strains, the C57BL/6J strain exhibited the largest decrease and had the highest mRNA levels of *Cat* under both hyperoxic and normoxic conditions compared to the other mouse strains (Figure 15).

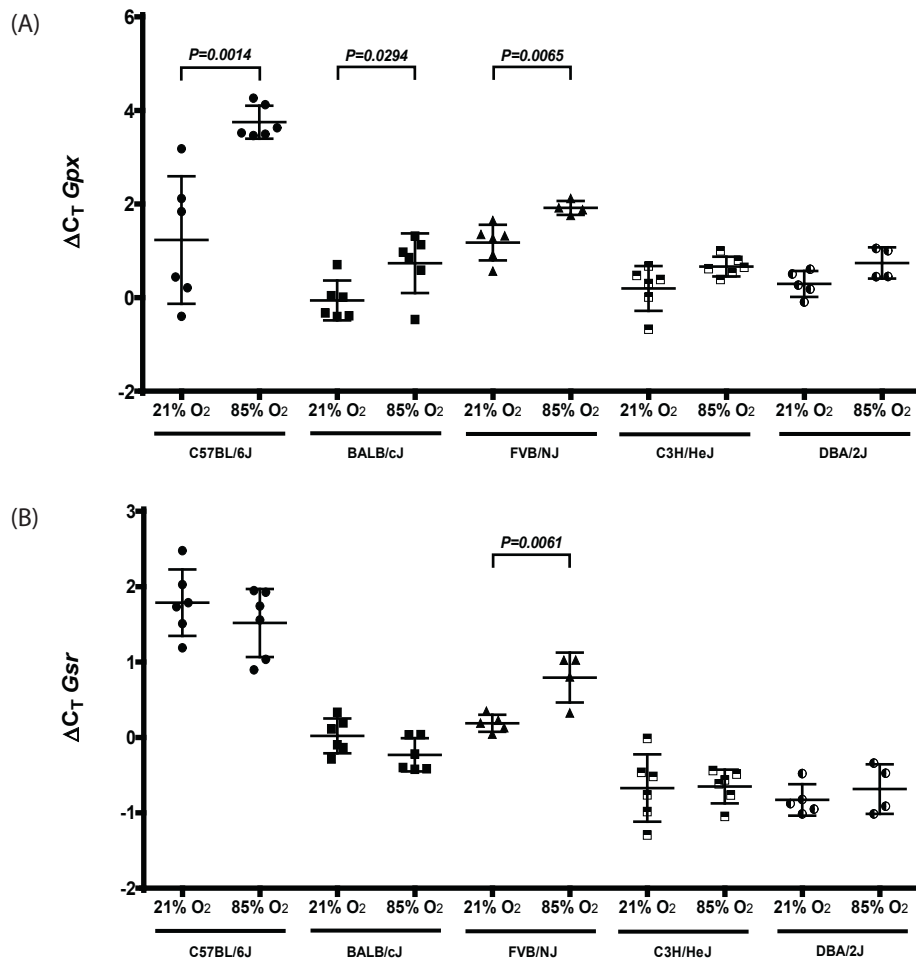


Figure 14 Expression of glutathione peroxidase 1 and glutathione disulfide reductase in five different inbred mouse strains exposed to normoxia or hyperoxia.

mRNA levels of (A) *Gpx* and (B) *Gsr* in lungs of mouse pups from inbred mouse strains on the 14th day of postnatal life. Parameters were assessed by real-time RT-PCR from five different inbred mouse strains exposed to normoxic (21% O₂) or hyperoxic (85% O₂) conditions for the first 14 days of postnatal life. Utilized primers are listed in Table 7.

Values represent mean $\Delta C_t \pm SD$ ($n = 4-6$, outliers were removed using the Grubbs test). Each dot represents an individual animal. Comparisons between the data from 21% O₂ and 85% O₂ exposed animals of the same strain were made by the unpaired Student *t* test. *P* values below 0.05 are indicated. mRNA, messenger RNA; real-time RT-PCR, real-time polymerase chain reaction; *Gpx*, glutathione peroxidase; *Gsr*, glutathione disulfide reductase. Adapted from [64]. Copyright 2020 by John Wiley and Sons. Adapted with permission.

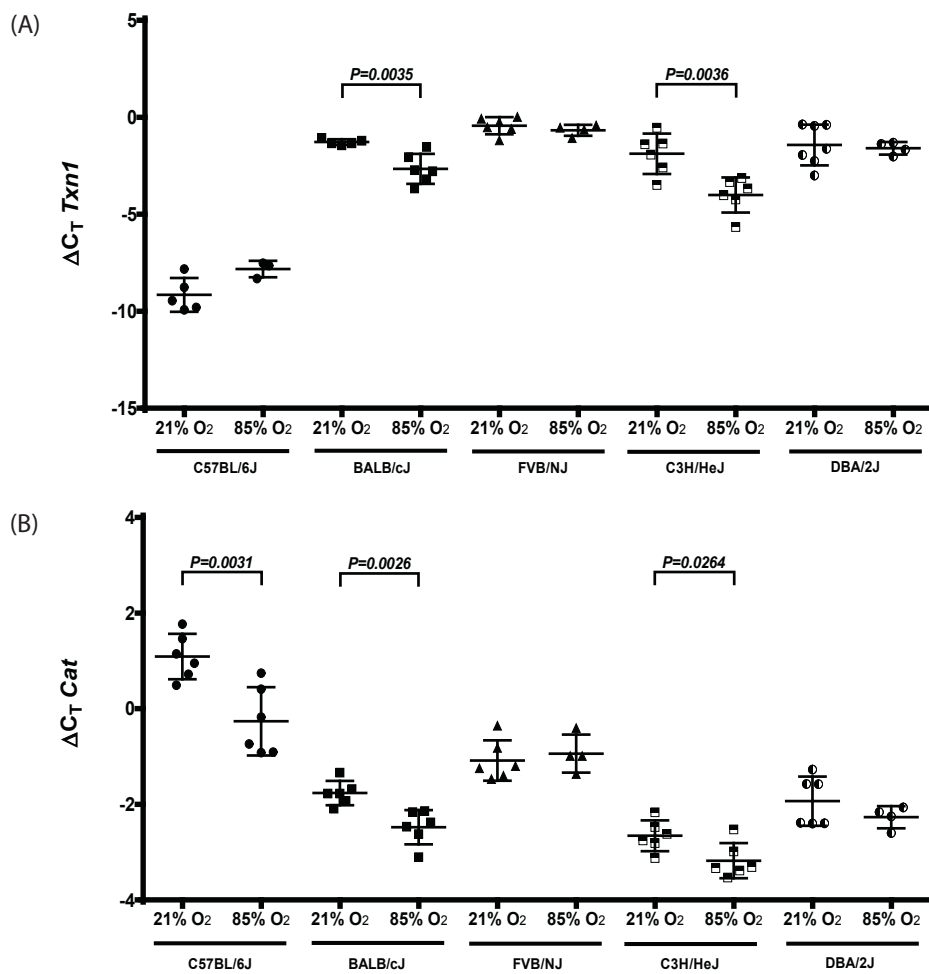


Figure 15 Expression of thioredoxin and catalase in five different inbred mouse strains exposed to normoxia or hyperoxia.

mRNA levels of (A) *Txn1* and (B) *Cat* in lungs of mouse pups from inbred mouse strains on the 14th day of postnatal life. Parameters were assessed by real-time RT-PCR from five different inbred mouse strains exposed to normoxic (21% O₂) or hyperoxic (85% O₂) conditions for the first 14 days of postnatal life. Utilized primers are listed in Table 7.

Values represent mean $\Delta C_t \pm SD$ ($n = 3-6$, outliers were removed using the Grubbs test). Each dot represents an individual animal. Comparisons between the data from 21% O₂ and 85% O₂ exposed animals of the same strain were made by the unpaired Student *t* test. P values below 0.05 are indicated. mRNA, messenger RNA; real-time RT-PCR, real-time polymerase chain reaction; *Txn*, thioredoxin; *Cat*, catalase. Adapted from [64]. Copyright 2020 by John Wiley and Sons. Adapted with permission.

The mRNA levels of *Txnrd1* and *Txnrd2*, which encode cytosolic and mitochondrial thioredoxin reductase enzymes (TXNRD), were profiled. Lung mRNA levels of *Txnrd1* were decreased in the C57BL/6J and BALB/cJ strains, while lung mRNA levels of *Txnrd2* were increased in the C57BL/6J, FVB/NJ and DBA/2J strains after exposure to hyperoxia. Other strains showed no significant changes (Figure 16).

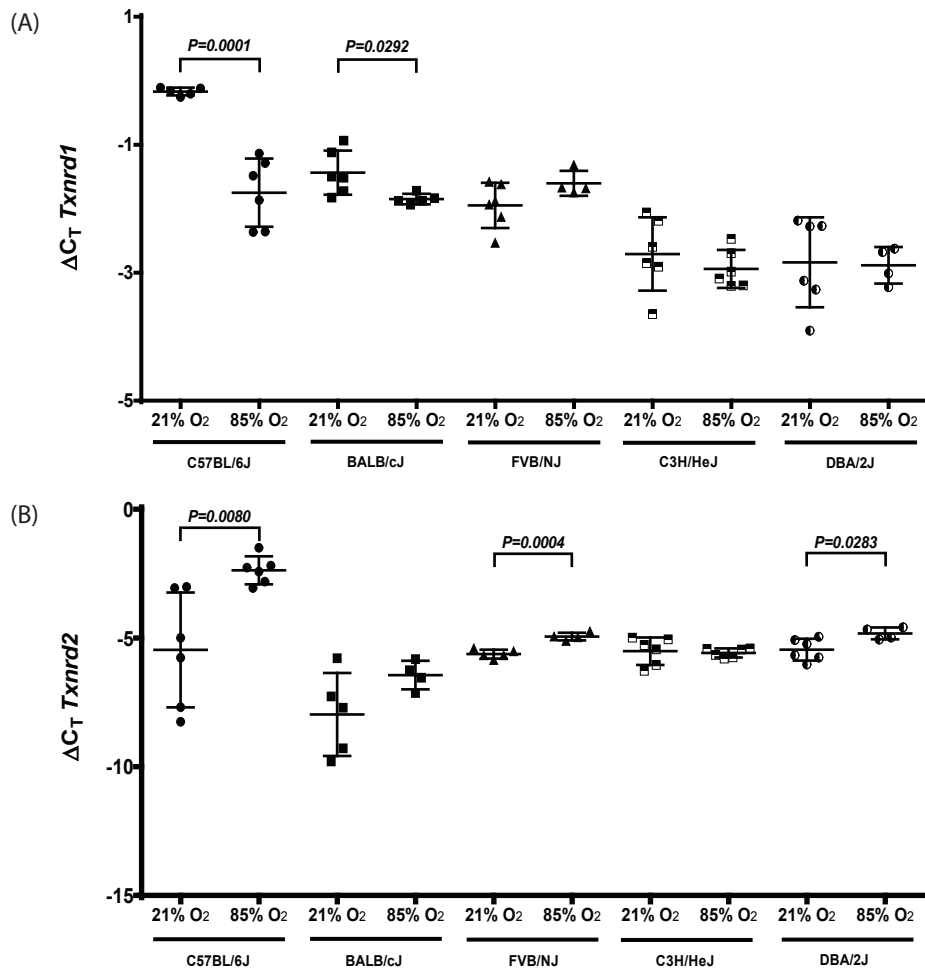


Figure 16 Expression of thioredoxin reductase 1 and 2 in five different inbred mouse strains exposed to normoxia or hyperoxia.

mRNA levels of (A) *Txnrd1* and (B) *Txnrd2* in lungs of mouse pups from inbred mouse strains on the 14th day of postnatal life. Parameters were assessed by real-time RT-PCR from five different inbred mouse strains exposed to normoxic (21% O₂) or hyperoxic (85% O₂) conditions for the first 14 days of postnatal life. Utilized primers are listed in Table 7. Values represent mean ΔC_T ± SD (n = 4–6, outliers were removed using the Grubbs test). Each dot represents an individual animal. Comparisons between the data from 21% O₂ and 85% O₂ exposed animals of the same strain were made by the unpaired Student *t* test. P values below 0.05 are indicated.

mRNA, messenger RNA; real-time RT-PCR, real-time polymerase chain reaction; *Txnrd*, thioredoxin reductase. Adapted from [64]. Copyright 2020 by John Wiley and Sons. Adapted with permission.

The mRNA expression levels of *Nfe2l2*, which encodes the transcription factor nuclear factor erythroid-derived 2-like 2 (NFE2L2), were reduced in the C57BL/6J and BALB/c strains. Among all the strains, the C57BL/6J strain displayed the most significant decrease and exhibited the highest mRNA levels of *Nfe2l2* under normoxic conditions compared to the other mouse strains. (Figure 17).

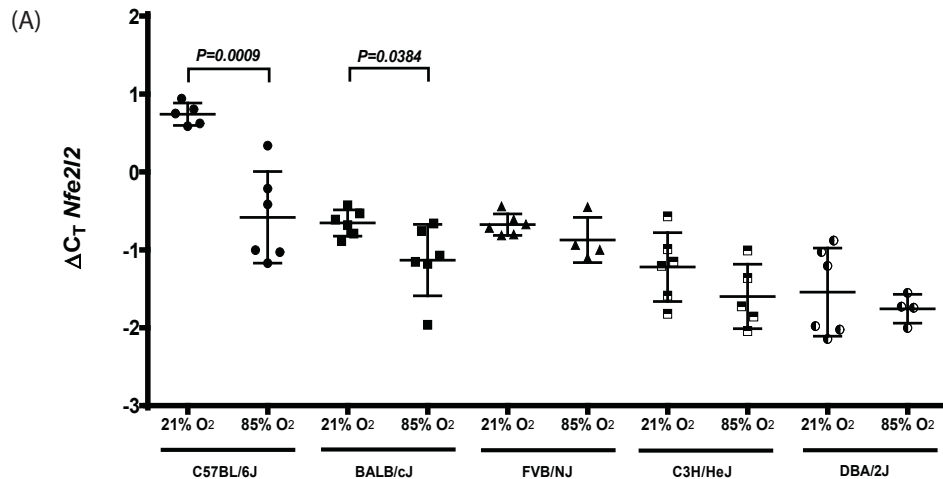


Figure 17 Expression of nuclear factor (erythroid-derived 2)-like 2 in five different inbred mouse strains exposed to normoxia or hyperoxia.

mRNA levels of *Nfe2l2* in lungs of mouse pups from inbred mouse strains on the 14th day of postnatal life. Parameters were assessed by real-time RT-PCR from five different inbred mouse strains exposed to normoxic (21% O₂) or hyperoxic (85% O₂) conditions for the first 14 days of postnatal life. Utilized primers are listed in Table 7.

Values represent mean $\Delta C_T \pm SD$ ($n = 4-6$, outliers were removed using the Grubbs test). Each dot represents an individual animal. Comparisons between the data from 21% O₂ and 85% O₂ exposed animals of the same strain were made by the unpaired Student *t* test. *P* values below 0.05 are indicated. mRNA, messenger RNA; real-time RT-PCR, real-time polymerase chain reaction; Nfe2l2, nuclear factor erythroid 2-related factor 2. Adapted from [64]. Copyright 2020 by John Wiley and Sons. Adapted with permission.

The mRNA levels of the peroxiredoxin (PRDX) family of antioxidant enzymes were also profiled. The mRNA levels of *Prdxn1* were found to be decreased in the C57BL/6J, BALB/cJ, and FVB/NJ strains, whereas the mRNA levels of *Prdxn5* were increased in the BALB/cJ and DBA/2J strains. The mRNA levels of *Prdxn6* were increased in the C57BL/6J and BALB/cJ strains after hyperoxia exposure. Notably, the C57BL/6J strain exhibited the lowest mRNA levels of *Prdx5* under both normoxic and hyperoxic conditions compared to other mouse strains (Figure 18).

The mRNA levels of *Prdx2*, *Prdx3*, and *Prdx4* remained unchanged in all strains (Figure 19).

Furthermore, the mRNA levels of the three members of the PON family (*Pon1*, *Pon2*, and *Pon3*), which encode paroxonase, were analyzed. Upregulated mRNA levels were observed for all three genes in the DBA/2J strain, while only *Pon2* showed upregulation in the C57BL/6J and BALB/cJ strains after hyperoxia exposure (Figure 20).

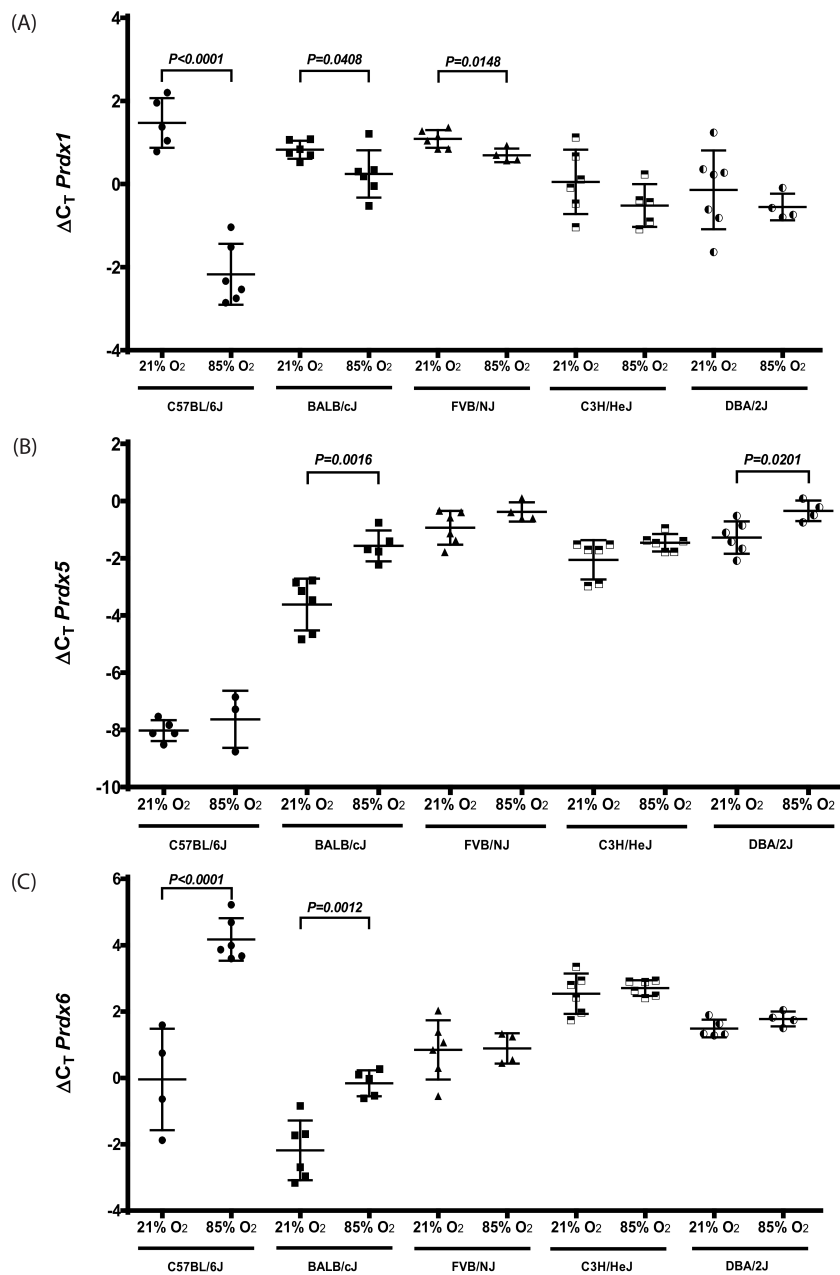


Figure 18 Expression of peroxiredoxin 1, 5 and 6 in five different inbred mouse strains exposed to normoxia or hyperoxia.

mRNA levels of (A) Prdx1, (B) Prdx5 and (C) Prdx6 in lungs of mouse pups from inbred mouse strains on the 14th day of postnatal life. Parameters were assessed by real-time RT-PCR from five different inbred mouse strains exposed to normoxic (21% O₂) or hyperoxic (85% O₂) conditions for the first 14 days postnatal life. Utilized primers are listed in Table 7.

Values represent mean $\Delta C_t \pm SD$ ($n = 3-7$, outliers were removed using the Grubbs test). Each dot represents an individual animal. Comparisons between the data from 21% O₂ and 85% O₂ exposed animals of the same strain were made by the unpaired Student *t* test. P values below 0.05 are indicated. mRNA, messenger RNA; real-time RT-PCR, real-time polymerase chain reaction; Prdx, peroxiredoxin. Adapted from [64]. Copyright 2020 by John Wiley and Sons. Adapted with permission.

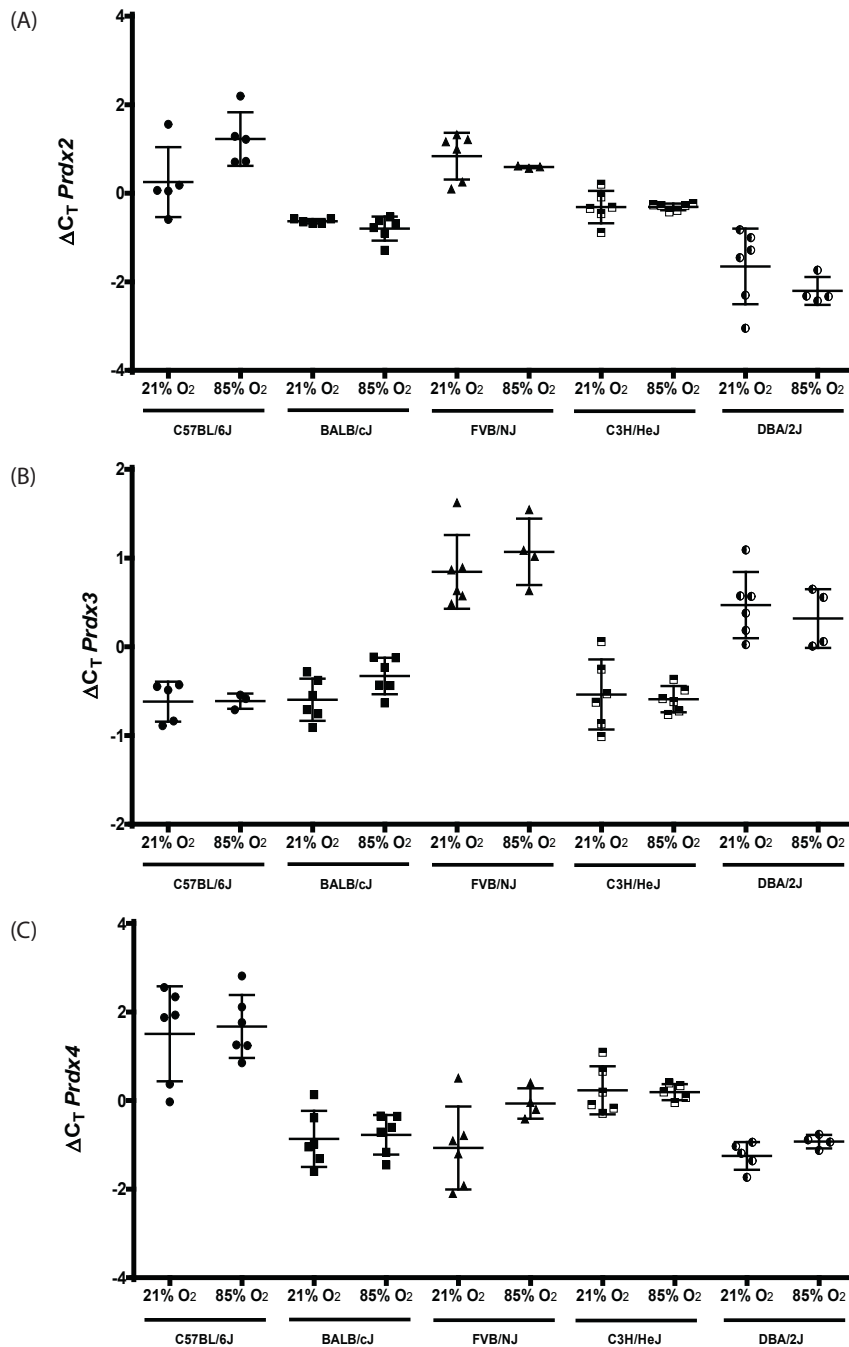


Figure 19 Expression of peroxiredoxin 2, 3 and 4 in five different inbred mouse strains exposed to normoxia or hyperoxia.

mRNA levels of (A) Prdx2, (B) Prdx3 and (C) Prdx4 in lungs of mouse pups from inbred mouse strains on the 14th day of postnatal life. Parameters were assessed by real-time RT-PCR from five different inbred mouse strains exposed to normoxic (21% O₂) or hyperoxic (85% O₂) conditions for the first 14 days of postnatal life. Utilized primers are listed in Table 7.

Values represent mean $\Delta C_t \pm SD$ ($n = 3-6$, outliers were removed using the Grubbs test). Each dot represents an individual animal. Comparisons between the data from 21% O₂ and 85% O₂ exposed animals of the same strain were made by the unpaired Student *t* test. *P* values below 0.05 are indicated. mRNA, messenger RNA; real-time RT-PCR, real-time polymerase chain reaction; Prdx, peroxiredoxin. Adapted from [64]. Copyright 2020 by John Wiley and Sons. Adapted with permission.

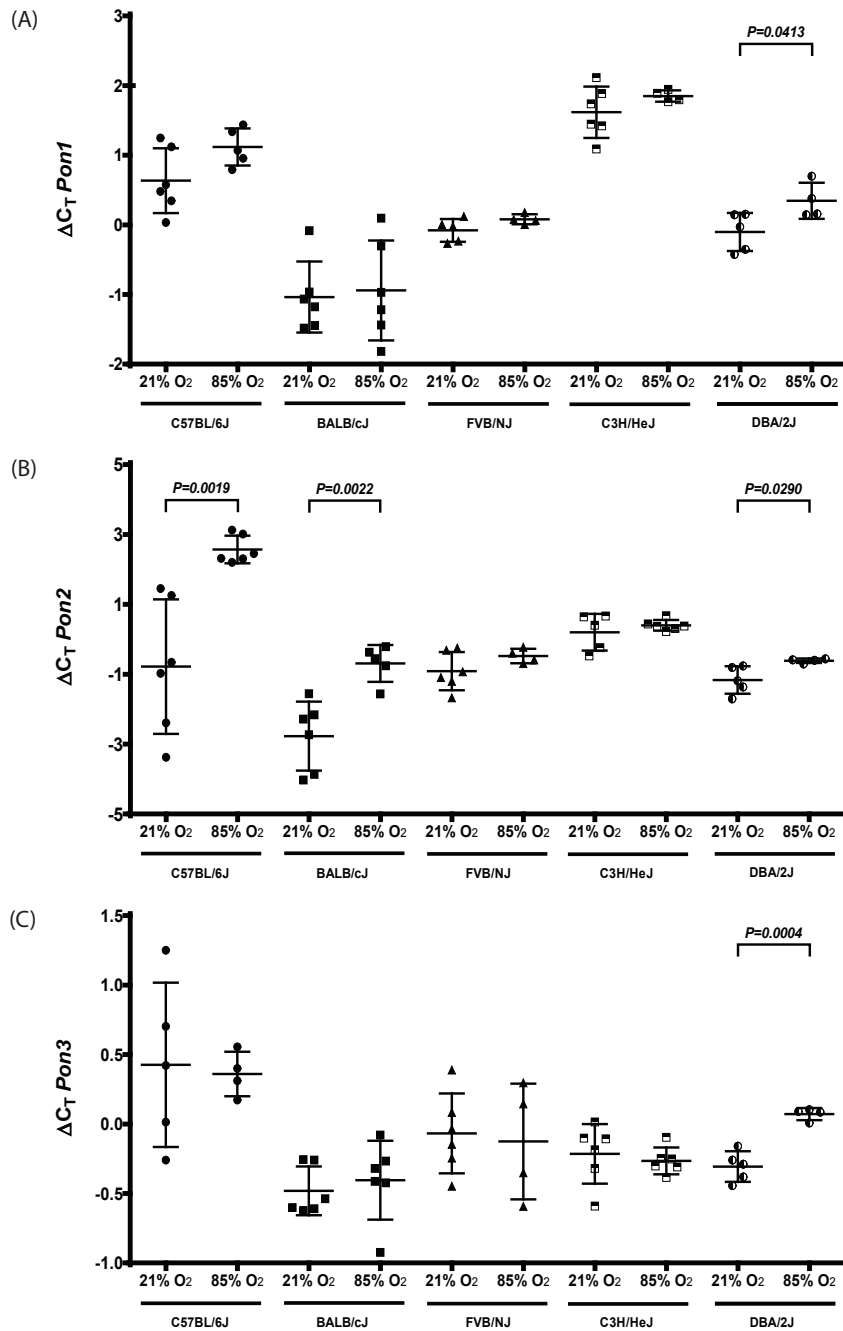


Figure 20 Expression of paroxonase 1,2 and 3 in five different inbred mouse strains exposed to normoxia or hyperoxia.

mRNA levels of (A) Pon1, (B) Pon2 and (C) Pon3 in lungs of mouse pups from inbred mouse strains on the 14th day of postnatal life. Parameters were assessed by real-time RT-PCR from five different inbred mouse strains exposed to normoxic (21% O₂) or hyperoxic (85% O₂) conditions for the first 14 days of postnatal life. Utilized primers are listed in Table 7.

Values represent mean $\Delta C_t \pm SD$ ($n = 4-6$, outliers were removed using the Grubbs test). Each dot represents an individual animal. Comparisons between the data from 21% O₂ and 85% O₂ exposed animals of the same strain were made by the unpaired Student *t* test. *P* values below 0.05 are indicated. mRNA, messenger RNA; real-time RT-PCR, real-time polymerase chain reaction; Pon, paroxonase. Adapted from [64]. Copyright 2020 by John Wiley and Sons. Adapted with permission.

The mRNA levels of *Hmox1*, which encodes hemoxygenase-1 remained unchanged in all strains except for the BALB/cJ strain following hyperoxia exposure. It is worth noting that the C57BL/6J mice displayed the highest mRNA levels of *Hmox1* compared to all other strains under both normoxic and hyperoxic conditions (Figure 21).

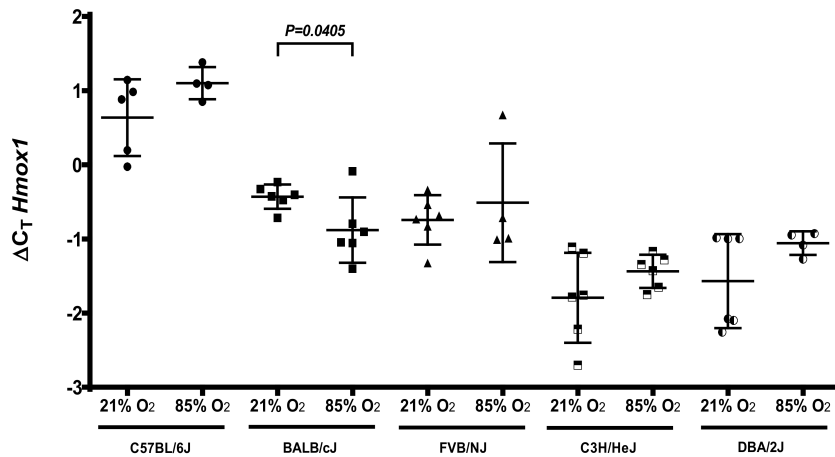


Figure 21 Expression of hemoxygenase-1 in five different inbred mouse strains exposed to normoxia or hyperoxia.

mRNA levels of *Hmox1* in lungs of mouse pups from inbred mouse strains on the 14th day of postnatal life. Parameters were assessed by real-time RT-PCR from five different inbred mouse strains exposed to normoxic (21% O₂) or hyperoxic (85% O₂) conditions for the first 14 days of postnatal life. Utilized primers are listed in Table 7.

Values represent mean ± SD ($n = 4-6$, outliers were removed using the Grubbs test). Each dot represents an individual animal. Comparisons between the data from 21% O₂ and 85% O₂ exposed animals of the same strain were made by the unpaired Student *t* test. *P* values below 0.05 are indicated. mRNA, messenger RNA; real-time RT-PCR, real-time polymerase chain reaction; *Hmox*, heme oxygenase. Adapted from [64]. Copyright 2020 by John Wiley and Sons. Adapted with permission.

5. Discussion

5.1 Method Discussion

5.1.1 Polymerase Chain Reaction

In this study we utilized PCR (Polymerase Chain Reaction) to exponentially amplify specific cDNA sequences derived from mouse lung tissue's total RNA. This allowed us to quantify gene expression levels and providing insights into the regulation of specific genes. One of the key advantages of PCR is its sensitivity, specificity, and rapid amplification capability, making it a valuable tool for gene expression analysis [66].

We specifically employed real-time PCR (RT-PCR) for gene expression analysis. This method presents several advantages over conventional PCR techniques, as it allows for the real-time detection and quantification of the PCR product during its synthesis, providing quantitative data rather than only qualitative results [67]. This is achieved through the monitoring of the fluorescence signal generated by the SYBR® Green dye binding to double-stranded DNA during the amplification process. To detect and analyze the fluorescence signal changes over the reaction, we employed the StepOnePlus™ Real-time PCR System, which enabled accurate and reliable quantification of gene expression levels. Furthermore, RT-PCR allows for the simultaneous analysis of multiple genes in a single reaction, increasing the efficiency and capacity of gene expression studies [67].

To evaluate the potential for non-specific amplification or contamination, the specificity of the primers was assessed prior to any PCR analyses by using a no reverse transcriptase control (NRT) template in the PCR reaction. In this control, a cDNA reaction was prepared by substituting the reverse transcriptase (RT) with RNase-free water. This enabled us to determine whether the primers could generate a PCR product in the absence of cDNA but in the presence of residual genomic DNA. It was anticipated that no product would be obtained since the primers were specifically designed to span introns, ensuring their specificity for the target sequences. As expected, no amplification was observed, further confirming the specificity of the primers and ruling out any potential non-specific amplification or contamination.

For DNA quantification and purity assessment, we used the NanoDrop® ND-1000 spectrophotometer. This ensured the quality of the isolated DNA samples.

The efficiency of all used RT-PCR primers was tested before in a separate primer dilution test in which the primers proved to function at a dilution up to 1:5000 (m/v).

A melting curve analysis was performed for each primer to differentiate the amplified PCR product from unspecific primer dimers. The PCR product has stronger binding forces compared to small primer dimers, requiring higher temperatures for denaturation. If the PCR product is successfully amplified, the fluorescence of the fluorescent dye should be detected at higher temperatures when the long double-stranded cDNA (amplified PCR product) denatures, resulting in the release of fluorescent dye. In contrast, primer dimers denature at lower temperatures, leading to the detection of the fluorescent dye at lower temperatures. A well resolved single-peak melting curve, free from any shoulders or sub-peaks, was considered a reliable indication of a specific product.

By conducting duplicate tests for each gene as technical replicates, we effectively minimized technical variations, including potential sources of error such as pipetting errors and instrument variability, thereby improving the reliability of our results. We then compared the duplicated C_t values obtained for the reference gene and the gene of interest to assess the consistency of the amplification process. This approach ensured the robustness of our gene expression analysis.

The choice of using the housekeeping gene *Polr2a* as the reference gene allowed us to assess the relative expression of the specific gene under investigation.

The suitability of the reference gene *Polr2a* for studies on hyperoxia in the lung has been previously examined by colleagues in the laboratory. In an unpublished observation conducted by the Morty laboratory, a comparison was made among five potential reference genes (*Gapdh*, *Polr2a*, *Hmbs*, *Actb*, and *Tub1*), and it was determined that *Polr2a* was the most suitable reference gene for studies on bronchopulmonary dysplasia.

Additionally, PCR was utilized to determine the sex of mouse pups. The amplification of a male-specific sequence (*Sry*) situated on the Y chromosome was utilized to identify male individuals. The presence of an independent control gene (*Il3*) was used to validate the amplification of the template DNA and functioned as an internal control for PCR amplification. Furthermore, a positive control was conducted using DNA samples from both a male and a female individual with known gender.

5.1.2 Immunoblot

The western blot, also referred to as immunoblot, is a frequently utilized method in molecular biology for the identification and visualization of specific proteins providing valuable information regarding their molecular weight, quantity, and presence [68]. In this study, we utilized western blotting to evaluate protein expression levels in lung tissue samples of mice, considering both its advantages and limitations.

Western blotting is a technique that enables the identification of target proteins using specific primary antibodies. Ensuring the specificity of primary antibodies is essential for obtaining reliable and accurate results [69]. Hence it is important to carefully select and validate antibodies to prevent non-specific binding and cross-reactivity. To ensure the specificity of the Western blots, the primary antibody employed in this study was carefully chosen based on its established specificity for the target antigen. The antibody's specificity has been previously validated and confirmed by the manufacturer.

Regarding the specificity of the Western blot analysis, it is important to note that we did not perform experiments using competing peptides or knockout cells to directly assess specificity. However, we carefully evaluated the Western blots based on the presence of clear, single bands that corresponded to the predicted molecular size of the target proteins. The observation of clear and distinct bands in the Western blots is indicative of positive specificity, suggesting that the antibodies used specifically recognized the intended target proteins.

Another potential limitation of western blotting is the occurrence of background signal, which can lead to false-positive results or obscure specific protein bands. To minimize background signal, thorough and efficient washing steps were implemented. This ensured the removal of any unbound or nonspecifically bound antibodies, improving the specificity of protein detection.

Inconsistent loading of protein onto the gel can lead to variations and inaccuracies, resulting in false results [69]. This variability in protein loading is a significant source of inconsistency between different laboratories [69]. By including β -Actin as a loading control, we ensured equal loading of protein samples within the polyacrylamide gel, enhancing the reliability of our results and instilling confidence in the accuracy of our protein expression measurements.

In our blots with SOD3, we consistently observed the presence of an additional band at 52 kDa, which coincided with the reported presence of extra bands at 54 kDa according

to the manufacturer⁹. Therefore, the detection of the additional band at 52 kDa aligns with our expectations. The manufacturer is uncertain about the identity of these extra bands

The bands corresponding to GSS and β -Actin were detected at their expected band sizes, providing further validation for the accuracy of our experimental results in those cases.

5.1.3 Statistical analysis

The data in this study are presented as scatter plots with mean \pm SD. Statistical significance of differences between groups was determined using the unpaired Student t-test ($P < 0.05$). To maintain data integrity, statistical outliers were identified and excluded from the analysis after screening with the Grubbs test.

We recognize the challenge of confidently assuming a normal distribution in this study, given the limited sample size of eight mice determined through a prospective power analysis. However, it is worth noting that previous studies with similar small sample sizes commonly employed the t-test for pairwise comparisons [70], [71]. Furthermore, a study by de Winter, J.C.F. specifically addresses the validity of the t-test in small sample sizes [72]. It emphasizes that the t-test does not significantly exceed the Type I error rate of 5% even with very few samples, suggesting that it remains a valid choice for pairwise comparisons. Additionally, the study suggests that a paired t-test can be employed when the within-pair correlation coefficient is high [72]. These findings align with our study, as we focused on pairwise comparisons between related samples with a high within-pair correlation coefficient.

Considering the findings of previous research and the specific characteristics of our data, the use of the t-test for pairwise comparisons in this study is justified despite the small sample size. It is important to acknowledge that the limited sample size poses a constraint on the generalizability and precision of our results. However, based on the common usage of the t-test in similar studies, we believe it provides valuable insights into the observed differences between groups.

⁹ <https://www.abcam.com/products/primary-antibodies/superoxide-dismutase-3ec-sod-antibody-4g11g6-ab80946.html#lb>

5.2 Selection of mouse strains and experimental design

Bronchopulmonary dysplasia (BPD) is a long-term lung complication that is most prevalent in preterm babies who require mechanical ventilation and oxygen therapy [15], [16]. Despite significant advances in treatment, BPD remains a common chronic lung disease that leads to significant morbidity and mortality in neonatal intensive care [18]. Therefore, there is a pressing need for advances in research to understand its pathomechanism.

Such studies are usually performed with animal models such as term-born mouse and rat pups [41], with researchers employing various mouse and rat strains [36]. However, the role of mouse and rat strains selected for experimentation on postnatal lung maturation is an essential factor to consider when designing and interpreting experiments [48], [49], [73]. It has been observed that the genetic background of mice can lead to different outcomes, even when identical genetic manipulations, treatment protocols or environmental exposures are applied [47]. The use of diverse mouse strains can result in discrepancies when comparing independent studies. These findings emphasize the need for a systematic evaluation of the susceptibility of different mouse strains to hyperoxia, enabling informed decisions on selecting the most suitable mouse strain for BPD studies using experimental models.

Therefore, we conducted a comprehensive side-by-side comparison of lung alveolarization and the gene expression of central components of the lung antioxidant response in six commonly used inbred mouse strains: C57BL/6J, BALB/cJ, FVB/NJ, C3H/HeJ, DBA/2J and 129S2/SvPasOrlRj. This selection includes five out of the seven groups of the laboratory mouse strain family tree based on 1638 informative single-nucleotide polymorphisms compared in 102 inbred mouse strains (see Figure 2) [63]. The C3H/HeJ and BALB/cJ strains are from divergent branches of the Bagg albino-derived group; the FVB/NJ strain is from the Swiss mouse group, the C57BL/6J strain is from the general C57/C58 group, the DBA/2J strain is from C.C. Little's DBA and related strain group and the 129S2/SvPasOrlRj is from the Castle group. Mouse strains from the Japan and New Zealand inbred strains group and the wild-derived strain group were not selected since they are not commonly used in preclinical studies on bronchopulmonary dysplasia.

With this selection, we approached a wide variety of genetically different strains, including the most used mouse strains in preclinical studies on bronchopulmonary dysplasia.

For the experiments, we exposed the six chosen strains to normoxic (21% O₂) and hyperoxic (85% O₂) conditions for the first 14 days of postnatal life. Among the six strains, five survived hyperoxic conditions until P14. However, the 129S2/SvPasOrlRj strain exhibited abnormal behaviors such as agitation, aggression, and leaving the nest under hyperoxic conditions, while the dams behaved normally under normoxic conditions. All 129S2/SvPasOrlRj pups exposed to hyperoxic conditions died by P4. The deceased pups were found dead in the litters, partially consumed, without any apparent cause of death. On the contrary, the 129S2/SvPasOrlRj pups under normoxic conditions survived without any issues. Due to these observations, we decided to exclude the 129S2/SvPasOrlRj strain from this experiment.

5.3 Lung development in mouse strains under hyperoxia

The mouse strains treated under normoxic conditions were used as the control group. Under normoxic conditions, the C57BL/6J strain demonstrated the highest number of alveoli and lung volume, while DBA/2J showed the lowest. The C3H/HeJ strain had the highest septal thickness, and the FVB/NJ strain had the lowest.

Visual inspection of the Richardson-stained, plastic-embedded lung tissue sections revealed that the mean diameter of the alveoli in normoxia-exposed C3H/HeJ mouse lungs appeared larger than in the other mouse strains. This was supported by the highest mean linear intercept (MLI) in the C3H/HeJ of all normoxia-treated strains, which serves as an approximate measure of the alveolar diameter. These findings are consistent with previous studies [74].

Hyperoxia caused the greatest magnitude of change in terms of alveoli number (74.5%), alveoli density (64.8%), MLI (94.5%) and lung volume (27.5%) in the C57BL/6J strain. The FVB/NJ strain exhibited the highest increase in septal thickness (65.4%) due to hyperoxia exposure, while the C57BL/6J was the least affected (30.3%). The C3H/cj strain showed the lowest magnitude of change in terms of alveolar density (35.9%) and MLI (31.7%). As expected, these results suggest an overall stunting of alveolarization and are align with previous studies using BPD animal models, which have reported

impaired alveolar formation, larger and fewer alveoli, reduced airspace septation, and thickening of alveolar walls following hyperoxia exposure compared to normoxia-treated animals [33], [34], [41].

The results suggest that the C57BL/6J strain is highly susceptible to the effects of hyperoxia, particularly in terms of alveoli number, alveoli density, MLI, and lung volume, while the C3H/HeJ strain is the least affected. This indicates that the C57BL/6J strain is more susceptible to hyperoxia exposure, resulting in a significant reduction in lung alveolarization. This is further supported by the significant decrease in alveoli density observed in the C57BL/6J strain, which reflects the degree of lung alveolarization.

Overall, the results support our hypothesis that mouse genetic background influences lung development in response to hyperoxia. All the strains exhibited varying degrees of lung perturbation after exposure to the injurious stimulus of 85% O₂ hyperoxia.

It is important to interpret these results with caution due to potential limitations that should be acknowledged. These limitations include inadequate control of inflation during fixation, compression-induced shrinkage, and inadequate tissue processing [75]. These factors can introduce biases in the estimated parameters. If the tissue is not adequately hardened during fixation, the lung may contract during sectioning, resulting in a decrease in the reference area [75]. To address these limitations, we followed Weibel et al.'s protocol and fixed the lung tissue for at least 24 hours with a fixation solution containing glutaraldehyde, paraformaldehyde, and HEPES by airway instillation under 20 cm H₂O hydrostatic pressure to ensure adequate results [75]. This method stabilized the lung tissue and prevented its collapse during further processing [75].

Another potential limitation of our study is the lack of uniform standardization in the process of lung preparation, including the steps from harvesting to histological preparation. This variability introduced by human handlers may influence the parameters of lung architecture in individual samples. However, to partially address this limitation, we took measures to minimize bias. Specifically, we assigned the task of handling all the lungs to the same person, ensuring consistency in the techniques and styles of preparation. This approach aimed to reduce the potential impact of inter-operator variability on the results.

5.4 Lung antioxidant gene expression in mouse strains under hyperoxia

It is known that the expression of antioxidant enzyme genes is stimulated by oxidative stress [65]. Therefore, we hypothesized that hyperoxia exposure would induce a lung antioxidant response in developing lungs. We further postulated that the five mouse strains would express their antioxidant response differently towards hyperoxia, depending on their susceptibility. If a strain is more susceptible to hyperoxia, it may not be capable of adequately engaging the antioxidant machinery to counteract oxidative stress since antioxidants form a defence mechanism against it [54]. Therefore, in this study, we investigated the expression of a range of genes that encode antioxidant enzymes and selected protein expression. The major antioxidant enzymes, superoxide dismutases, catalase and glutathione peroxidase, play a fundamental role in the antioxidant defence of the lung [57]. These enzymes are also considered first-line defence antioxidants, meaning that they actively prevent the formation of free radicals or reactive species in cells [76].

Superoxide dismutase (SOD) is considered the most potent antioxidant in cells, playing a crucial role in protecting against injury by reactive oxygen species (ROS) [77],[76]. Superoxide, the primary ROS, is produced as a by-product of oxygen metabolism [57]. SOD catalyzes the dismutation of two molecules of superoxide anion free radical (O_2^-) into molecular oxygen (O_2) and hydrogen peroxide (H_2O_2), which serves as its counterpart [76]. In mammals, SOD exists in three isoforms, SOD1, SOD2, and SOD3 [76], [78]. SOD3 or EC-SOD has been shown to have a protective function in the lungs and plays a significant role in reducing the harmful impacts of hyperoxia on lung alveolization [79]. Zelko et al. demonstrated that SOD3 mRNA levels were undetectable until late gestation in mice and rats, indicating that SOD3 is essential for protecting fetal lungs against hyperoxia after birth [78]. SOD1, or CuZn-SOD, and SOD2, or Mn-SOD, have also been shown to play a role in protecting against hyperoxia-induced pulmonary toxicity [80], [81]. Research conducted in mice have suggested that SOD2 might not play a substantial role in modulating the impact of hyperoxia on lung alveolarization. It is crucial to acknowledge that this observation is limited to mice and may not generalize to other organisms or experimental models [82].

In our study, we observed that hyperoxia exposure resulted in an increase or no change in the mRNA levels encoding SOD1, SOD2, and SOD3 in all strains that we investigated. The expression of SOD3 mRNA and the protein expression level correlated in all strains, except for the BALB/cJ mouse pups. Interestingly, in the case of BALB/cJ mice, we discovered a discrepancy between the measured levels of SOD3 protein and the *Sod3* gene mRNA levels. Specifically, we observed an increase in SOD3 protein levels despite no corresponding increase in *Sod3* gene mRNA levels. Also, Zelko et al. found an interesting discrepancy between the enzymatic activity and protein level of SOD3. They documented the expression pattern of SOD3 in the lung of rabbits at various developmental stages, from preterm to adulthood. Interestingly, they observed that while the activity of SOD3 increased nearly sixfold from the preterm stage to adulthood, the protein level of SOD3 remained relatively constant during these developmental transitions. [78]. The reason behind this discrepancy between enzymatic activity and protein level of SOD3 is not fully understood. One possible explanation suggested by Zelko et al. is that a portion of the intracellularly localized SOD3 protein may be inactive. They noted that the localization of SOD3 shifts from intracellular compartments in fetuses to extracellular spaces after birth and into adulthood, which could contribute to changes in its functionality [78].

Other two major antioxidant enzymes, glutathione peroxidase and catalase scavenge hydrogen peroxide (H_2O_2) generated by the dismutation reaction of SOD [83], [84]. The mRNA levels of *Gpx1*, which encodes for glutathione peroxidase, were increased in the C57BL/6J, BALB/cJ, and FVB/NJ strains after hyperoxia exposure and remained unchanged in the other strains, which is consistent with its protective function. In contrast, the mRNA levels of *Cat*, which encodes catalase, were noted to decrease or remain unchanged after hyperoxia exposure, while previous studies had documented an increase in catalase levels [85], [86]. The reason for this discrepancy is unclear.

Antioxidants such as heme oxygenase-1, redox proteins including thioredoxin (TXN1), thioredoxin reductase (TXNRD), peroxiredoxins (PRDX), and other glutathione-metabolizing lung enzymes (glutathione synthetase, glutathione-disulfide reductase) play a crucial role in the pulmonary antioxidant defenses [57] and have been investigated in this study. Glutathione synthetase and glutathione-disulfide reductase are further glutathione metabolizing lung enzymes next to glutathione peroxidase. The lung

mRNA levels of *Gss* (encoding for glutathione synthetase) increased in C57BL/6J, BALB/cJ, and DBA/2J strains. Consistent with this finding, we also observed an increase in GSS protein levels in all five mouse strains after hyperoxia exposure. However, the lung mRNA levels of *Gsr* (encoding for glutathione-disulfide reductase) were unchanged in all strains except in the FVB/NJ strain after hyperoxia exposure. Disturbances to glutathione dynamics were noted in previous studies with hyperoxia-exposed newborn rat lungs, where glutathione-disulfide reductase remained unchanged throughout hyperoxia exposure at any time point [87]. Another study reported that overexpression of glutathione reductase in alveolar type II cells in adult mice did not protect against hyperoxic lung injury and that the mice were even more susceptible to hyperoxic lung injury. However, no neonatal mice were used in this study [88]. These findings suggest that a higher glutathione disulfide level in the lung does not significantly protect against hyperoxia-induced pulmonary toxicity. [88]. Further research is needed to establish the role of the glutathione metabolizing machinery. Thioredoxin (TXN) is an antioxidant protein that acts as a protein reductase by cysteine thiol-disulfide exchange [89] and forms the TRX system together with two thioredoxin reductase isozymes (TXNRD). Thioredoxin reductase is the only enzyme that catalyzes the reduction of thioredoxin [90]. TXN can also act as a direct antioxidant by reducing the reactive oxygen species hydrogen peroxide (H_2O_2) through the enzyme TRX peroxidases, also known as peroxiredoxin [91]. Previous studies have shown the importance of the TRX system in protecting against hyperoxia-induced injuries [89], [92].

TRX transgenic (TRX-Tg) mice, which carry an overexpressed human TRX gene driven by the β -actin promoter, as well as mice that are systemically administered recombinant human TRX, have demonstrated remarkable resistance to injury across a range of human disease models [93]. These diseases include viral pneumonia [94], acute lung injury [95], myocarditis [96] and chronic obstructive pulmonary disease (COPD) [97].

In a recent study, the impact of TRX on hyperoxic lung injury was investigated using newborn mice with TRX transgene (TRX-Tg) and wildtype (WT) mice. These mice were exposed to either 21% or 95% O_2 for a duration of four days. The findings revealed that newborn TRX-Tg mice displayed a reduced incidence of hyperoxic lung injury compared to the newborn WT mice. This favorable outcome in lung development can be attributed to TRX's ability to suppress proinflammatory cytokines [93].

In another investigation Das et al. investigated the effects of hyperoxia exposure (90% O₂) for four days on thioredoxin-deficient mice and mice overexpressing TRX (TRX-Tg). Thioredoxin-deficient mice failed to recover and showed high mortality, decreased mitochondrial energy metabolism, increased p53, and increased synthesis of proinflammatory cytokines. On the other hand, mice overexpressing TRX (TRX-Tg) were resilient to hyperoxia-induced lung injury and displayed reduced harmful effects [89].

In conclusion, the findings from various studies consistently demonstrate that thioredoxin (TRX) plays a protective role against hyperoxia-induced lung injury, as evidenced by decreased occurrence of lung damage, lower mortality rates, preserved mitochondrial energy metabolism, and reduced synthesis of proinflammatory cytokines in TRX-overexpressing mice compared to deficient mice.

The potential utilization of TRX as a biomarker in human samples, such as serum or tracheal aspirates, for assessing the development and severity of BPD should be considered and investigated [93]. Further research is necessary to conduct preclinical studies in animal models of BPD, aiming to evaluate the effectiveness of recombinant human TRX as a treatment option [93].

Further studies by Li et al. reported that aurothioglucose inhibition of thioredoxin reductase-1 (TXNRD1) attenuates neonatal hyperoxic lung injury through activation of nuclear factor E2-related factor 2 (NFE2L2) using the C3H/HeN mouse model [92]. NFE2L2 activation increases the transcription of many classical antioxidants, controls the expression of genes encoding antioxidants, and has a protective function against oxidative stress, contributing to normal lung maturation [92], [98]. Interestingly, a follow-up study by Li et al. reported that aurothioglucose had different effects when comparing the C57BL/6 and C3H/HeN strain [99]. Although aurothioglucose inhibited TXNRD1 activity and moderately attenuated hyperoxia-induced septal wall thickening in the C57BL/6 models, it did not activate NFE2L2 or attenuate neonatal hyperoxic lung injury, such as improving alveolarization, as it did in the hyperoxia-exposed C3H/HeN models [99]. These findings suggest a strain-dependent response, indicating that the effects of aurothioglucose differ between C3H/HeN and C57BL/6 models. The results of our study indicate a 5.2-fold higher baseline mRNA levels of *Txnrd1* in the C57BL/6J strain than in the C3H/HeJ strain, while the *Txn1* baseline mRNA levels were 155-fold higher in the C3H/HeJ strain than in the C57BL/6J strain. Furthermore,

hyperoxia exposure decreased the lung mRNA levels of *Txn1* in the C3H/HeJ strain, but not in the C57BL/6J strain, while hyperoxia exposure decreased mRNA levels of *Txnrd1* and increased mRNA levels of *Txnrd2* in the C57BL/6J strain, but not the C3H/HeJ strain. Additionally, *Nfe2l2* mRNA levels were decreased by hyperoxia exposure in the C57BL/6J strain, but not in the C3H/HeJ strain. The differences in baseline levels of *Txn1* and *Txnrd1* in the C57BL/6J and C3H/HeJ strain, and the varying strain-dependent impact of hyperoxia on the lung mRNA levels of *Txn1* and *Txnrd1*, might suggest an explanation for the strain-dependent effects of aurothioglucose.

In addition to conventional antioxidants, atypical antioxidants like the three members of the paraoxonase family encoded by *Pon1*, *Pon2* and *Pon3* [100] were also investigated. PON1 and PON3 play an important role as antioxidants in preventing oxidative modification of low-density lipoprotein (LDL) [101], while PON2 has been shown to protect cells against oxidative damage [102].

Notably, in response to hyperoxia exposure, the DBA/2J strain exhibited an upregulation of *Pon1*, *Pon2*, and *Pon3* expression, suggesting their potential role in combating oxidative stress. On the other hand, the C57BL/6J and BALB/cJ strains specifically upregulated *Pon2* expression in response to hyperoxia. Future studies should delve deeper into the role of PON in arrested alveolarization to better understand its contribution to lung development and explore its therapeutic implications.

Overall, the collected results demonstrated a strain dependency in postnatal lung maturation through hyperoxia exposure in different inbred mice strains. The C57BL/6J strain appeared to be the most severely affected by hyperoxia, exhibiting major stunting of alveolarization typical for the BPD phenotype. Interestingly, despite the pronounced lung phenotype, the C57BL/6J strain demonstrated a significant upregulation of various antioxidants, including SOD1, SOD2, SOD3, GSS, GPX, PON2, TXNRD2, and PRDX6. These antioxidant responses were even more pronounced in the C57BL/6J strain compared to the other strains, suggesting a complex interplay between oxidative stress and antioxidant defense mechanisms specific to this strain. Since antioxidants usually form a defense mechanism against oxidative stress caused by hyperoxia [54], these results might suggest that extensive engagement of antioxidants could lead to lung perturbation in the postnatal maturation of mice. On the contrary, the C57BL/6J strain also strongly downregulated other antioxidants (CAT, TXNRD1, PRDX1) through

hyperoxia exposure. Future research should consider the association between the expression of these three antioxidants and the postnatal lung maturation of mice under hyperoxia exposure.

It is worth considering the use of outbred mouse strains instead of the commonly employed inbred strains in studies on bronchopulmonary dysplasia (BPD). Inbred strains are extensively utilized in laboratory research worldwide [103] due to their reduced genetic variability, which enhances the reproducibility of studies [44].

However, the human population exhibits genetic diversity, leading some researchers to propose that outbred strains may offer a more accurate model [104]. In fact, a study reported that outbred mice exhibit phenotypic stability in experiments comparable to, and sometimes even greater than, inbred mice. This could be attributed to their biological system appearing to be less vulnerable to environmental variations, resulting in improved reproducibility [104]. These novel insights highlight the potential benefits of incorporating outbred mouse strains in future studies to enhance our understanding of BPD pathogenesis and improve translational relevance.

6. Conclusion

The findings from our study indicate that the genetic background of five different inbred mouse strains (C57BL/6J, BALB/cJ, FVB/NJ, C3H/HeJ, and DBA/2J) has a significant impact on the postnatal maturation of lung architecture when exposed to normoxia (21% O₂) or hyperoxia (85% O₂) for 14 days after birth. Our data suggest that hyperoxia-driven perturbations on lung maturation are strain-dependent, with the C57BL/6J strain being the most severely affected by hyperoxia, showing the greatest changes in alveolar density and size. Moreover, we observed a discrepancy in the baseline gene expression of the lung antioxidant machinery and the gene expression after exposure to hyperoxia among the different strains.

Our study highlights the importance of considering the genetic background of mice in studies investigating lung development and the impact of environmental stressors such as hyperoxia. Further research is needed to determine how the lung antioxidant machinery influences the strain-dependent hyperoxia-driven perturbations on lung maturation. In summary, our study demonstrates that the genetic background of mice significantly influences the response of the lungs to hyperoxia, shedding light on the complex interplay between genetics and environmental factors in lung development.

7. Summary

Bronchopulmonary dysplasia (BPD) is a common complication of preterm birth that can cause significant morbidity and mortality in neonates. Despite identifying several risk factors and causes, the exact pathogenesis of BPD remains unclear, and further research is needed to understand it. Animal models are commonly used to study BPD to simulate the condition and test different stimuli, but the use of various mouse strains can sometimes yield conflicting results. Several reports suggest that the mouse strain used in experimental studies is a critical factor that can impact the results and data obtained and should therefore be carefully considered during experiment design and interpretation.

As a result, there is a pressing need for a comparative analysis of lung alveolarization and the gene expression of critical mediators of the lung antioxidant response in various commonly used mouse strains. By conducting such analyses, researchers can make informed decisions on the most appropriate mouse strain to employ in BPD studies.

To this end, this study conducted a comprehensive comparison of lung alveolarization and the gene expression of key mediators of the lung antioxidant response in six commonly used inbred mouse strains (C57BL/6J, BALB/cJ, FVB/NJ, C3H/HeJ, DBA/2J and 129S2/SvPasOrlRj). The mice were exposed to normoxic or hyperoxic conditions for the first 14 days of postnatal life. Lung perturbation was evaluated using design-based stereology. Gene expression of the lung antioxidant response was assessed using real-time reverse transcriptase polymerase chain reaction and immunoblot.

The study revealed that hyperoxia caused varying degrees of changes in lung architecture in all five mouse strains, with the C57BL/6J strain being the most sensitive to hyperoxia. The C57BL/6J strain showed the most significant changes in terms of alveoli number, alveoli density, mean linear intercept (MLI), and lung volume. In contrast, the FVB/NJ strain demonstrated the most significant increase in septal thickness following exposure to hyperoxia, while the C57BL/6J strain was the least affected in this aspect. Additionally, the C3H/cj strain showed the smallest degree of change in terms of alveolar density and mean linear intercept (MLI).

Additionally, the gene expression of key mediators of the lung antioxidant response exhibited variations among the different strains, indicating a strain-dependent influence. The C57BL/6J strain showed the most significant alterations in gene expression, with a notable upregulation of a wide range of antioxidants such as SOD1, SOD2, SOD3, GSS, GPX, PON2, TXNRD2, and PRDX6 compared to the other strains. Baseline gene

expression also differed among the strains under normoxic and hyperoxic conditions. In conclusion, this study shows that the mouse genetic background significantly affects the outcome of lung development under the influence of hyperoxia.

8. Zusammenfassung

Die bronchopulmonale Dysplasie (BPD) ist nach wie vor eine der häufigsten Frühgeburtskomplikationen, die zu erheblicher Morbidität und Mortalität auf neonatalen Intensivstationen führt. Obwohl bereits mehrere Ursachen und Risikofaktoren für die BPD identifiziert wurden, fehlt es noch immer an genauen Erkenntnissen über den Pathomechanismus. Daher besteht ein dringender Bedarf an weiterer Forschung auf diesem Gebiet. Zur Durchführung solcher Studien werden oft Tiermodelle verwendet, bei denen verschiedene Faktoren wie die Hyperoxie eingesetzt werden, um den Phänotyp von Patienten mit BPD nachzuahmen. Aktuell gibt es jedoch kein Konsens darüber, welcher Mausstamm am ehesten für BPD-Studien geeignet sind. Teilweise ergeben sich widersprüchliche Daten. Verschiedene Berichte weisen darauf hin, dass die Wahl des Mausstammes ein wichtiger Faktor ist, der bei der Planung und Interpretation von Experimenten zu berücksichtigen ist. Es ist daher von großer Bedeutung, einen detaillierten Vergleich der Lungenalveolarisation und der Genexpression von Schlüsselmediatoren der antioxidativen Reaktion in häufig verwendeten Mausstämmen durchzuführen. Durch einen solchen Vergleich können fundierte Entscheidungen getroffen werden, welcher Mausstamm am besten geeignet ist, um die BPD zu untersuchen und die Ergebnisse korrekt zu interpretieren.

In dieser Studie wurde ein umfassender Vergleich der Lungenalveolarisation und der Genexpression von Schlüsselmediatoren der antioxidativen Reaktion der Lunge in sechs häufig verwendeten Mausstämmen (C57BL/6J, BALB/cJ, FVB/NJ, C3H/HeJ, DBA/2J und 129S2/SvPasOrlRj) durchgeführt. Hierzu wurden fünf verschiedene Stämme in den ersten 14 Tagen nach der Geburt normoxischen (21% O₂) oder hyperoxischen (85% O₂) Bedingungen ausgesetzt. Die daraus resultierte Lungenentwicklungsstörung wurde mittels design-basierter Stereologie beurteilt. Die Quantifizierung der Genexpression der antioxidativen Reaktion der Lunge wurde mittels Real-Time PCR und Immunoblot bewertet.

Bei allen fünf Mäusestämmen führte der schädliche Reiz der Hyperoxie (85% O₂) zu Veränderungen der postnatalen Reifung und zur anomalen Lungenarchitektur, jedoch in unterschiedlichem Ausmaß. Hyperoxie verursachte insbesondere im C57BL/6J- Stamm das grösste Ausmaß an Veränderungen in Bezug auf Alveolenzahl, Alveolendichte,

MLI und Lungenvolumen. Der FVB/NJ-Stamm wies die höchste Zunahme der Septumdicke durch Hyperoxie-Exposition auf, wobei der C57BL/6J- Stamm am wenigsten betroffen war. Der C3H/cj-Stamm zeigte das geringste Ausmaß an Veränderung in Bezug auf alveoläre Dichte und MLI.

Auch die Genexpression von Schlüsselmediatoren der antioxidativen Reaktion in der Lunge auf Hyperoxie war abhängig vom Mausstamm. Besonders im C57BL/6J-Stamm war die Veränderung der Genexpression signifikant. Unter dem Einfluss von Hyperoxie wurden hier eine Vielzahl von Antioxidantien (SOD1, SOD2, SOD3, GSS, GPX, PON2, TXNRD2 und PRDX6) hochreguliert. Die Genexpression variierte in allen fünf Mausstämmen unter normoxischen und hyperoxischen Bedingungen. Zusammenfassend hatte der genetische Hintergrund der Mäuse einen erheblichen Einfluss auf die Ergebnisse der Lungenentwicklung unter Hyperoxie.

9. References

- [1] M. G. Levitzky, *Pulmonary Physiology, Eighth Edition. Madison: McGraw Hill Professional*, 8th ed. McGraw-Hill Education / Medical, 2013.
- [2] E. R. Weibel, *The Pathway for Oxygen: Structure and Function in the Mammalian Respiratory System*, 1st ed. Bern: Harvard University Press, 1984.
- [3] S. Kotecha, "Lung growth for beginners," *Paediatr. Respir. Rev.*, vol. 1, no. 4, pp. 308–313, 2000, doi: 10.1053/prrv.2000.0069.
- [4] P. H. Burri, "Structural aspects of postnatal lung development - Alveolar formation and growth," *Biol. Neonate*, vol. 89, no. 4, pp. 313–322, 2006, doi: 10.1159/000092868.
- [5] P. H. Burri, "Fetal and Postnatal Development of the Lung," *Annu. Rev. Physiol.*, vol. 46, no. 1, pp. 617–628, 1984, doi: 10.1146/annurev.ph.46.030184.003153.
- [6] I. Mižíková and R. E. Morty, "The extracellular matrix in bronchopulmonary dysplasia: Target and source," *Front. Med.*, vol. 2, no. DEC, pp. 1–20, 2015, doi: 10.3389/fmed.2015.00091.
- [7] S. Joshi and S. Kotecha, "Lung growth and development," *Early Hum. Dev.*, vol. 83, no. 12, pp. 789–794, 2007, doi: 10.1016/j.earlhumdev.2007.09.007.
- [8] C. M. Chao, E. El Agha, C. Tiozzo, P. Minoo, and S. Bellusci, "A breath of fresh air on the mesenchyme: Impact of impaired mesenchymal development on the pathogenesis of bronchopulmonary dysplasia," *Front. Med.*, vol. 2, no. APR, pp. 1–13, 2015, doi: 10.3389/fmed.2015.00027.
- [9] P. K. Jeffery, "The development of large and small airways," *Am. J. Respir. Crit. Care Med.*, vol. 157, no. 5 II SUPPL., 1998, doi: 10.1164/ajrccm.157.5.rsaa-1.
- [10] P. H. Burri, "The Postnatal Growth of the Rat Lung III," *Anat. Rec.*, vol. 180, pp. 77–98, 1973.
- [11] S. Kotecha, "Lung growth: Implications for the newborn infant," *Arch. Dis. Child. Fetal Neonatal Ed.*, vol. 82, no. 1, pp. 69–75, 2000, doi: 10.1136/fn.82.1.F69.
- [12] W. H. Northway, R. Rosan, and D. Porter, "Pulmonary disease following respirator therapy of hyaline-membrane disease. Bronchopulmonary dysplasia.," *N. Engl. J. Med.*, pp. 276(7):357-368., 1967, doi: 10.1056/NEJM196702162760701.
- [13] J. Y. Islam, R. L. Keller, J. L. Aschner, T. V. Hartert, and P. E. Moore, "Understanding the short- and long-term respiratory outcomes of prematurity and bronchopulmonary dysplasia," *Am. J. Respir. Crit. Care Med.*, vol. 192, no. 2, pp. 134–156, 2015, doi: 10.1164/rccm.201412-2142PP.
- [14] M. C. Walsh *et al.*, "Summary proceedings from the bronchopulmonary dysplasia group," *Pediatrics*, vol. 117, no. 3, 2006, doi: 10.1542/peds.2005-

- 0620I.
- [15] J. Gien and J. P. Kinsella, "Pathogenesis and treatment of bronchopulmonary dysplasia," *Curr. Opin. Pediatr.*, vol. 23, no. 3, pp. 305–313, 2011, doi: 10.1097/MOP.0b013e328346577f.
- [16] T. Shahzad, S. Radajewski, C.-M. Chao, S. Bellusci, and H. Ehrhardt, "Pathogenesis of bronchopulmonary dysplasia: when inflammation meets organ development," *Mol. Cell. Pediatr.*, vol. 3, no. 1, 2016, doi: 10.1186/s40348-016-0051-9.
- [17] J. Balany and V. Bhandari, "Understanding the impact of infection, inflammation, and their persistence in the pathogenesis of bronchopulmonary dysplasia," *Front. Med.*, vol. 2, no. December, pp. 1–10, 2015, doi: 10.3389/fmed.2015.00090.
- [18] L. Gortner *et al.*, "Rates of bronchopulmonary dysplasia in very preterm neonates in Europe: Results from the MOSAIC cohort," *Neonatology*, vol. 99, no. 2, pp. 112–117, 2011, doi: 10.1159/000313024.
- [19] C. Siffel, K. D. Kistler, J. F. M. Lewis, and S. P. Sarda, "Global incidence of bronchopulmonary dysplasia among extremely preterm infants: a systematic literature review.," *J. Matern. neonatal Med. Off. J. Eur. Assoc. Perinat. Med. Fed. Asia Ocean. Perinat. Soc. Int. Soc. Perinat. Obstet.*, vol. 34, no. 11, pp. 1721–1731, Jun. 2021, doi: 10.1080/14767058.2019.1646240.
- [20] L. Gortner and S. Meyer, "Die Bronchopulmonale Dysplasie Frühgeborener: Pathophysiologie, Klinik, Diagnostik und Therapie," *Intensivmed. und Notfallmedizin*, vol. 44, no. 8, pp. 475–485, 2007, doi: 10.1007/s00390-007-0808-4.
- [21] W. H. Northway *et al.*, "Late Pulmonary Sequelae of Bronchopulmonary Dysplasia," *N. Engl. J. Med.*, vol. 323, no. 26, pp. 1793–1799, 1990.
- [22] L. Didon, A. B. Roos, G. P. Elmberger, F. J. Gonzalez, and M. Nord, "Lung-specific inactivation of CCAAT/enhancer binding protein α causes a pathological pattern characteristic of COPD," *Eur. Respir. J.*, vol. 35, no. 1, pp. 186–197, 2010, doi: 10.1183/09031936.00185008.
- [23] J. Stocks, A. Hislop, and S. Sonnappa, "Early lung development: Lifelong effect on respiratory health and disease," *Lancet Respir. Med.*, vol. 1, no. 9, pp. 728–742, 2013, doi: 10.1016/S2213-2600(13)70118-8.
- [24] K. Beam, S. Aliaga, S. K. Ahlfeld, M. Cohen-Wolkowicz, B. Smith, and M. M. Laughon, "A systematic review of randomized controlled trials for the prevention of bronchopulmonary dysplasia in infants," *J. Perinatol.*, vol. 34, no. 9, pp. 705–710, 2014, doi: 10.1038/jp.2014.126.
- [25] W. A. Carlo *et al.*, "Association of antenatal corticosteroids with mortality and neurodevelopmental outcomes among infants born at 22 to 25 weeks' gestation," *Obstet. Gynecol. Surv.*, vol. 67, no. 4, pp. 215–217, 2012, doi: 10.1097/OGX.0b013e31825021ef.
- [26] L. W. Doyle, J. L. Cheong, S. Hay, B. J. Manley, and H. L. Halliday, "Late (≥ 7

- days) systemic postnatal corticosteroids for prevention of bronchopulmonary dysplasia in preterm infants.,” *Cochrane database Syst. Rev.*, vol. 11, no. 11, p. CD001145, Nov. 2021, doi: 10.1002/14651858.CD001145.pub5.
- [27] M. J. Goetz *et al.*, “Msc based therapies to prevent or treat bpd—a narrative review on advances and ongoing challenges,” *Int. J. Mol. Sci.*, vol. 22, no. 3, pp. 1–27, 2021, doi: 10.3390/ijms22031138.
- [28] R. A. Polin *et al.*, “Surfactant replacement therapy for preterm and term neonates with respiratory distress,” *Pediatrics*, vol. 133, no. 1, pp. 156–163, 2014, doi: 10.1542/peds.2013-3443.
- [29] N. Claure and E. Bancalari, “Bronchopulmonary Dysplasia: Definitions and Epidemiology,” in *Bronchopulmonary Dysplasia*, vol. 33, no. 6, V. Bhandari, Ed. Switzerland: Springer, 2016, pp. 167–182.
- [30] M. E. De Paepe, “Bronchopulmonary Dysplasia: Pathology of bronchopulmonary dysplasia,” in *Bronchopulmonary Dysplasia*, 33rd ed., Switzerland, Ed. Switzerland: Springer, 2016, pp. 149–164.
- [31] J. A. Voynow, “‘New’ bronchopulmonary dysplasia and chronic lung disease,” *Paediatr. Respir. Rev.*, vol. 24, pp. 17–18, 2017, doi: 10.1016/j.prrv.2017.06.006.
- [32] A. J. Jobe, “The New BPD: An Arrest of Lung Development,” *Pediatr. Res.*, vol. 46(6), pp. 641–643, 1999, doi: 10.1203/00006450-199912000-00007.
- [33] F. Mosca, M. Colnaghi, and M. Fumagalli, “BPD: Old and new problems,” *J. Matern. Neonatal Med.*, vol. 24, no. SUPPL. 1, pp. 80–82, 2011, doi: 10.3109/14767058.2011.607675.
- [34] C. M. Alvira and R. E. Morty, “Can We Understand the Pathobiology of Bronchopulmonary Dysplasia?,” *J. Pediatr.*, vol. 190, pp. 27–37, 2017, doi: 10.1016/j.jpeds.2017.08.041.
- [35] A. N. Husain, N. H. Siddiqui, and J. T. Stocker, “Pathology of arrested acinar development in postsurfactant bronchopulmonary dysplasia,” *Hum. Pathol.*, vol. 29, no. 7, pp. 710–717, 1998, doi: 10.1016/S0046-8177(98)90280-5.
- [36] J. Berger and V. Bhandari, “Animal models of bronchopulmonary dysplasia. The term mouse models,” *Am. J. Physiol. - Lung Cell. Mol. Physiol.*, vol. 307, no. 12, pp. L936–L947, 2014, doi: 10.1152/ajplung.00159.2014.
- [37] H. Ehrhardt *et al.*, “Absence of TNF- α enhances inflammatory response in the newborn lung undergoing mechanical ventilation,” *Am. J. Physiol. - Lung Cell. Mol. Physiol.*, vol. 310, no. 10, pp. L909–L918, 2016, doi: 10.1152/ajplung.00367.2015.
- [38] M. O’Reilly and B. Thébaud, “Animal models of bronchopulmonary dysplasia. The term rat models,” *Am. J. Physiol. - Lung Cell. Mol. Physiol.*, vol. 307, no. 12, pp. L948–L958, 2014, doi: 10.1152/ajplung.00160.2014.
- [39] D. M. G. Silva, C. Nardiello, A. Pozarska, and R. E. Morty, “Recent advances in the mechanisms of lung alveolarization and the pathogenesis of bronchopulmonary dysplasia,” *Am. J. Physiol. - Lung Cell. Mol. Physiol.*, vol.

- 309, no. 11, pp. L1239–L1272, 2015, doi: 10.1152/ajplung.00268.2015.
- [40] L. C. Wickramasinghe, P. van Wijngaarden, C. Johnson, E. Tsantikos, and M. L. Hibbs, “An Experimental Model of Bronchopulmonary Dysplasia Features Long-Term Retinal and Pulmonary Defects but Not Sustained Lung Inflammation,” *Front. Pediatr.*, vol. 9, no. August, pp. 1–13, 2021, doi: 10.3389/fped.2021.689699.
- [41] C. Nardiello, I. Mižíková, and R. E. Morty, “Looking ahead: where to next for animal models of bronchopulmonary dysplasia?,” *Cell Tissue Res.*, vol. 367, no. 3, pp. 457–468, 2017, doi: 10.1007/s00441-016-2534-3.
- [42] P. K. H. Chow, R. T. H. Ng, and B. E. Ogden, *Using animal models in biomedical research: a primer for the investigator*. Wspc, 2008.
- [43] L. Silver, “Inbred Strain,” in *Brenner’s Encyclopedia of Genetics: Second Edition*, Elsevier Inc., 2013, pp. 53–53.
- [44] M. F. W. Festing, “Inbred Strains,” in *Encyclopedia of Immunology*, Elsevier, 1998, pp. 1369–1372.
- [45] J. A. Beck *et al.*, “Genealogies of mouse inbred strains,” *Nat. Genet.*, vol. 24, no. 1, pp. 23–25, 2000, doi: 10.1038/71641.
- [46] P. A. Overbeek, *Factors Affecting Transgenic Animal Production*. Elsevier Inc., 2014.
- [47] C. D. Sigmund, “Viewpoint: Are studies in genetically altered mice out of control?,” *Arterioscler. Thromb. Vasc. Biol.*, vol. 20, no. 6, pp. 1425–1429, 2000, doi: 10.1161/01.ATV.20.6.1425.
- [48] J. L. Nichols *et al.*, “Genome-wide association mapping of acute lung injury in neonatal inbred mice,” *FASEB J.*, vol. 28, no. 6, pp. 2538–2550, 2014, doi: 10.1096/fj.13-247221.
- [49] G. S. Whitehead, L. H. Burch, K. G. Berman, C. A. Piantadosi, and D. A. Schwartz, “Genetic basis of murine responses to hyperoxia-induced lung injury,” *Immunogenetics*, vol. 58, no. 10, pp. 793–804, Oct. 2006, doi: 10.1007/s00251-006-0147-9.
- [50] K. J. Beauchemin *et al.*, “Temporal dynamics of the developing lung transcriptome in three common inbred strains of laboratory mice reveals multiple stages of postnatal alveolar development,” *PeerJ*, vol. 2016, no. 9, p. e2318, Aug. 2016, doi: 10.7717/PEERJ.2318.
- [51] B. A. Freeman and J. D. Crapo, “Biology of disease: free radicals and tissue injury,” *Lab. Investig.*, 1982.
- [52] J. K. Miller, E. Brzezinska-Slebodzinska, and F. C. Madsen, “Oxidative Stress, Antioxidants, and Animal Function,” *J. Dairy Sci.*, vol. 76, no. 9, pp. 2812–2823, 1993, doi: 10.3168/jds.S0022-0302(93)77620-1.
- [53] W. F. Petrone, D. K. English, K. Wong, and J. M. McCord, “Free radicals and inflammation: Superoxide-dependent activation of a neutrophil chemotactic

- factor in plasma,” *Proc. Natl. Acad. Sci. U. S. A.*, vol. 77, no. 2 II, pp. 1159–1163, 1980, doi: 10.1073/pnas.77.2.1159.
- [54] H. Sies, “Oxidative stress: Oxidants and antioxidants,” *Exp. Physiol.*, vol. 82, no. 2, pp. 291–295, 1997, doi: 10.1113/expphysiol.1997.sp004024.
- [55] B. Salehi *et al.*, “Antioxidants: Positive or negative actors?,” *Biomolecules*, vol. 8, no. 4, pp. 1–11, 2018, doi: 10.3390/biom8040124.
- [56] A. I. Khlebnikov, I. A. Schepetkin, N. G. Domina, L. N. Kirpotina, and M. T. Quinn, “Improved quantitative structure-activity relationship models to predict antioxidant activity of flavonoids in chemical, enzymatic, and cellular systems,” *Bioorganic Med. Chem.*, vol. 15, no. 4, pp. 1749–1770, 2007, doi: 10.1016/j.bmc.2006.11.037.
- [57] E. Birben, “Oxidative, stress and antioxidants?,” *World Allergy Organ. J.*, vol. 44, no. 5, pp. 219–224, 2009, doi: 10.1016/j.cnd.2009.09.001.
- [58] Y. S. Ho, M. S. Dey, and J. D. Crapo, “Antioxidant enzyme expression in rat lungs during hyperoxia,” *Am. J. Physiol. - Lung Cell. Mol. Physiol.*, vol. 270, no. 5 14-5, 1996, doi: 10.1152/ajplung.1996.270.5.1810.
- [59] R. P. Michel and L. M. Cruz-Orive, “Application of the Cavalieri principle and vertical sections method to lung: estimation of volume and pleural surface area,” *J. Microsc.*, vol. 150, no. 2, pp. 117–136, 1988, doi: 10.1111/j.1365-2818.1988.tb04603.x.
- [60] C. C. W. Hsia, D. M. Hyde, M. Ochs, and E. R. Weibel, “An official research policy statement of the American Thoracic Society/European Respiratory Society: Standards for quantitative assessment of lung structure,” *Am. J. Respir. Crit. Care Med.*, vol. 181, no. 4, pp. 394–418, 2010, doi: 10.1164/rccm.200809-1522ST.
- [61] “What is the threshold cycle or Ct value? - QIAGEN.” <https://www.qiagen.com/us/resources/faq?id=783d4566-9ad9-4fab-9936-182beda65617&lang=en> (accessed Aug. 01, 2020).
- [62] M. Bradford, “A rapid and sensitive method for the quantitation of microgram quantities of protein utilizing the principle of protein-dye binding,” *Anal. Biochem.*, vol. 72, no. 1–2, pp. 248–254, 1976, doi: 10.1016/0003-2697(76)90527-3.
- [63] P. M. Petkov *et al.*, “An efficient SNP system for mouse genome scanning and elucidating strain relationships,” *Genome Res.*, vol. 14, no. 9, pp. 1806–1811, 2004, doi: 10.1101/gr.2825804.
- [64] J. Tiono *et al.*, “Mouse genetic background impacts susceptibility to hyperoxia-driven perturbations to lung maturation,” *Pediatr. Pulmonol.*, vol. 54, no. 7, pp. 1060–1077, 2019, doi: 10.1002/ppul.24304.
- [65] B. Maitre, L. Jornot, and A. F. Junod, “Effects of inhibition of catalase and superoxide dismutase activity on antioxidant enzyme mRNA levels,” *Am. J. Physiol. - Lung Cell. Mol. Physiol.*, vol. 265, no. 6 9-6, 1993, doi: 10.1152/ajplung.1993.265.6.1636.

- [66] L. Garibyan and N. Avashia, "Polymerase chain reaction," *J. Invest. Dermatol.*, vol. 133, no. 3, pp. 1–4, 2013, doi: 10.1038/jid.2013.1.
- [67] H. D. VanGuilder, K. E. Vrana, and W. M. Freeman, "Twenty-five years of quantitative PCR for gene expression analysis," *Biotechniques*, vol. 44, no. 5, pp. 619–626, 2008, doi: 10.2144/000112776.
- [68] B. T. Kurien and R. H. Scofield, "Chapter 3 Introduction to Protein Blotting," *Methods*, vol. 536, no. 4, doi: 10.1007/978-1-59745-542-8.
- [69] R. Ghosh, J. E. Gilda, and A. V. Gomes, "The necessity of and strategies for improving confidence in the accuracy of western blots," *Expert Rev. Proteomics*, vol. 11, no. 5, pp. 549–560, 2014, doi: 10.1586/14789450.2014.939635.The.
- [70] S. Leary, P. Das, D. Ponnalagu, H. Singh, and V. Bhandari, "Genetic Strain and Sex Differences in a Hyperoxia-Induced Mouse Model of Varying Severity of Bronchopulmonary Dysplasia," *Am. J. Pathol.*, vol. 189, no. 5, pp. 999–1014, 2019, doi: 10.1016/j.ajpath.2019.01.014.
- [71] C. Nardiello, J. Ruiz-Camp, W. Seeger, and R. E. Morty, "The role of miR-135b in normal and aberrant post-natal lung development," p. OA3230, 2017, doi: 10.1183/1393003.congress-2017.oa3230.
- [72] J. C. F. de Winter, "Using the student's t-test with extremely small sample sizes," *Pract. Assessment, Res. Eval.*, vol. 18, no. 10, pp. 1–12, 2013.
- [73] B. B. Hudak, L. Y. Zhang, and S. R. Kleeberger, "Inter-strain variation in susceptibility to hyperoxic injury of murine airways," *Pharmacogenetics*, vol. 3, no. 3, pp. 135–143, 1993, doi: 10.1097/00008571-199306000-00003.
- [74] S. E. Soutiere, C. G. Tankersley, and W. Mitzner, "Differences in alveolar size in inbred mouse strains," *Respir. Physiol. Neurobiol.*, vol. 140, no. 3, pp. 283–291, 2004, doi: 10.1016/j.resp.2004.02.003.
- [75] E. R. Weibel, C. C. W. Hsia, and M. Ochs, "How much is there really? Why stereology is essential in lung morphometry," *J. Appl. Physiol.*, vol. 102, no. 1, pp. 459–467, 2007, doi: 10.1152/jappphysiol.00808.2006.
- [76] O. M. Ighodaro and O. A. Akinloye, "First line defence antioxidants-superoxide dismutase (SOD), catalase (CAT) and glutathione peroxidase (GPX): Their fundamental role in the entire antioxidant defence grid," *Alexandria J. Med.*, vol. 54, no. 4, pp. 287–293, Dec. 2018, doi: 10.1016/j.ajme.2017.09.001.
- [77] P. Saxena, K. Selvaraj, S. K. Khare, and N. Chaudhary, "Superoxide dismutase as multipotent therapeutic antioxidant enzyme: Role in human diseases," *Biotechnol. Lett.*, vol. 44, no. 1, pp. 1–22, 2022, doi: 10.1007/s10529-021-03200-3.
- [78] I. N. Zelko, T. J. Mariani, and R. J. Folz, "Superoxide dismutase multigene family: A comparison of the CuZn-SOD (SOD1), Mn-SOD (SOD2), and EC-SOD (SOD3) gene structures, evolution, and expression," *Free Radic. Biol. Med.*, vol. 33, no. 3, pp. 337–349, 2002, doi: 10.1016/S0891-5849(02)00905-X.
- [79] C. Delaney *et al.*, "Lack of EC-SOD worsens alveolar and vascular development

- in a neonatal mouse model of bleomycin-induced bronchopulmonary dysplasia and pulmonary hypertension,” *Pediatr. Res.*, vol. 78, no. 6, pp. 634–640, 2015, doi: 10.1038/pr.2015.166.
- [80] J. R. Wispes *et al.*, “Human Mn-superoxide dismutase in pulmonary epithelial cells of transgenic mice confers protection from oxygen injury,” *J. Biol. Chem.*, vol. 267, no. 33, 1992, doi: 10.1016/S0021-9258(18)35927-1.
- [81] I. Fridavich, “Superoxide radical and superoxide dismutases,” *Annual Review of Biochemistry*, vol. 64. Annual Reviews Inc., pp. 97–112, 1995, doi: 10.1146/annurev.bi.64.070195.000525.
- [82] A. Gupta, M. Perez, K. Jin Lee, J. M. Taylor, and K. N. Farrow, “SOD2 Activity Is not Impacted by Hyperoxia in Murine Neonatal Pulmonary Artery Smooth Muscle Cells and Mice,” *Int. J. Mol. Sci.*, vol. 16, pp. 6373–6390, 2015, doi: 10.3390/ijms16036373.
- [83] D. E. Handy and J. Loscalzo, “The role of glutathione peroxidase-1 in health and disease,” *Free Radic. Biol. Med.*, vol. 188, no. April, pp. 146–161, 2022, doi: 10.1016/j.freeradbiomed.2022.06.004.
- [84] Y. S. Ho, M. S. Dey, and J. D. Crapo, “Antioxidant enzyme expression in rat lungs during hyperoxia,” *Am. J. Physiol. - Lung Cell. Mol. Physiol.*, vol. 270, no. 5 14-5, May 1996, doi: 10.1152/ajplung.1996.270.5.1810.
- [85] M. Hoffman, J. B. Stevens, and A. P. Autor, “Adaptation to hyperoxia in the neonatal rat: Kinetic parameters of the oxygen-mediated induction of lung superoxide dismutases, catalase and glutathione peroxidase,” *Toxicology*, vol. 16, no. 3, pp. 215–225, 1980, doi: 10.1016/0300-483X(80)90118-3.
- [86] R. J. Folz, A. M. Abushamaa, and H. B. Suliman, “Extracellular superoxide dismutase in the airways of transgenic mice reduces inflammation and attenuates lung toxicity following hyperoxia,” *J. Clin. Invest.*, vol. 103, no. 7, pp. 1055–1066, 1999, doi: 10.1172/JCI3816.
- [87] K. A. Kennedy and N. L. Lane, “Effect of in vivo hyperoxia on the glutathione system in neonatal rat lung,” *Exp. Lung Res.*, vol. 20, no. 1, pp. 73–83, 1994, doi: 10.3109/01902149409064374.
- [88] K. M. Heyob, L. K. Rogers, and S. E. Welty, “Glutathione reductase targeted to type II cells does not protect mice from hyperoxic lung injury,” *Am. J. Respir. Cell Mol. Biol.*, vol. 39, no. 6, pp. 683–688, 2008, doi: 10.1165/rcmb.2008-0112OC.
- [89] K. C. Das, “Thioredoxin-deficient mice, a novel phenotype sensitive to ambient air and hypersensitive to hyperoxia-induced lung injury,” *Am. J. Physiol. - Lung Cell. Mol. Physiol.*, vol. 308, pp. 429–442, 2015, doi: 10.1152/ajplung.00285.2014.
- [90] D. Mustacich and G. Powis, “Thioredoxin reductase,” 2000. doi: <https://doi.org/10.1042/bj3460001>.
- [91] A. Holmgren, “Thioredoxin,” *Annu. Rev. Biochem.*, vol. 54, no. 1, pp. 237–271, Jun. 1985, doi: <https://doi.org/10.1146/annurev.bi.54.070185.001321>.

- [92] Q. Li *et al.*, “Thioredoxin Reductase Inhibition Attenuates Neonatal Hyperoxic Lung Injury and Enhances Nuclear Factor E2-Related Factor 2 Activation,” *Am. J. Physiol. Cell. Mol. Physiol.*, vol. 55, pp. 419–428, 2016, doi: 10.1165/rcmb.2015-0228OC.
- [93] N. Nagano *et al.*, “Attenuation of hyperoxic lung injury in newborn thioredoxin-1-overexpressing mice through the suppression of proinflammatory cytokine mRNA expression,” *Biomedicines*, vol. 8, no. 3, 2020, doi: 10.3390/biomedicines8030066.
- [94] H. Nakamura, S. Tamura, I. Watanabe, T. Iwasaki, and J. Yodoi, “Enhanced resistancy of thioredoxin-transgenic mice against influenza virus-induced pneumonia,” *Immunol. Lett.*, vol. 82, no. 1, pp. 165–170, 2002, doi: [https://doi.org/10.1016/S0165-2478\(02\)00033-0](https://doi.org/10.1016/S0165-2478(02)00033-0).
- [95] M. Kaimul Ahsan, H. Nakamura, M. Tanito, K. Yamada, H. Utsumi, and J. Yodoi, “Thioredoxin-1 suppresses lung injury and apoptosis induced by diesel exhaust particles (DEP) by scavenging reactive oxygen species and by inhibiting DEP-induced downregulation of Akt,” *Free Radic. Biol. Med.*, vol. 39, no. 12, pp. 1549–1559, 2005, doi: <https://doi.org/10.1016/j.freeradbiomed.2005.07.016>.
- [96] K. Shioji, H. Nakamura, H. Masutani, and J. Yodoi, “Redox Regulation by Thioredoxin in Cardiovascular Diseases,” *Antioxid. Redox Signal.*, vol. 5, no. 6, pp. 795–802, Dec. 2003, doi: 10.1089/152308603770380106.
- [97] A. Sato *et al.*, “Thioredoxin-1 Ameliorates Cigarette Smoke-Induced Lung Inflammation and Emphysema in Mice,” *J. Pharmacol. Exp. Ther.*, vol. 325, no. 2, pp. 380 LP – 388, May 2008, doi: 10.1124/jpet.107.134007.
- [98] T. Nguyen, P. Nioi, and C. B. Pickett, “The Nrf2-Antioxidant Response Element Signaling Pathway and Its Activation by Oxidative Stress * ARE-mediated Pathway,” *J. Biol. Chem.*, 2009, doi: 10.1074/jbc.R900010200.
- [99] Q. Li *et al.*, “Aurothioglucose does not improve alveolarization or elicit sustained Nrf2 activation in C57BL/6 models of bronchopulmonary dysplasia,” *Am. J. Physiol. Cell. Mol. Physiol.*, vol. 314, pp. 736–742, 2018, doi: 10.1152/ajplung.00539.
- [100] N. Martinelli, L. Consoli, D. Girelli, E. Grison, R. Corrocher, and O. Olivieri, *Paraoxonases. Ancient Substrate Hunters and Their Evolving Role in Ischemic Heart Disease*, 1st ed., vol. 59. Elsevier Inc., 2013.
- [101] S. T. Reddy *et al.*, “Human Paraoxonase-3 Is an HDL-Associated Enzyme With Biological Activity Similar to Paraoxonase-1 Protein but Is Not Regulated by Oxidized Lipids,” *Arterioscler. Thromb. Vasc. Biol.*, 2001, doi: 10.1161/01.atv.21.4.542.
- [102] C. J. Ng *et al.*, “Paraoxonase-2 is a ubiquitously expressed protein with antioxidant properties and is capable of preventing cell-mediated oxidative modification of low density lipoprotein,” *J. Biol. Chem.*, 2001, doi: 10.1074/jbc.M105660200.
- [103] M. F. W. Festing, “Evidence Should Trump Intuition by Preferring Inbred Strains

-
- to Outbred Stocks in Preclinical Research,” *ILAR J.*, 2014, doi: 10.1093/ilar/ilu036.
- [104] A. H. Tuttle, V. M. Philip, E. J. Chesler, and J. S. Mogil, “Comparing phenotypic variation between inbred and outbred mice,” *Nat. Methods*, vol. 15, no. 12, pp. 994–996, 2018, doi: 10.1038/s41592-018-0224-7.

10. Declaration

Erklärung zur Dissertation

„Hiermit erkläre ich, dass ich die vorliegende Arbeit selbständig und ohne unzulässige Hilfe oder Benutzung anderer als der angegebenen Hilfsmittel angefertigt habe. Alle Textstellen, die wörtlich oder sinngemäß aus veröffentlichten oder nichtveröffentlichten Schriften entnommen sind, und alle Angaben, die auf mündlichen Auskünften beruhen, sind als solche kenntlich gemacht. Bei den von mir durchgeführten und in der Dissertation erwähnten Untersuchungen habe ich die Grundsätze guter wissenschaftlicher Praxis, wie sie in der „Satzung der Justus-Liebig-Universität Gießen zur Sicherung guter wissenschaftlicher Praxis“ niedergelegt sind, eingehalten sowie ethische, datenschutzrechtliche und tierschutzrechtliche Grundsätze befolgt. Ich versichere, dass Dritte von mir weder unmittelbar noch mittelbar geldwerte Leistungen für Arbeiten erhalten haben, die im Zusammenhang mit dem Inhalt der vorgelegten Dissertation stehen, oder habe diese nachstehend spezifiziert. Die vorgelegte Arbeit wurde weder im Inland noch im Ausland in gleicher oder ähnlicher Form einer anderen Prüfungsbehörde zum Zweck einer Promotion oder eines anderen Prüfungsverfahrens vorgelegt. Alles aus anderen Quellen und von anderen Personen übernommene Material, das in der Arbeit verwendet wurde oder auf das direkt Bezug genommen wird, wurde als solches kenntlich gemacht. Insbesondere wurden alle Personen genannt, die direkt und indirekt an der Entstehung der vorliegenden Arbeit beteiligt waren. Mit der Überprüfung meiner Arbeit durch eine Plagiatserkennungssoftware bzw. ein internetbasiertes Softwareprogramm erkläre ich mich einverstanden.“

Ort, Datum

Unterschrift

11. Publication directory

Parts of this dissertation were published and presented as a poster at a conference:

Tiono J, Surate Solaligue DE, Mižíková I, Nardiello C, Vadász I, Böttcher-Friebertshäuser E, Ehrhardt H, Herold S, Seeger W, Morty RE. Mouse genetic background impacts susceptibility to hyperoxia-driven perturbations to lung maturation. *Pediatr Pulmonol.* 2019 Jul;54(7):1060-1077. doi: 10.1002/ppul.24304.

Poster Presentation at the American Thoracic Society 2017 International Conference. Washington, DC, United States. Poster Title: Advancements in the biology of bpd and other congenital pediatric lung diseases.

https://www.atsjournals.org/doi/abs/10.1164/ajrccm-conference.2017.195.1_MeetingAbstracts.A6392

12. Acknowledgements

With this concluding part of my dissertation, I seize the opportunity to express my deepest gratitude to Prof. Dr. Rory E. Morty for his unwavering support and guidance throughout the entirety of this project. His mentorship and the chance to work within the Morty Laboratory at the Max Planck Institute for Heart and Lung Research in Bad Nauheim have been instrumental, offering profound insights into the realm of scientific research. I am equally thankful for the invaluable experiences gained from participating in the ATS Congress in Washington, DC, and the MBML retreat, which were both memorable and rich in learning.

Special thanks are extended to Prof. Dr. Werner Seeger for the honor of conducting my dissertation research within the Department of Internal Medicine at Justus-Liebig University Giessen.

My heartfelt appreciation goes out to the entire Morty Laboratory team (David E Surate, Claudio Nardiello, Ivana Mižiková, Jordi Ruiz Camp, Alberto Rodríguez and Monika Haselbauer) for all the help and support during my laboratory work, as well as for the enjoyable times we shared both inside and outside of work.

I am profoundly grateful to the laboratory mice, whose indispensable participation played a pivotal role in this study.

Lastly, my deepest appreciation is for my family and friends, particularly my parents, who have consistently encouraged my curiosity and instilled in me the belief that knowledge is the pathway to success.